



**Technische Universität München**

Fakultät für Medizin

III. Medizinische Klinik und Poliklinik, Klinikum rechts der Isar

In vivo monitoring of cancer specific TCR-engineered  
human T cells by Immuno-PET to analyze pharmacokinetics of  
T-cell based immunotherapies

Sabine Mall

Vollständiger Abdruck der von der Fakultät für Medizin der Technischen Universität München zur Erlangung des akademischen Grades eines Doktors der Naturwissenschaften (Dr.rer.nat.) genehmigten Dissertation.

Vorsitzender: Prof. Dr. Dirk H. Busch  
Prüfer der Dissertation: 1. Prof. Dr. Angela Krackhardt  
2. Prof. Dr. Iris Antes

Die Dissertation wurde am 09.03.2016 bei der Technischen Universität München eingereicht und durch die Fakultät für Medizin am 03.08.2016 angenommen.

## TABLE OF CONTENT

<b>LIST OF FIGURES</b>	<b>4</b>
<b>LIST OF TABLES</b>	<b>5</b>
<b>SUMMARY</b>	<b>6</b>
<b>ZUSAMMENFASSUNG</b>	<b>7</b>
<b>1 INTRODUCTION</b>	<b>8</b>
<b>1.1 Cancer Immunotherapies</b>	<b>8</b>
1.1.1 Immune Check-point inhibitors	8
1.1.2 Cytokines	9
1.1.3 Vaccination therapy	10
1.1.4 T-cell therapy	11
<b>1.2 Noninvasive imaging technologies for T-cells</b>	<b>16</b>
1.2.1 Optical imaging (Fluorescence and bioluminescence imaging)	17
1.2.2 Magnetic resonance tomography (MRI)	17
1.2.3 Nuclear imaging (Positron emission tomography and Single photon emission tomography)	17
<b>2 AIM OF THIS STUDY</b>	<b>23</b>
<b>3 MATERIAL</b>	<b>24</b>
<b>3.1 Material</b>	<b>24</b>
3.1.1 Technical equipment	24
3.1.2 Consumable supplies	25
3.1.3 Reagents and chemicals	26
3.1.4 Kits	28
3.1.5 Cytokines	29
3.1.6 Antibodies and HLA-multimers	29
3.1.7 Buffers	30
3.1.8 Media	31
3.1.9 DNA vectors and Primer	32
3.1.10 Restriction enzymes	32
3.1.11 Primary cells and cell lines	33
3.1.12 Mouse models	33
3.1.13 Software	34
<b>4 METHODS</b>	<b>35</b>
<b>4.1 Molecular biology</b>	<b>35</b>
4.1.1 Agarose Gel electrophoresis	35
4.1.2 Restriction digest	35
4.1.3 Ligation	36
4.1.4 Transformation of chemically competent E.coli	36
4.1.5 Plasmid preparation from e.coli - Mini-Prep and Maxi prep	36
4.1.6 Analytical digest	37
4.1.7 Isolation of genomic DNA from human cells	37
4.1.8 Detection of retroviral particles - Downgrading to Safety-Level S1	37

<b>4.2</b>	<b>Polymerase chain reaction (PCR) methods</b>	<b>38</b>
4.2.1	PCR	38
4.2.2	Quantitative PCR (qPCR) of genomic DNA	39
<b>4.3</b>	<b>Cell culture methods</b>	<b>39</b>
4.3.1	Freezing and thawing of cells	40
4.3.2	Counting of cells	40
4.3.3	Cultivation of cell lines	40
<b>4.4</b>	<b>Purification of primary cells</b>	<b>41</b>
4.4.1	Isolation of peripheral blood mononuclear cells (PBMC)	41
4.4.2	Purification of CD8+ CD62L+ CD45RA- T <sub>CM</sub> cells	41
4.4.3	Activation of primary cells	42
<b>4.5</b>	<b>Gene transfer techniques</b>	<b>42</b>
4.5.1	Production of virus particles	42
4.5.2	Transduction of activated PBMC or T <sub>CM</sub>	42
4.5.3	Transduction of cell lines	43
4.5.4	Cloning of cells by limiting dilution	43
<b>4.6</b>	<b>Flow cytometry and flow cytometry based assays</b>	<b>44</b>
4.6.1	Staining of surface molecules	44
4.6.2	HLA-Multimer staining of T cells	44
4.6.3	Fc-Receptor blocking experiments	44
4.6.4	FACS Sorting of cells	45
<b>4.7</b>	<b>Functional analysis of T cells</b>	<b>45</b>
4.7.1	24h Co-incubation assay	45
4.7.2	Enzyme linked immunosorbent Assay (ELISA)	45
4.7.3	Flow cytometry based cytotoxicity assay	46
<b>4.8</b>	<b>Purification, conjugation and labeling of aTCRmu-IgG and aTCRmu-F(ab')<sub>2</sub></b>	<b>46</b>
4.8.1	aTCRmu-IgG purification and F(ab') <sub>2</sub> fragmentation	46
4.8.2	DFO Conjugation and <sup>89</sup> Zr labeling of aTCRmu-IgG and aTCRmu-F(ab') <sub>2</sub>	47
4.8.3	Determination of specific binding of <sup>89</sup> Zr-aTCRmu-IgG or <sup>89</sup> Zr-aTCRmu-F(ab') <sub>2</sub> to 2.5D6 transduced T-cells (cell test).	47
<b>4.9</b>	<b>Animal models</b>	<b>48</b>
4.9.1	EL4 Tumor model	48
4.9.2	ML2 Tumor model	49
4.9.3	Adoptive T-cell transfer	49
4.9.4	Total body Irradiation (TBI) of mice	49
<b>4.10</b>	<b>PET/CT imaging</b>	<b>49</b>
<b>4.11</b>	<b>Ex vivo analysis</b>	<b>50</b>
4.11.1	Biodistribution analysis	50
4.11.2	Autoradiography	50
4.11.3	Preparation of single cell suspension of organs	51
4.11.4	Histology and Immunohistochemistry	51
<b>4.12</b>	<b>Statistics</b>	<b>52</b>
<b>5</b>	<b>RESULTS</b>	<b>53</b>
<b>5.1</b>	<b>Principle of the applied T-cell tracking method</b>	<b>53</b>
<b>5.2</b>	<b>Characterization of TCR2.5D6 transduced T<sub>CM</sub></b>	<b>54</b>
5.2.1	Characterization of TCR2.5D6 transduced T <sub>CM</sub> in vitro	54
<b>5.3</b>	<b>Characterization of the anti-TCRmu-antibody as tracer for TCR-transduced T-cells</b>	<b>56</b>
5.3.1	Functionality of T <sub>CM</sub> after labeling with <sup>89</sup> Zr-aTCRmu-IgG or <sup>89</sup> Zr-aTCRmu-F(ab') <sub>2</sub>	56
<b>5.4</b>	<b>In vivo PET/CT imaging</b>	<b>58</b>
5.4.1	Development of an experimental workflow for confirmation of imaging data	58

5.4.2	Development of a positive control model for in vivo imaging using EL4 cells	58
5.4.3	Development of an imaging model for human TCR-transgenic T cells	61
5.4.4	Intratumoral detection of T-cells using <sup>89</sup> Zr-aTCRmu-IgG	62
5.4.5	Intratumoral detection of T cells using <sup>89</sup> Zr-aTCRmu-F(ab') <sub>2</sub>	65
5.4.6	Confirmation of in vivo imaging of intratumoral T cells tracked by <sup>89</sup> Zr-aTCRmu-F(ab') <sub>2</sub>	69
5.4.7	Characterization of in vivo cytotoxic activity of TCR2.5D6 transduced T <sub>CM</sub>	70
5.4.8	Detection of intravenously injected T cells at the tumor site using <sup>89</sup> Zr-aTCRmu-F(ab') <sub>2</sub>	73
5.4.9	Presence of TCR2.5D6 transduced T cells detected by <sup>89</sup> Zr-aTCRmu-F(ab') <sub>2</sub> within ML2-B7 tumor tissue	76
<b>5.5</b>	<b>Qualitative and quantitative evaluation of T-cell distribution by <sup>89</sup>Zr-aTCRmu-F(ab')<sub>2</sub> PET-imaging</b>	<b>80</b>
5.5.1	Qualitative and quantitative evaluation of <sup>89</sup> Zr-aTCRmu-F(ab') <sub>2</sub> signals in ML2-B7 tumors	80
5.5.2	Heterogenous T-cell distribution detected by <sup>89</sup> Zr-aTCRmu-F(ab') <sub>2</sub> PET imaging	83
5.5.3	Mapping of T-cell distribution at the tumor site by <sup>89</sup> Zr-aTCRmu-F(ab') <sub>2</sub> PET imaging	87
<b>6</b>	<b>DISCUSSION</b>	<b>90</b>
6.1	Monitoring of TCR transgenic T-cells by Immuno-PET	90
6.2	Functionality of T cells after TCRmu-labeling and development of TCRmu-F(ab') <sub>2</sub>	93
6.3	<sup>89</sup> Zirconium - an ideal radionuclide for T-cell imaging?	95
6.4	Confirmation of imaging data by ex vivo analysis	97
6.5	Differential distribution of TCR-transgenic T-cells during tumor rejection	97
6.6	Potential clinical translation of the presented T-cell tracking methodology	100
6.7	Conclusion and outlook	104
<b>7</b>	<b>REFERENCES</b>	<b>106</b>
<b>8</b>	<b>ABBREVIATIONS</b>	<b>120</b>
<b>9</b>	<b>ACKNOWLEDGEMENTS</b>	<b>123</b>
<b>10</b>	<b>CURRICULUM VITAE</b>	<b>124</b>

## LIST OF FIGURES

Figure 1. Principle of T-cell tracking presented in this work.....	53
Figure 2. Characterization of TCR2.5D6 transduced CD8+ T <sub>CM</sub> cells.....	54
Figure 3. Generation of a stable HLA-B7 expressing ML2 cell line.....	55
Figure 4. Functionality of TCR2.5D6-transduced T <sub>CM</sub> .....	55
Figure 5. Functionality of T <sub>CM</sub> after in vitro labeling with <sup>89</sup> Zr-aTCRmu-IgG or <sup>89</sup> Zr-aTCRmu-F(ab') <sub>2</sub> .....	57
Figure 6. PET/CT imaging and ex vivo analysis of murine TCR expressing EL4 cells.....	60
Figure 7. Experimental setup of in vivo imaging model for human TCR transgenic T-cells. ....	61
Figure 8. Tracking of TCR2.5D6-transduced T <sub>CM</sub> after intratumoral injection by <sup>89</sup> Zr-aTCRmu-IgG.....	64
Figure 9. Expression of Fc-receptors on ML2 cells. ....	64
Figure 10. Investigation of different imaging time points to detect TCR-transduced T <sub>CM</sub> after injection of <sup>89</sup> Zr-aTCRmu-F(ab') <sub>2</sub> .....	66
Figure 11. Tracking of TCR2.5D6-transduced T <sub>CM</sub> injected directly into the tumor by <sup>89</sup> Zr-aTCRmu-F(ab') <sub>2</sub> . ....	69
Figure 12. Ex vivo detection of TCR2.5D6-transduced T-cells following direct injection into the tumors.....	70
Figure 13. Anti-tumor activity of TCR2.5D6-transduced T <sub>CM</sub> in vivo in a myeloid sarcoma model.....	72
Figure 14. Tracking of intravenously injected TCR2.5D6-transduced T <sub>CM</sub> within ML2-B7 tumors using <sup>89</sup> Zr-aTCRmu-F(ab') <sub>2</sub> .....	74
Figure 15. Ex vivo analysis of tracer uptake confirming specific tracking of intravenously injected TCR2.5D6-transduced T <sub>CM</sub> within ML2-B7 tumors by <sup>89</sup> Zr-aTCRmu-F(ab') <sub>2</sub> . ....	76
Figure 16. Presence of aTCRmu positive T cells within ML2-B7 tumors analyzed ex vivo.....	77
Figure 17. Presence of TCR2.5D6 positive T cells in the tumor of i.v. injected mice. ....	78
Figure 18. Presence of aTCRmu positive T cells within ML2-B7 tumors analyzed ex vivo.....	79
Figure 19. Differential distribution of <sup>89</sup> Zr-aTCRmu-F(ab') <sub>2</sub> signals within ML2-B7 tumors of mice injected with 2.5D6TCR-transgenic T <sub>CM</sub> .....	81
Figure 20. Analysis of tumor volume and <sup>89</sup> Zr-aTCRmu-F(ab') <sub>2</sub> uptake in ML2-B7 tumors according the classification into group I-III. ....	82
Figure 21. Growing kinetics of ML2 tumors of different size before and after intravenous injection of TCR2.5D6-transduced or non-transduced T <sub>CM</sub> . ....	84
Figure 22. Differential distribution of <sup>89</sup> Zr-aTCRmu-F(ab') <sub>2</sub> signals within ML2-B7 tumors of mice injected with 2.5D6TCR-transgenic T <sub>CM</sub> in comparison to <sup>18</sup> F-FDG imaging.....	86
Figure 23. T-cell imaging by PET/CT using <sup>89</sup> Zr-aTCRmu-F(ab') <sub>2</sub> facilitates mapping of T cells within ML2-B7 tumors of mice injected with TCR2.5D6-transgenic T <sub>CM</sub> . ....	88

## LIST OF TABLES

Table 1. Advantages and disadvantages from of different imaging modalities used for T-cell tracking (modified from (Liu and Li 2014)) .....	17
Table 2. Characteristics and application of different nuclides used for imaging of T-cells by PET/SPECT.....	18
Table 3. Advantages and disadvantages of different labeling strategies for T-cell imaging by PET/CT.....	22
Table 4. Technical equipment .....	25
Table 5. Consumable supplies.....	26
Table 6. Reagents and chemicals .....	28
Table 7. Kits .....	29
Table 8. Cytokines .....	29
Table 9. Antibodies used for flow cytometry .....	29
Table 10. Antibodies for immunohistochemistry.....	30
Table 11. Multimer.....	30
Table 12. Buffers .....	31
Table 13. Media.....	31
Table 14. Vectors .....	32
Table 15. Primers for detection of human and murine TCR sequences.....	32
Table 16. Probes for detection of human and murine TCR sequences.....	32
Table 17. Primer for detection of viral envelope .....	32
Table 18. Restriction enzymes .....	32
Table 19. Primary cells and cell lines.....	33
Table 20. Mouse strains .....	33
Table 21. Software .....	34
Table 22. Reaction mix for restriction digest .....	35
Table 23. Reaction mix for ligation .....	36
Table 24. Reaction mix for analytical digest.....	37
Table 25. Reaction mix for PCR with KOD polymerase .....	38
Table 26. PCR program for KOD polymerase .....	39
Table 27. Reaction mix for qPCR .....	39
Table 28. PCR program for qPCR.....	39
Table 29. Concentrations of <sup>89</sup> Zr-labeled aTCRmu for determination of specific binding .....	48
Table 30. Experimental setup of ex vivo analysis for confirmation of imaging data. ....	58
Table 31. Uptake in tumor or different organs compared to recently published antibody-based studies. ....	104
Table 32. Uptake in tumor or different organs compared to recently published reporter-gene-based studies. ....	104

## SUMMARY

Adoptive transfer of T-cells genetically modified by T-cell receptors (TCR) is an attractive novel therapeutic strategy for cancer patients. Highly sensitive in vivo imaging technologies are critical for improved understanding of T-cell migration, expansion and functionality in vivo as well as mechanisms of effective tumor rejection or evasion. Moreover, clinical translation of such technologies would further provide possibilities to improve these therapeutic approaches in humans. We targeted the murine constant TCR beta domain of a murine-human hybrid TCR by an anti-murine TCR monoclonal antibody (aTCRmu) for tracking specifically TCR-transgenic effector cells. For proof of concept, we established a xenogenic mouse model of myeloid sarcoma and transferred human central memory T cells ( $T_{CM}$ ) transgenic for the leukemia-reactive, myeloperoxidase-specific TCR2.5D6. The aTCRmu-F(ab')<sub>2</sub> was labeled with Zirconium-89 (<sup>89</sup>Zr) to mark human TCR-transgenic T cells in vitro and track them in vivo by positron emission tomography/computer tomography (PET/CT) imaging.

Binding of non-labeled or <sup>89</sup>Zr-labeled aTCRmu-F(ab')<sub>2</sub> did not impair functionality of TCR-transgenic T cells in vitro. In vivo application of <sup>89</sup>Zr-labeled aTCRmu-F(ab')<sub>2</sub> resulted in highly sensitive and specific visualization of TCR-transgenic  $T_{CM}$  confirmed by ex vivo analyses. Moreover, we detected diverse T cell distribution patterns on the tumor site by PET/CT imaging depending on the tumor size and rejection phase. Correlation of PET/CT images with semi-quantitative evaluation of T-cell infiltration based on immunohistochemical analysis allowed mapping of differential T-cell distributions within the tumor. This F(ab')<sub>2</sub> based T-cell-tracking technology enables non-invasive imaging of TCR-transgenic T cells independently of the TCR-specificity. Furthermore, the in vivo labeling of cells by this technology opens the possibility to track T cells on differential time points most critical for decision making processes of immunotherapy. Moreover, the high sensitivity and simple application make this approach especially attractive for direct clinical translation.

**Key words:** Cancer immunotherapy, T-cell receptor (TCR) transgenic T-cells, T-cell imaging, Immuno-PET/CT

## ZUSAMMENFASSUNG

Der Transfer von genetisch modifizierten T-Zellen, die mit einem tumor-spezifischen T-Zell-Rezeptor (TZR) ausgestattet wurden, ist ein neuer und äußerst attraktiver Ansatz in der Tumor-Therapie. Um mehr über die Migration, Expansion und Funktionalität von transgenen T-Zellen in vivo zu lernen und somit diese Therapien weiter zu optimieren, sind hochsensitive bildgebende Verfahren nötig. In diesem Projekt haben wir die murine konstante Domäne eines murin-humanen hybrid TZR als Zielstruktur gewählt um spezifisch transgene T-Zellen in vivo zu detektieren. In einem xenogenen Mausmodell wurden solide Tumoren aus myeloischen Zellen, sogenannte Chlorome, etabliert. Zentrale Gedächtnis T-Zellen ( $T_{CM}$ ) wurden mit dem leukämie-reaktiven, Myeloperoxidase-spezifischen TCR2.5D6 transduziert und deren intravenöser Transfer resultierte in einer starken Immunreaktivität gegen die Tumore. Dieses Modell wurde zur Etablierung der in vivo - Bildgebung von TZR-transgenen T-Zellen verwendet. Hierzu wurde ein monoklonaler Antikörper (aTCRmu) verwendet, der spezifisch an murine TZR sowie an humane TZR-transgene Effektor Zellen bindet. Der aTCRmu-IgG und dessen  $F(ab')_2$  Fragment wurden mit Zirkonium-89 ( $^{89}Zr$ ) markiert um humane TZR-transgene T-Zellen in vitro zu markieren und in vivo mit Hilfe der Positronen-Emissions-Tomographie/Computer-Tomographie (PET/CT) zu detektieren. Die Bindung von nicht-markiertem oder  $^{89}Zr$ -markiertem aTCRmu- $F(ab')_2$  führte zu keinem Funktionalitätsverlust bei TZR-transgenen  $T_{CM}$  in vitro. Nach der intravenösen Gabe von  $^{89}Zr$ -aTCRmu- $F(ab')_2$  konnten TZR-transgene  $T_{CM}$  am Tumor mittels PET/CT visualisiert werden. Dieses spezifische und sensitive in vivo Detektion wurde durch ex vivo Analysen bestätigt. Durch die Korrelation der PET/CT Bilder mit der Immunhistochemie-basierenden, semi-quantitativen Bestimmung der T-Zell-Infiltration konnte die Verteilung der T-Zellen innerhalb des Tumors klar abgebildet werden. Diese Methode ermöglicht die Verfolgung von TCR-transgenen T-Zellen in vivo, unabhängig von der Spezifität des TZR. Des Weiteren kann durch die in vivo Markierung der Zellen die Bildgebung an unterschiedlichen Zeitpunkten durchgeführt werden, was vor allem für Entscheidungsprozesse in der Immuntherapie von Relevanz ist. Die hohe Sensitivität und die einfache Anwendung machen diesen Ansatz attraktiv für eine direkte klinische Translation.

**Schlagerworte:** Immuntherapie, T-Zell-Rezeptor (TZR) transgene T-Zellen, Bildgebung von T-Zellen, Immuno-PET/CT



# 1 INTRODUCTION

## 1.1 CANCER IMMUNOTHERAPIES

Cancer is one of the leading causes of death worldwide. More than 10 million new cases were diagnosed and 8.2 million died from the disease per year as reported by the world health organization (WHO) world cancer report 2014 (Steward 2014). Although the identification of different oncogenes and tumor-suppressor-genes resulted in improved treatment for some patients, there is still a need to develop and optimize novel therapeutic approaches. Taken into account that spontaneous anti-tumor responses occur frequently in cancer patients and the presence of T-cells within tumors are often associated with a better clinical outcome (Clemente, Mihm et al. 1996; Zhang, Conejo-Garcia et al. 2003; Galon, Costes et al. 2006) immunotherapy is getting more and more important for different cancer entities. Several immunotherapeutic approaches, which interact on different phases of immune response, are currently under investigation:

### 1.1.1 IMMUNE CHECK-POINT INHIBITORS

A very promising approach of immunotherapy has emerged in the past decade with the use of immune-checkpoint inhibitors such as anti- cytotoxic T-lymphocyte antigen-4 (CTLA-4) (Leach, Krummel et al. 1996) or anti- programmed cell death 1 protein (PD-1) (Freeman, Long et al. 2000) antibodies.

Antigens are presented by the major histocompatibility complex (MHC) on the surface of antigen presenting cells (APC) to the TCR. The TCR signal can be modulated in different ways by a variety of molecules. To induce an activation of T cells, a co-stimulatory signal is necessary. The CD28-B7 interaction mediates such a co-stimulatory signal. Therefore, B7 molecules on APC bind to CD28 on the T cells leading to the activation of the T cells. On the other side, CTLA-4 binds also to B7 resulting in a strong inhibitory signal for the T cells (Egen and Allison 2002; Schneider, Downey et al. 2006). CTLA-4 blocking by antibodies prevents therefore the binding to B7 and the T cell inhibition. This leads to an enhanced immune response against tumor associated antigens shown in pre-clinical models (Leach, Krummel et al. 1996; van Elsas, Hurwitz et al. 1999). Ipilimumab, a humanized monoclonal antibody binding to anti-CTLA4 showed survival benefits for melanoma-patients (Hodi, Butler et al. 2008) and was the first immune checkpoint inhibitor approved by the food and drug

administration in USA (FDA) and in Germany for the therapy of metastatic melanoma (Hodi, O'Day et al. 2010). Several phase I and phase II clinical trials show benefits in different tumor entities such as non-small cell lung cancer (NSCLC) (Lynch, Bondarenko et al. 2012), renal cell carcinoma (RCC) (Yang, Hughes et al. 2007) and prostate cancer (van den Eertwegh, Versluis et al. 2012; Kwon, Drake et al. 2014). However, a phase III study comparing ipilimumab to placebo treatment did not show benefits for prostate cancer (Kwon, Drake et al. 2014).

Another promising target is PD-1 which was found to be upregulated in tumor infiltrating lymphocytes (TILs) (Ahmadzadeh, Johnson et al. 2009; Sfanos, Bruno et al. 2009) whereas a high amount of tumors show increased levels of programmed cell death ligand 1 (PD-L1) expression (Thompson, Kuntz et al. 2006; Wu, Zhu et al. 2006). Binding of PD-L1 to PD-1 leads to T-cell anergy and decreased processing of antigens by APCs (Dong, Strome et al. 2002; Taube, Anders et al. 2012). Nivolumab and pembrolizumab, both anti-PD-1 antibodies showed efficacy in the treatment and were approved in USA as well as Germany for treatment of metastatic melanoma. Several clinical studies involving a variety of other tumor entities such as RCC, NSCLC, melanoma, prostate cancer (Topalian, Hodi et al. 2012; Borghaei, Paz-Ares et al. 2015; Brahmer, Reckamp et al. 2015) and Hodgkin's lymphoma (Ansell, Lesokhin et al. 2015) are being conducted and show clinical responses. Combination therapies of anti-CTLA-4 and PD-1 antibodies showed improved anti-tumor response in a murine model (Curran, Montalvo et al. 2010) and significantly longer progression free survival compared to anti-CTLA-4 treatment alone in patients with advanced melanoma (Larkin, Chiarion-Sileni et al. 2015). New immune checkpoints are evaluated in pre-clinical tumor models as potential new targets and include LAG-3 (Triebel, Jitsukawa et al. 1990), TIM-3 (Sakuishi, Apetoh et al. 2010) as well as the co-stimulatory molecules OX40 (Curti, Kovacsovics-Bankowski et al. 2013) and 4-1BB (CD137) (Melero, Shuford et al. 1997).

### *1.1.2 CYTOKINES*

Human Interleukin-2 (IL-2) is a cytokine which is produced after antigen activation and promotes T cells cytotoxicity as well as differentiation processes in response to antigens as reviewed in (Jiang and Zhou 2015). On the other side, IL-2 is essential for the development of regulatory T-cells (T-Reg) thereby limiting inappropriate immune reactions by mediating tolerance (Sim, Martin-Orozco et al. 2014). IL-2 has been shown to be effective in different cancer therapies showing complete remission in 5-10% of patients with metastatic

melanoma and renal cell carcinoma and was approved by the FDA in 1998 (Rosenberg, Yang et al. 1994; Atkins, Lotze et al. 1999). A limitation of the therapeutic effect of IL-2 treatment is the induction of severe toxicity, including hypotension, capillary leak syndrome and heart toxicities (Rosenberg, Lotze et al. 1987; Rosenberg, Lotze et al. 1989).

Other cytokines in use are human interferons (IFN), secreted glycoproteins, which have important roles in regulating and linking the innate and adaptive immune system. They are involved in the defense of microbes and were shown to have an important role in the naturally occurring antitumor immune response as reviewed in (Kotredes and Gamero 2013). IFN $\alpha$ 2a and IFN $\alpha$ 2b are approved for the management of different cancer types including chronic myelogenous leukemia (CML) (Niederle, Kloke et al. 1993; 1994) and melanoma (Kirkwood, Strawderman et al. 1996). To improve IFN therapy, several combinational therapies are under investigation (O'Brien, Guilhot et al. 2003; Di Pucchio, Pilla et al. 2006).

### *1.1.3 VACCINATION THERAPY*

A possible way to induce immunity against tumors might be by vaccination therapy. Many different strategies are under development and can be classified into 3 major groups including cell vaccines, protein or peptide vaccines and genetic (DNA, RNA and viral) vaccines. In depth investigation of the use of cellular vaccines was performed either with whole tumor cells or dendritic cells (DC). Granulocyte macrophage colony stimulating factor (GM-CSF)-transduced tumor cell vaccines (GVAX) have been studied in several trials with encouraging data but phase III clinical trials failed to achieve survival benefit for metastatic prostate cancer patients and were terminated (Small E 2009). One DC-vaccine, Sipleucel-T, was approved by the FDA for the treatment of metastatic prostate cancer. These are ex vivo generated DCs cultured with a fusion protein of prostatic acid phosphatase (PAP) and GM-CSF. The Sipleucel-T treatment showed a 4-month prolonged median survival in patients with prostate cancer (Kantoff, Higano et al. 2010). A certain limitation of cell based vaccination therapies is the complex preparation. Therefore, vaccination modalities using proteins or peptides deriving from tumor-associated antigens (TAA) have advantages also in regard to cost effectiveness. In a phase II clinical trial RCC-patients were treated with IMA901, a vaccine consisting of 10 peptides derived from tumor-associated antigens (Walter, Weinschenk et al. 2012). Although not all patients benefit from this therapy, the

immune response against multiple peptides correlated to the patient's overall survival. Another study used the melanoma associated antigen A3 (MAGE-A3) in a phase II study for patients with MAGE-A3 positive NSCLC and observed positive trends in overall survival (Vansteenkiste, Zielinski et al. 2013). The strategy of genetic vaccination has the advantage of easy delivery of multiple antigens combined with the activation of different arms of the immune system. Whereas DNA-vaccines are mainly in preclinical use, one phase I/II study was performed for a RNA based vaccine in melanoma patients. In this study mRNAs coding for Melan-A, tyrosinase, gp100, MAGE-A1, MAGE-A3 and survivin were applied with the adjuvant GM-CSF and an increase of vaccine-directed T-cells were observed (Weide, Pascolo et al. 2009). A recently published pre-clinical study showed the determination of the individual tumor derived mutasome by identification of tumor specific neo-epitopes using exome sequencing and production of a specific polytropic mRNA vaccine which induced a strong immune response against the tumor (Kreiter, Vormehr et al. 2015). Another genetic approach is the use of viral systems, such as PROSTAVAC which delivers prostate specific antigen (PSA) in combination with costimulatory molecules and showed encouraging results in a phase II study (Kantoff, Schuetz et al. 2010).

#### *1.1.4 T-CELL THERAPY*

The fact that adoptive immunotherapy might have a high potential in cancer treatment was shown by the therapeutic efficiency of donor lymphocyte infusions (DLI) after stem cell transplantation. This procedure increased the graft-versus-leukemia effect (GvL) after stem cell transplantation in CML as well as in acute myeloid leukemia (AML), although to a much lower extent (Kolb, Mittermuller et al. 1990; Collins, Shpilberg et al. 1997; Kolb, Simoes et al. 2004; Kolb 2008). The first specific T-cell based therapy was reported by Rosenberg et. al. using TILs for the immunotherapy of metastatic melanoma (Rosenberg, Packard et al. 1988). In several studies they subsequently showed that adoptive transfer of autologous, in vitro expanded T cells derived from patients tumors showed efficacy against melanoma (Dudley, Yang et al. 2008; Dudley, Gross et al. 2010; Rosenberg, Yang et al. 2011). Although TIL-culture could be grown from many tumor entities, until now anti-tumor responses could be convincingly only observed for melanoma.

This led to the idea to genetically engineer lymphocytes with tumor-specific receptors for application of cell therapy for multiple tumor entities. Several technologies have been

developed to redirect the specificity of T cells: The integration of genes encoding for either conventional alpha/beta TCRs or chimeric antigen receptors (CARs) represent the two main technologies.

A CAR is composed of an extracellular single chain antibody linked to an intracellular TCR signaling domain, including co-stimulatory domains such as CD28 (Maher, Brentjens et al. 2002) or 4-1BB (CD137) (Imai, Mihara et al. 2004). CAR T-cells are able to recognize extracellular tumor-antigens independent of the MHC restriction. Clinical trials with anti-CD19 CAR T-cells have demonstrated very promising results in hematological malignancies showing remission of patients with therapy resistant CLL and acute lymphocytic leukemia (ALL) (Porter, Levine et al. 2011; Grupp, Kalos et al. 2013; Davila, Riviere et al. 2014; Maude, Frey et al. 2014).

T cells engineered with common alpha/beta TCRs, are able to target the tumors in context of MHC class I peptides. These peptides may derive from extracellular as well as intracellular proteins representing an advantage by enhancing the selection of interesting targets enormously. T cells engineered with a TCR against MART-1 melanoma melanocyte antigen showed specific tumor regression in a pre-clinical mouse model (Kessels, Wolkers et al. 2001). This TCR was further used the first time in humans by retroviral transduction and re-infusion of autologous lymphocytes showing regression of metastatic melanoma lesions in two patients (Morgan, Dudley et al. 2006). TCR specific for NY-ESO1, MART-1 and gp100 have shown clinical efficacy in early TCR-gene-therapy trials in synovial cell carcinoma and melanoma (Morgan, Dudley et al. 2006; Johnson, Morgan et al. 2009; Robbins, Morgan et al. 2011).

#### 1.1.4.1 Optimal T-cell subpopulations for T-cell therapy

An important question confronting the use of genetically engineered cells in adoptive cell therapy of cancer is the selection of the ideal human effector T-cell subpopulation used for genetic transfer of immunoreceptors. Pre-clinical mouse models showed improved antitumor responses when T cells in early stages of differentiation (such as naïve or central memory cells) are transduced and transferred (Klebanoff, Gattinoni et al. 2005). Within the memory pool it was shown that central memory T-cells ( $T_{CM}$ ) show increased antitumor activity compared to effector memory T cells ( $T_{EM}$ ) (Klebanoff, Finkelstein et al. 2004; Wu, Zhang et al. 2013). This was supported by studies in monkeys which show improved in vivo

persistence of infused  $T_{CM}$  compared to  $T_{EM}$  (Berger, Jensen et al. 2008). More recently, CD8+ T memory stem cells ( $T_{SCM}$ ) were characterized. This subpopulation of T cells derives from the naive T-cell compartment and was characterized by the CD45RO-CD45RA+CD62L+CCR7+CD27+CD28+IL7Ra+ phenotype. Compared with the known memory populations ( $T_{EM}$ ,  $T_{CM}$ ), they show increased proliferative capacity, reconstitute more efficiently into immunodeficient hosts and show superior antitumor capacity (Gattinoni, Lugli et al. 2011).

Most of the present studies in cancer immunotherapy were performed with CD8+ T cells. However, the role of CD4+ T cells becomes increasingly important in elimination of tumor cells (Quezada, Simpson et al. 2010; Tran, Turcotte et al. 2014; Sommermeyer, Hudecek et al. 2015). In a recent study, a combination of CD4+ naive T cells ( $T_N$ ) and CD8+  $T_{CM}$  cells, transduced with a CAR, was associated to enhanced antitumor capacity compared to the single treatment of each subpopulation (Sommermeyer, Hudecek et al. 2015). This may indicate that a combination of different T-cell subpopulations might enhance efficacy of adoptive T-cell therapy. Nevertheless, this needs to be further explored.

#### 1.1.4.2 Toxicity of adoptive cell therapies

T-cell therapies have the potential to be very potent in tumor therapy (Morgan, Dudley et al. 2006; Johnson, Morgan et al. 2009; Robbins, Morgan et al. 2011). However, there are several risks in the use of T-cell therapies, which need to be addressed. These adverse effects can be divided either into “on-target, off-tumor” or “off-target, off-tumor” toxicities.

Engineered T-cells have the potency to recognize small levels of antigen on cells. Therefore, the targeting of normal, non-mutated self-antigens, which are overexpressed on tumor cells may incorporate a risk for "on-target, off-tumor" toxicity in treated patients. Ideal antigen targets would be those which are presented exclusively on the tumor cell such as peptides deriving from mutated proteins. Their identification is currently an important topic and under investigation (Schumacher, Bunse et al. 2014; Yadav, Jhunjunwala et al. 2014; Tran, Ahmadzadeh et al. 2015). Alternatively, selection of a target which is only expressed on normal cells which are not essential for survival of the patient would be possible. This was shown for the therapy with an anti-CD19 CAR leading to depletion of all B cells. As a consequence patients need to be supplemented with immunoglobulins (Kalos, Levine et al. 2011; Brentjens, Davila et al. 2013; Grupp, Kalos et al. 2013; Lee, Kochenderfer et al.

2015)."On target, off tumor" toxicity was also shown in a study conducted by Johnson et.al. in which two different TCR were used for therapy of metastatic melanoma. One TCR (DMF5) derived from human TILs and showed specificity against a peptide of MART-1. The other TCR was isolated from mice immunized with a peptide deriving from the gp100 protein. The human and the murine TCR were transduced into human peripheral blood lymphocytes (PBL) and adoptively transferred into cancer patients. Objective cancer regression was seen in 30% and 19% of patients who received the human or mouse TCR, respectively. However, severe cytotoxicity was observed in the skin, eyes and ears because of expression of the targeted antigens in these organs (Johnson, Morgan et al. 2009). These toxicities could be observed in mouse models as well (Palmer, Chan et al. 2008). A TCR against carcinoembryonic antigen (CEA) was used for the treatment of metastatic colorectal cancer which was refractory to standard treatment. All patients showed decrease in serum-CEA and one patient had an objective regression of lung and liver metastases. However, all patients developed severe colitis representing the dose limiting adverse event (Parkhurst, Yang et al. 2011).

Other toxicities can result from previously unknown cross-reactivity against normal self-peptides resulting in "off-target, off-tumor" toxicities. An example is MAGE-A3, a cancer testis antigen which was not known to be expressed in any normal tissue. Targeting of a MAGE-A3 peptide in a clinical trial showed a clinical regression of the cancer in 5 of 9 patients. However, treatment caused severe brain damage because the TCR recognized a related epitope of the MAGE-A12, expressed at very low levels in the brain (Morgan, Chinnasamy et al. 2013). A recently published clinical study for melanoma and myeloma treatment used an affinity-maturated HLA-A\*01-restricted TCR targeting MAGE-A3. This TCR recognized an unrelated HLA-A\*01 restricted peptide presented in the cardiac muscle resulting in lethality of 2 patients (Linette, Stadtmauer et al. 2013). Several toxicities were also observed in CAR-studies, such as severe liver toxicities caused by a carbonic-anhydrase 9 specific CAR (Lamers, Sleijfer et al. 2013) or acute pulmonary toxicity after treatment of a patient with an anti-ERBB2 CAR (Morgan, Yang et al. 2010).

These observed toxicities need to be addressed carefully. However, beside the observed adverse effects, T-cell-therapy showed objective cancer regression in nearly all presented clinical trials as described (Johnson, Morgan et al. 2009; Morgan, Yang et al. 2010; Parkhurst,

Yang et al. 2011; Morgan, Chinnasamy et al. 2013). These trials show the strong power of T-cell based immunotherapy for cancer, but also the need for improvement of safety mechanisms for this therapeutic approach. There are several different attempts to improve the safety of TCR transfer:

- Optimization of the construct to reduce cross-reactivity by mispairing with endogenous TCR. Unlike CAR constructs, TCR are not modified at the intracellular domain to achieve optimal signal intensity. Modifications in the TCR alpha and beta chain sequences have been introduced to reduce mispairing with endogenous TCR chains and to improve the expression of the TCR. The exchange of the human constant domains with their murine counterparts and introduction of a disulfide bond linking the constant domains of the alpha and beta chain has improved pairing between the introduced chains and reduced mispairing with endogenous chains (Cohen, Zhao et al. 2006; Cohen, Li et al. 2007; Kuball, Dossett et al. 2007). Other studies investigated knockdown of endogenous TCRs by zinc-finger-nucleases or transcription-activator-like effector nucleases (TALEN) (Provasi, Genovese et al. 2012; Berdien, Mock et al. 2014).
- Incorporation of “suicide genes” which enable the destruction of cells in case of unforeseen toxicities. A prominent suicide-gene is the herpes simplex virus1-thymidine kinase (HSV1-tk) and its mutants which have a high affinity for Ganciclovir (GCV) (Moolten 1986). The HSV-tk/GCV approach was mostly used in allogeneic hematopoietic stem cell transplantation in the context of controlling graft-versus-host disease (GvHD) (Bonini, Ferrari et al. 1997). Limitations of HSV-tk/GCV is the potential immunogenicity of the enzyme and the need of Ganciclovir-administration in case of a cytomegalic-infection, which is a frequent complication in stem-cell transplantation. Furthermore, active cell proliferation is required in order to mediate cell death and ensure efficacy of the suicide mechanism (Morgan 2012). A newly and very promising suicide gene is induced Caspase9 which showed first clinical efficiency in therapy against GvHD (Di Stasi, Tey et al. 2011; Zhou, Dotti et al. 2015).
- Genetic modification of cells to express a protein which allows targeting and depletion of the cells by specific antibodies. Several different epitopes are under evaluation in preclinical models. CD20 can be targeted by the clinically approved therapeutic antibody rituximab which induces cell depletion by complement



dependent cytotoxicity (CDC) (Introna, Barbui et al. 2000; Serafini, Manganini et al. 2004; Griffioen, van Egmond et al. 2009). On the basis of the CD20, a novel suicide gene consisting of the epitopes from CD34 and CD20 was constructed to enable CD34 selection and cell tracking as well as CD20 mediated cell depletion (Philip, Kokalaki et al. 2014). Other groups showed the introduction of truncated human epithelial growth factor receptor (EGFR) (Wang, Chang et al. 2011) or even a 10 amino-acid long c-myc tag (Kieback, Charo et al. 2008) into cells to eliminate them by cetuximab or an anti-tag specific antibody, respectively.

## 1.2 NONINVASIVE IMAGING TECHNOLOGIES FOR T-CELLS

Although cancer immunotherapies showed a remarkable development within the last years, these therapies still require substantial improvement. Therefore, a better understanding of the in vivo behavior of such transferred T cells is urgently needed. Conventional immune-monitoring methods, such as immunohistochemistry, flow cytometry or T-cell frequency analysis reveal only limited information about pharmacodynamics and pharmacokinetics of T-cells. Body distribution and functionality of T cells over time remain mostly invisible by these methods. Non-invasive tracking of infused T cells can provide information about their distribution, viability and functionality such as homing, infiltration and retention at the tumor in real-time and, importantly, allow serial imaging over different time points of treatment. Therefore, non-invasive imaging technologies have an important role in the development and optimization of effective T-cell therapies as they can improve monitoring of the therapy having importance for decision-making processes in clinical trials. Several imaging modalities are applied for T-cell tracking in preclinical and clinical studies and each method has their advantages and disadvantages. Table 1 summarizes the different labeling strategies used for non-invasive imaging of T-cells.

Imaging modality	Tissue penetration	Sensitivity	Spatial resolution	Cost	Clinical translation
Optical Fluorescence/bioluminescence	<2 cm	High ~10 <sup>-9</sup> to 10 <sup>-12</sup> M for fluorescence; ~10 <sup>-15</sup> to 10 <sup>-17</sup> M for bioluminescence	2-5mm	Low	Limited
MRI	unlimited	Low 10 <sup>-3</sup> to 10 <sup>-5</sup> M	<0.1mm (preclinical ) ~1mm (clinical )	High	Yes
PET/SPECT	unlimited	High 10 <sup>-11</sup> to 10 <sup>-12</sup> M for PET 10 <sup>-10</sup> to 10 <sup>-11</sup> for SPECT	1-2 mm preclinical 5-10mm (clinical )	High	Yes

**Table 1. Advantages and disadvantages from of different imaging modalities used for T-cell tracking** (modified from (Liu and Li 2014))

### 1.1.5 OPTICAL IMAGING (FLUORESCENCE AND BIOLUMINESCENCE IMAGING)

Optical imaging provides a high sensitivity with detection limits in the picomolar range and provides fast results about distribution, function and survival of T cells at very low cost. They are widely used for in vivo imaging in small animal models either for whole-body imaging or for intravital imaging approaches (Swirski, Berger et al. 2007; Dobrenkov, Olszewska et al. 2008; Prins, Shu et al. 2008; Rabinovich, Ye et al. 2008; Chewing, Dugger et al. 2009; Charo, Perez et al. 2011). However, the application in the clinic is limited due to poor penetration in deep tissues.

### 1.1.6 MAGNETIC RESONANCE TOMOGRAPHY (MRI)

MRI has a high spatial resolution and shows the best soft tissue contrast but has only low sensitivity. Superparamagnetic iron oxide nanoparticles (SPIO) or perfluorocarbon (PFC) have been mostly used to label different cell types including T lymphocytes (Lewin, Carlesso et al. 2000; Kircher, Allport et al. 2003; Daldrup-Link, Meier et al. 2005; Srinivas, Turner et al. 2009; Liu, Ye et al. 2012; Hitchens, Liu et al. 2015).

### 1.1.7 NUCLEAR IMAGING (POSITRON EMISSION TOMOGRAPHY AND SINGLE PHOTON EMISSION TOMOGRAPHY)

Nuclear imaging, as positron emission tomography (PET) and single photon emission computed tomography (SPECT) imaging have been well established in the clinic and are widely used for T-cell tracking as well. The sensitivity of both, bioluminescence imaging (BLI) and nuclear imaging, has been reported to be similar, as low as 10<sup>4</sup>-10<sup>5</sup> labeled cells (Rabinovich, Ye et al. 2008; Shu, Radu et al. 2009) However, nuclear imaging may allow

higher tissue penetration capability (Koya, Mok et al. 2010) and has been demonstrated to be highly quantitative (Dobrenkov, Olszewska et al. 2008). To compare BLI and nuclear imaging, human prostate specific membrane antigen (PSMA)-specific human T lymphocytes were transduced with a fusion reporter gene construct containing HSV1-tk and luciferase and subsequently adoptively transferred into a murine lung tumor model of prostate carcinoma. T-cell biodistribution was monitored by BLI and PET imaging (Dobrenkov, Olszewska et al. 2008). This study showed that BLI imaging did not allow evaluation of small differences in T-cell lung infiltration or a precise quantitative analysis of T-cell persistence whereas PET imaging allowed precise quantification of T-cell distribution on the tumor site. A combination of PET with CT solves the spatial resolution problem of the PET. Thus, nuclear imaging is not only important for translation but offers also technical advantages when compared to BLI. To track T cells by nuclear imaging, various nuclides, which show different characteristics in half live or emitted  $\beta^+$  energies have been used and are summarized in Table 2.

Nuclid	Half life (van Dongen, Visser et al. 2007)(Verel, Visser et al. 2005)	Max $\beta^+$ Energy (keV) (Verel, Visser et al. 2005)(van Dongen, Visser et al. 2007)	Intrinsic spatial resolution loss (mm) (van Dongen, Visser et al. 2007)	Tracer	Application	Reference
<sup>99m</sup> Tc	0.87	2,438	3.2	<sup>99m</sup> Tc-HMPAO	In vitro labeling	(Botti, Negri et al. 1997)
<sup>111</sup> In	67.3 h	247	n.d.	<sup>111</sup> I-oxine	In vitro labeling – SPECT	(Botti, Negri et al. 1997)
<sup>18</sup> F	1.83 h	634	0.7	<sup>18</sup> F-FDG	In vitro or in vivo T cell labeling	(Eriksson, Sadeghi et al. 2011) (Adonai, Nguyen et al. 2002)
				<sup>18</sup> F-FHBG <sup>18</sup> F-FIAC <sup>18</sup> F-FMAU <sup>18</sup> F-FEAU <sup>18</sup> F-FIAU	Reporter gene imaging	(Dubey, Su et al. 2003) (Green, Nguyen et al. 2004) (Kim, Dubey et al. 2004) (Yaghoubi, Couto et al. 2006) (Dobrenkov, Olszewska et al. 2008) (Dotti, Tian et al. 2009) (Shu, Radu et al. 2009) (Chan, Wu et al. 2011) (Koehe, Doubrovin et al. 2003) (Yaghoubi, Jensen et al. 2009) (McCracken, Vatakis et al. 2015)
<sup>124</sup> I	100.3 h	1535	2.3	<sup>124</sup> I <sup>124</sup> I-FIAU	Reporter gene imaging	(Penheiter, Russell et al. 2012) (Doubrovin, Doubrovina et al. 2007)
<sup>64</sup> Cu	12,7 h	653	0.7	<sup>64</sup> Cu-PTSM	In vitro labeling	(Adonai, Nguyen et al. 2002) (Griessinger, Kehlbach et al. 2014)
				<sup>64</sup> Cu2+-Gold nanoparticles	In vitro labeling	(Bhatnagar, Li et al. 2013)
				<sup>64</sup> Cu antibody	In vitro labeling	(Griessinger, Maurer et al. 2015)
				<sup>64</sup> Cu antibody fragments (minibody)	In vitro labeling	(Tavare, McCracken et al. 2014)
<sup>89</sup> Zr	78.4 h	897	1.0	<sup>89</sup> Zr-labeled antibody – fragments (cys – diabody)	In vivo labeling	(Tavare, McCracken et al. 2015) (Tavare, Escuin-Ordinas et al. 2015)

**Table 2. Characteristics and application of different nuclides used for imaging of T-cells by PET/SPECT.**

Labeling of T cells by described nuclides can be performed either by direct cell labeling or using indirect labeling strategies. Direct cell labeling with radionuclids is a simple and therefore often used labeling technique.  $^{18}\text{F}$ -Fluorodesoxyglucose ( $^{18}\text{F}$ -FDG), a well-established radiotracer was used in a porcine model to label T lymphoblasts and study their biodistribution and showed quantitative evaluation of directly labeled cells (Eriksson, Sadeghi et al. 2011). Two radiopharmaceutical tracking methods for T-cells are approved for clinical application: Technetium-99m-hexamethylpropylene amine oxime ( $^{99\text{m}}\text{Tc}$ -HMPAO) and indium-111 ( $^{111}\text{In}$ )-oxiquinolone are used for ex vivo labeling of autologous leukocytes to detect infections or inflammations in vivo (Hughes 2003). A comparative study showed that labeling efficiencies of  $^{111}\text{In}$ -oxine and  $^{18}\text{F}$ -FDG were better than  $^{99\text{m}}\text{Tc}$ -HMPAO, whereas the retention was the highest with  $^{111}\text{In}$ -oxine. However, all presented radiolabels caused reduced cell proliferation and functionality of labeled T cells was impaired (Botti, Negri et al. 1997). Another tracer used for direct T-cell labeling and in vivo imaging is  $^{64}\text{Cu}$ -pyruvaldehydebis-(N4-methylthiosemicarbazone) ( $^{64}\text{Cu}$ -PTSM). This cell label was used in a study to track T cells in a rat glioma model (Adonai, Nguyen et al. 2002) and in a murine model using OT-1 specific T cells (Griessinger, Kehlbach et al. 2014). However, the latter study showed that labeling with  $^{64}\text{Cu}$ -PTSM lead to reduced viability and functionality as well as induction of double strand breaks in T-cells. Furthermore, a disadvantage of all direct cell-labeling methods is the high efflux and therefore loss of the label, as shown for  $^{99\text{m}}\text{Tc}$ -HMPAO,  $^{18}\text{F}$ -FDG and  $^{64}\text{Cu}$ -PTSM (Botti, Negri et al. 1997; Adonai, Nguyen et al. 2002). To maximize the retention of the radiolabel in the cell,  $^{64}\text{Cu}^{2+}$  gold nanoparticles were examined for T-cells as well as CAR-transduced T cells (Bhatnagar, Li et al. 2013). In a recent study, cancer specific T cells were labeled by gold nanoparticles and tracked in vivo by classical X-ray computed tomography (CT) (Meir, Shamalov et al. 2015). The safety of this new tracking method using nanoparticles needs to be evaluated in further studies. Recently, a  $^{64}\text{Cu}$ -radiolabeled antibody recognizing a defined variable TCR domain was used to label murine T-cell populations with mono-specificity (cOVA-TCR-Tg-TH1 cells or Tag2-TCRtg-T cells) in vitro and follow their distribution in vivo (Griessinger, Maurer et al. 2015). However, this study also showed decreased viability of T cells after labeling procedure and imaging was performed only for 48h post injection.

Although direct T-cell labeling is easy and therefore widely used, long term in vivo tracking of T cells is restricted due to dilution of the probes during cells division. Longitudinal tracking of

directly labeled T cells is also challenging because of the short half-life of most PET radionuclides which are in clinical use (Table 2). Furthermore, dead and alive labeled cells cannot be distinguished leading to false positive results. Another option for longitudinal labeling of T cells is the use of reporter genes that activate or mediate the accumulation of an imaging probe within the cells (indirect labeling). This probe can be injected multiple times to track the infused T cells in vivo and to determine the biodistribution over time as the reporter gene will not be diluted by cell division. Furthermore, only alive cells will be tracked by this method, as only viable cells transcribe the reporter gene into a protein which can metabolize the PET probe. One of the most explored PET-reporter genes is the herpes simplex virus thymidine kinase 1 (HSV1-tk) and its mutants (HSV1-sr39tk and HSV1-A167Ytk) (Gambhir, Bauer et al. 2000) and different substrates including  $^{18}\text{F}$ -FIAC,  $^{18}\text{F}$ -FEAU,  $^{18}\text{F}$ -FHBG and  $^{124}\text{I}$ -FIAU have been used as PET probes for tracking T cells (Dubey, Su et al. 2003; Green, Nguyen et al. 2004; Kim, Dubey et al. 2004; Yaghoubi, Couto et al. 2006; Dobrenkov, Olszewska et al. 2008; Dotti, Tian et al. 2009; Shu, Radu et al. 2009; Chan, Wu et al. 2011). HSV1-tk has been used to track tumor-specific T cells in a mouse model bearing human tumor xenografts (Koehne, Doubrovin et al. 2003) as well as in non-human primates (Dotti, Tian et al. 2009). Furthermore, HSV1-tk was also used in a first clinical study of therapeutic cytotoxic T cells using  $^{18}\text{F}$ -FHBG (Yaghoubi, Jensen et al. 2009). HSV-tk has an important safety feature, as it can function as a suicide gene that allows ablation of the cells by the administration of Gancycovir as described in section 1.1.4.2. On the other side, this reporter gene derives from a viral particle and therefore might be a risk of immunogenicity in humans. Several other reporter genes, such as the human sodium iodine symporter (NIS) (Penheiter, Russell et al. 2012), human norepinephrine transporter (hNET) (Doubrovin, Doubrovina et al. 2007) or the recently published hdCK3mut (McCracken, Vatakis et al. 2015) were used in preclinical studies to track specifically T-cells. As these reporter genes derive from the human system, immunogenicity might be avoided, but background signal will be present in organs where these genes are expressed. For example the NIS symporter is strongly expressed in the thyroid, stomach and salivary glands (Huang, Batra et al. 2001). Another disadvantage of reporter gene imaging is the influence of the metabolic stage of cells impacting on reporter gene expression and therefore accumulation of the PET probe within the cell (Shu, Guo et al. 2005). Furthermore, the insertion of a reporter gene leads to

large constructs which need to be introduced into the T cells potentially leading to reduced expression as well as bearing the risk of insertional mutagenesis.

Direct in vivo labeling by application of radioactively labeled antibodies or fragments represents an alternative approach to monitor T cells in vivo serially and over longer time without reduction of signal. This technique has several advantages in comparison to the usage of reporter genes due to the simple application and the avoidance of further genetic manipulation associated to enhanced technical and regulatory hurdles. On the other side, false positive signals deriving from dead cells cannot be excluded. Therefore, ex vivo analysis need to be performed in preclinical assays to evaluate specificity and safety of the tracer. <sup>111</sup>Indium-labeled antibodies targeting CD4 have been used to specifically track CD4+ cells in a murine colitis model (Kanwar, Gao et al. 2008). In a recent study, <sup>64</sup>Cu-labeled antibody-fragments, so called minibodies, have been used to detect endogenous CD8-positive cells by PET imaging (Tavare, McCracken et al. 2014). However, application of minibodies seems to be not ideal as they suffered from aggregation problems in vivo. Furthermore, as described above, <sup>64</sup>Cu-labeling induces double strand breaks in labeled cells. By the use of <sup>89</sup>Zr-labeled anti-CD4 and anti-CD8 cys-diabodies T-cell reconstitution post stem cell transplantation was monitored in a murine model (Tavare, McCracken et al. 2015). Furthermore, using the presented <sup>89</sup>Zr-labeled anti-CD8 cys-diabodies, Tavare et al showed in another study the biodistribution and tumor infiltration of endogenous CD8-T-cells by PET/CT in murine models during the treatment with the checkpoint inhibitor anti-PDL1 and anti-CD137 (Tavare, Escuin-Ordinas et al. 2015). However, the developed immuno-PET tracer are so far limited to murine targets without any potential for direct clinical application. Moreover in these studies, the impact of labeling on T-cell function has not been investigated. Until now, no tracking of human genetically modified T cells expressing clinically relevant TCR with diverse specificities has been previously accomplished by Immuno-PET. Table 3 summarizes advantages and disadvantages of previously described T-cell labeling strategies for PET/CT imaging compared to the here presented study.

## In vivo tracking of TCR-engineered human T cells by Immuno-PET

Method	Reference	Description	Advantage	Disadvantage
Antibody based	Griessinger PNAS 2015	<sup>64</sup> Cu anti TCR mAb binding to specific TCR of murine T cells	<ul style="list-style-type: none"> <li>Imaging of TCR transgenic T cells shown in 2 different in vivo models</li> </ul>	<ul style="list-style-type: none"> <li>ex vivo labeling of cells enables detection only on short time frame post injection. Imaging over several time points is not possible</li> <li>Antibody has a specificity for a single murine TCR, no broad application possible. No clinical translation possible</li> <li><sup>64</sup>Cu induces double strand breaks and cell death</li> </ul>
	Tavare PNAS 2014	<sup>64</sup> Cu anti CD8 minibodies binding to murine endogenous CD8 cells	<ul style="list-style-type: none"> <li>minibodies show good binding efficiency</li> </ul>	<ul style="list-style-type: none"> <li><sup>64</sup>Cu induces double strand breaks and cell death</li> <li>Minibodies problematic pharmacokinetics, aggregation problem described</li> <li>Detection of murine T cells limits direct clinical translation</li> </ul>
	Tavare JNM 2014	<sup>89</sup> Zr anti CD8 and CD4 cys diabodies binding to murine endogenous CD8/CD4 cells (BL/6 mice)	<ul style="list-style-type: none"> <li>cys diabodies show very good binding efficiency and pharmacokinetics</li> </ul>	<ul style="list-style-type: none"> <li>Detection of murine T cells limits direct clinical translation</li> </ul>
	Tavare Cancer Research 2016	<sup>89</sup> Zr anti CD8 and CD4 cys diabodies binding to murine endogenous CD8 cells and OT-I transferred cells	<ul style="list-style-type: none"> <li>Use of different models</li> <li>Imaging of different T cell distribution of T cells with or without PDL1 therapy confirming our results</li> </ul>	<ul style="list-style-type: none"> <li>Detection of murine T cells limits direct clinical translation</li> </ul>
	Mall et al Cancer Research in revision	<sup>89</sup> Zr anti TCRmu F(ab') <sub>2</sub> binding to human TCR transgenic transferred T cells	<ul style="list-style-type: none"> <li>use of human TCR transgenic T cells allows testing binding effect on human cells</li> <li>binding to constant murine domain and therefore general use possible</li> <li>in vitro and in vivo functionality of T cells</li> </ul>	<ul style="list-style-type: none"> <li>F(ab')<sub>2</sub> not ideal, antibody derived tracer with lower molecular size for better secretion (&lt; 60kDa glomerular cut-off) and still high retention on the tumor would be better</li> <li>Murinization might be immunogenic</li> </ul>
Reporter gene based	McCracken JCI 2015	<sup>18</sup> F-FMAU imaging of hdCK3mut+ F5+ transgenic human T cells (i.v. transferred and HSC engraftment)	<ul style="list-style-type: none"> <li>Only detection of alive T cells</li> <li>sequential imaging over very long time periods possible</li> <li>use of human T cells</li> <li>Small size and human origin of transgene (but mutated)</li> <li>in vitro shown that hdCK3mut is not disturbing T cell function</li> </ul>	<ul style="list-style-type: none"> <li>Insertional mutagenesis</li> <li>silencing of reporter gene</li> <li>although human cell composition was shown to be equivalent for every group, only very low cell number of TCR+ (3,9%) transgenic T cells were detected after HSC engraftment in mice and authors did not clarify if this might be due to hdCK3mu expression or negative thymic selection. Furthermore, no anti-tumor efficacy shown and therefore in vivo impact of transgene and labeling not known, although ex vivo splenocytes tested for IFN<math>\gamma</math> secretion after specific stimulation</li> <li>hdCK3mut could cause toxicity during immune cell activation by changing cellular nucleotide pool. It is unknown if constitutive expression of dCK in cells does not lead to changes in cell function.</li> <li>sensitivity of imaging dependent on reporter gene expression: metabolic stage of the cells influences reporter expression</li> <li>For HSC transduction – lineage specific promoter necessary. In this work all transduced cells express the reporter gene but only CD3 cells the TCR → false negative results (detection of myeloid derived suppressor cells, macrophages on the tumor)</li> <li>Uptake of the PET reporter probe in other human cells. <sup>18</sup>F-FMAU is a thymidine analog and will be phosphorylated by thymidine kinases and therefore high background in highly replicating organs such as tumors might limit application.</li> <li>Indeed, very low signal to noise ratio in compared to antibody based methods</li> <li>hdCK3mut is a mutated form of hCK3 as these mutations might be immunogenic</li> </ul>
Direct labeling	Botti, EJNM 1997	<sup>111</sup> In-oxiquinolone	<ul style="list-style-type: none"> <li>some of the PET probes are clinically approved</li> </ul>	<ul style="list-style-type: none"> <li>false positive results: no discrimination between dead and alive cells or free label</li> <li>short time frame of imaging post cell injection (depending on the half life of the tracer)</li> <li>No long term follow up of the injected cells possible</li> <li>frequent cellular toxicity</li> </ul>
	Erikson, NuclMedBiol, 2011	<sup>18</sup> F-FDG		
	Botti, EJNM 1997	<sup>99m</sup> Tc-HMPAO		
	Griessinger, JNM 2014 Adonai, PNAS 2002	<sup>64</sup> Cu-PTSM		
	Bhatnagar, IntegrBiol, 2013	gold-nanoparticles coupled to <sup>64</sup> Cu		

**Table 3. Advantages and disadvantages of different labeling strategies for T-cell imaging by PET/CT**

## 2 AIM OF THIS STUDY

Adoptive transfer of T cells genetically modified by T-cell receptors (TCR) specifically recognizing malignant cells is an evolving therapeutic option in cancer. Clinical efficacy of TCR-transgenic T cells targeting melanoma-associated differentiation antigens and cancer testis antigens have been demonstrated in patients with melanoma and sarcoma (Cohen, Zhao et al. 2006; Johnson, Morgan et al. 2009; Robbins, Morgan et al. 2011). Novel target structures and TCR recognizing these targets are currently under intensive investigation and combinatorial approaches may further improve long-term efficacy. However, some TCR have demonstrated high toxicity with even fatal outcome in early clinical trials (Linette, Stadtmauer et al. 2013; Morgan, Chinnasamy et al. 2013). Understanding of the in vivo behavior of such genetically modified T cells in preclinical models may have high value for optimization of this approach with respect to novel TCR constructs but also combinatorial therapies. Moreover, clinically applicable approaches may be highly useful to understand pharmacodynamics and pharmacokinetics of TCR-modified T cells in humans. Furthermore, tracking of transduced T cells is not only of essential relevance regarding efficacy and optimization of T-cell therapy but could also represent an important safety mechanism by depletion of autoreactive T cells. To monitor real time survival, distribution and anti-tumor responses of T cells in vivo, non-invasive in vivo imaging is the model of choice. In this project we aimed to develop a general approach for tracking TCR-transgenic T cells in vivo with high potential for clinical translation. Therefore, a strategy of non-invasive in vivo imaging and tracking of TCR transgenic T cells should be developed. This tracking method should be established for the use as a general tracking method independent of TCR specificity. Furthermore, imaging of specific T cells should be possible over longer time periods to follow T-cell distribution during the course of immunotherapy. TCR-transgenic T cells should be analyzed in vitro to confirm binding specificity of the tracer as well as functionality of T cells after labeling procedure. Next, the in vivo binding of the tracer to the target should be analyzed and imaging data should be confirmed by involvement of ex vivo analysis. Furthermore, a clinically relevant tumor model should be established for analysis of in vivo pharmacokinetics and pharmacodynamics of human T cells transgenic for cancer specific TCR.



### 3 MATERIAL

#### 3.1 MATERIAL

##### 3.1.1 TECHNICAL EQUIPMENT

Device	Company
Analytical balance 440-35N	Denver Instrument, Göttingen, Germany
Analytical balance SI-64	Denver Instrument, Göttingen, Germany
Axiovert 40C microscope	Carl Zeiss Microscopy, Oberkochen, Germany
Centrifuge 5417R	Eppendorf AG, Hamburg, Germany
Centrifuge 5810R	Eppendorf AG, Hamburg, Germany
Centrifuge J2-HS	Beckman Coulter, Brea, USA
Cryotome CM1950	Leica Biosystems, Nussloch, Germany
DAKO Autostainer	Dako, Agilent Technologies, Glostrup, Denmark
Electrophoresis Apparatus	VWR, Darmstadt, Germany
Electrophoresis Chamber	G&P Kunststofftechnik, Kassel, Germany
FACS Aria	BD Bioscience, Franklin Lakes, USA
Freezer (-20°C)	Liebherr-International AG, Bulle, Switzerland
Freezer (-80°C)	Buchner Labortechnik, Pfaffenhofen, Germany
Gamma counter 1480Wizard3	Wallac, PerkinElmer, Waltham, USA
Gamma counter 2480Wizard2	PerkinElmer, Waltham, USA
Incubator BBD6220	Heraeus Holding, Hanau, Germany
Inveon small animal PET/CT scanner	Siemens, Knoxville, USA
Irradiation Cabinet	Gulmay, Byfleet, UK
Laminar Flow	BDK, Sonnenbühl-Genkigen, Germany
Laminar Flow HERAsafe	Heraeus Holding, Hanau, Germany
LSRII cytometer	BD bioscience, Franklin Lakes, USA
MACS MultiStand	Miltenyi Biotec, Bergisch Gladbach, Germany
MACSmix Tube Rotator	Miltenyi Biotec, Bergisch Gladbach, Germany
Magnet agitator	Janke & Kunkel, Staufen, Germany
Megafuge 1.0R	DJB Labcare Ltd, Buckinghamshire, UK
Microscope BX53	Olympus, Tokio, Japan

MidiMACS™ Separator	Miltenyi Biotec, Bergisch Gladbach, Germany
MoFlo high performance cell sorter	Dako, Agilent Technologies, Glostrup, Denmark
Multichannel pipets	Eppendorf AG, Hamburg, Germany
NanoDrop ND-100	Peqlab Biotechnologie, Erlangen, Germany
Nanophotometer	Implen GmbH, Munich, Germany
Neubauer Counting Chamber	Karl Hech, Sondheim/Röhn, Germany
phosphorimager CR35BIO	Raytest GmbH, Straubenhardt, Germany
Pipetboy	INTEGRA Biosciences, Fernwald, Germany
SE-HPLC BioSep™ (SEC-s3000 LC Column)	Phenomenex, Aschaffenburg, Germany
StepOnePlus	Applied Biosystems, life technologies, Carlsbad, USA
TGradient Thermocycler	Biometra, Göttingen, Germany
Thermomixer comfort	Eppendorf AG, Hamburg, Germany
UV-transilluminator Biodoc Analyze	Biometra, Göttingen, Germany
Vortexer	Bender & Hobe, Switzerland
Microplate reader (Sunrise)	Tecan, Männedorf, Switzerland

**Table 4. Technical equipment**

### 3.1.2 CONSUMABLE SUPPLIES

Consumable	Company
Aspiration pipet (2ml)	Sarstedt, Nümbrecht, Germany
Serological pipets (2/5/10/25/50ml)	Sarstedt, Nümbrecht, Germany
Cell culture flask	Greiner Bio-One, Frickenhausen, Germany
50ml/15ml tube	BD bioscience, Franklin Lakes, USA
Filter tips (10µl, 200µl, 1000µl)	Sarstedt, Nümbrecht, Germany
Gloves latex	Sempermed, Wien, Austria
Gloves nitrile	KCL, Eichenzell, Germany
ImmunoPlates	Nunc, Roskilde, Denmark
Inoculating loops	VWR, Darmstadt, Germany
MACS cell separation Columns (LD, LS, MS)	Miltenyi Biotec, Bergisch Gladbach, Germany
Freezing Container	Nunc, Roskilde, Denmark
Parafilm	Pechiney Plastic Packaging, Chicago, USA
Petri dishes	Greiner Bio-One, Frickenhausen, Germany

Pipet tips (10µl, 200µl, 1000µl)	Sarstedt, Nümbrecht, Germany
Round bottom flow cytometry tubes	BD bioscience, Franklin Lakes, USA
Sealing foil	Alpha laboratories, Hampshire, UK
Sub-Q syringes (1ml)	BD bioscience, Franklin Lakes, USA
Syringes (5ml, 10ml, 50ml)	BD bioscience, Franklin Lakes, USA
Cell strainer (40µm)	BD bioscience, Franklin Lakes, USA
Cell culture treated 96 well U-bottom plates	TPP Techno Plastic products, Trasadingen, Switzerland
Sephadex G-25 M, PD10 column	GE Healthcare, Buckinghamshire, UK
phosphor imaging plate	Fujifilm, Tokyo, Japan
Cell culture treated 6/12/24/96 well plates	TPP Techno Plastic products, Trasadingen, Switzerland
Reaction tubes (0.5µl)	Peqlab Biotechnologie, Erlangen, Germany
Microtubes (1.2ml)	Alpha laboratories, Hampshire, UK
Reaction tubes (1.5µl and 2ml)	Sarstedt, Nümbrecht, Germany
Non-treated 6/24-well plates	BD bioscience, Franklin Lakes, USA
Stericup 0,22µm Vacuum Filter Units	Merck Millipore, Darmstadt, Germany
Syringe filter (0,22µm and 0.45µm)	TPP Techno Plastic products, Trasadingen, Switzerland
CryoPure tube (1,6ml)	Sarstedt, Nümbrecht, Germany

**Table 5. Consumable supplies**

### 3.1.3 REAGENTS AND CHEMICALS

Reagent	Company
100bp DNA ladder	New England Biolabs, Ipswich, UK
1kb DNA ladder	New England Biolabs, Ipswich, UK
6x Gel loading dye	Fermentas, St.Leon-Rot, Germany
7-Aminoactinomycine D (7-AAD)	Sigma-Aldrich, Taufkirchen, Germany
Agarose	Roth, Karlsruhe, Germany
AIM-V	Invitrogen, Carlsbad, USA
Ampicillin	Sigma-Aldrich, Taufkirchen, Germany
Bovine serum albumine (BSA)	Sigma-Aldrich, Taufkirchen, Germany
DEPC-H <sub>2</sub> O	Invitrogen, Carlsbad, USA

1,4 Dithiothreitol (DTT)	Sigma-Aldrich, Taufkirchen, Germany
Desferrioxamine (DFO-Bz-NCS)	Macrocyclics, Inc, Dallas, USA
Diaminobenzidine	KPL, Gaithersburg, USA
DMEM	Invitrogen, Carlsbad, USA
DMSO	Sigma-Aldrich, Taufkirchen, Germany
D-PBS	Invitrogen, Carlsbad, USA
EDTA	Invitrogen, Carlsbad, USA
Eosin	Merck, Darmstadt, Germany
Ethanol	Merck, Darmstadt, Germany
Ethidium Bromide	Roth, Karlsruhe, Germany
Fetal bovine Serum (FCS)	Invitrogen, Carlsbad, USA
Ficoll	Biochrom, Berlin, Germany
Gene Ruler 1kb DNA ladder	PeqLab, Erlangen, Germany
Gentamycine	Merck, Darmstadt, Germany
goat serum	Abcam, Cambridge; UK
H <sub>2</sub> SO <sub>4</sub> (1M)	Roth, Karlsruhe, Germany
Haematoxylin	Merck, Darmstadt, Germany
HBSS	Invitrogen, Carlsbad, USA
Heparine	B.Braun, Melsungen, Germany
HEPES	Invitrogen, Carlsbad, USA
Human Serum	TU Munich, München Germany
Isofluran	CP Pharma, Burgendorf, Germany
Isopropanol	Merck, Darmstadt, Germany
Kanamycin	Sigma-Aldrich, Taufkirchen, Germany
LB Agar	Invitrogen, Carlsbad, USA
LB Broth Base	Invitrogen, Carlsbad, USA
L-Glutamine	Invitrogen, Carlsbad, USA
Milk-powder	Sigma-Aldrich, Taufkirchen, Germany
Mycophenolic acid (MPA)	Sigma-Aldrich, Taufkirchen, Germany
NaCl	Merck, Darmstadt, Germany
NaN <sub>3</sub>	Merck, Darmstadt, Germany
NEB5α	New England Biolabs, Ipswich, UK

Non essential amino-acids	Invitrogen, Carlsbad, USA
OneShot TOP10	Invitrogen, Carlsbad, USA
Penicilline/Streptomycine	Invitrogen, Carlsbad, USA
Paraformaldehyde (PFA)	Sigma-Aldrich, Taufkirchen, Germany
Protamine sulfate	MP Biomedicals, Illkirch, France
Protein A Sepharose	GE Healthcare Life Sciences
Proteinase K	GeneAll, seoul, Korea
Restriction enzymes	New England Biolabs, Ipswich, UK
RetroNectin	Takara, Japan
RNase Out	Invitrogen, Carlsbad, USA
RPMI	Invitrogen, Carlsbad, USA
S.O.C. Medium	Invitrogen, Carlsbad, USA
Sodium Pyruvate	Invitrogen, Carlsbad, USA
TransIT Transfection Reagent	Mirus, Madison, USA
Trypsine EDTA (0.5%)	PAA laboratories, Pasching, Austria
Tween20	Sigma Aldrich, Taufkirchen, Germany
Typan blue	Invitrogen, Carlsbad, USA
Zirconium-89	BV Cyclotron VU, Amsterdam, Netherlands

**Table 6. Reagents and chemicals**

### 3.1.4 KITS

Reagent	Company
Anti-PE/Anti-APC/Anti-FITC Microbeads	Miltenyi Biotec, Bergisch Gladbach, Germany
BCA Protein Assay Kit	Thermo Fischer Scientific, Waltham, USA
Dynabeads human T activator CD3/CD28	Invitrogen, Carlsbad, USA
Endotoxin free plasmid preparation	Macherey-Nagel, Düren, Germany
Human IFN $\gamma$ ELISA Set	BD Bioscience, Franklin Lakes, USA
iVIEW DAB detection kit	Ventana Medical Systems, Roche
JetStar 2.0 Plasmid Purification Kit	Genomed, Löhne, Germany
KAPA Probe Fast Universal Mastermix	PeqLab, Erlangen, Germany
KOD Hot Start Polymerase Kit	Merck, Darmstadt, Germany
NucleoSpin Gel and PCR Purification Kit	Macherey-Nagel, Düren, Germany

QiAamp DNA mini kit	Qiagen, Venlo, Netherlands
QiAmp Viral RNA Mini Kit	Qiagen, Venlo, Netherlands
T4 Ligase	Thermo Fischer Scientific, Waltham, USA
TMB substrate Reagent Set	BD bioscience, Franklin Lakes, USA

**Table 7. Kits**

### 3.1.5 CYTOKINES

Cytokine	Company
Human IL-2	PeptoTech, London, UK
Human IL-7	PeptoTech, London, UK
Human IL-15	PeptoTech, London, UK

**Table 8. Cytokines**

### 3.1.6 ANTIBODIES AND HLA-MULTIMERS

#### 3.1.6.1 Antibodies used for flow cytometry

Antibody	Clone	Isotype	Company
Isotype control	MOPC-21	mIgG <sub>1</sub>	BD Bioscience, Franklin Lakes, USA
α-hCD16	3G8	mIgG <sub>1</sub> k	BD Bioscience, Franklin Lakes, USA
α-hCD3	UCHT-1	mIgG <sub>1</sub> k	BD Bioscience, Franklin Lakes, USA
α-hCD32	FLI8.26	mIgG <sub>2b</sub> k	BD Bioscience, Franklin Lakes, USA
α-hCD4	RPA-T4	mIgG <sub>1</sub> k	BD Bioscience, Franklin Lakes, USA
α-hCD45	J.33	mIgG <sub>1</sub>	Beckman Coulter, Brea, USA
α-hCD45RA	HI100	mIgG <sub>2b</sub> k	BD Bioscience, Franklin Lakes, USA
α-hCD45RO	UCHL1	mIgG <sub>2</sub> k	BD Bioscience, Franklin Lakes, USA
α-hCD5	BL1a	mIgG <sub>2a</sub>	Beckman Coulter, Brea, USA
α-hCD62L	DREG-56	mIgG <sub>1</sub> k	BD Bioscience, Franklin Lakes, USA
α-hCD64	10.1	mIgG <sub>1</sub> k	BD Bioscience, Franklin Lakes, USA
α-hCD8	RPA-T8	mIgG <sub>1</sub> k	BD Bioscience, Franklin Lakes, USA
α-mTCRb (TCRmu)	H57-597	hIgG <sub>2</sub> k	BD Bioscience, Franklin Lakes, USA

**Table 9. Antibodies used for flow cytometry**

### 3.1.6.2 Antibodies used for immunohistochemistry

Antibody	Clone	Isotype	Dilution	Company
$\alpha$ -CD3	SP7	rIgG	1:150	DCS, Hamburg, Germany
$\alpha$ -CD3	MRQ-39	rIgG <sub>1</sub>	1:500	Cell Marque, Rocklin, USA
$\alpha$ -CD5	4C7	mIgG <sub>1</sub> k	1:150	Novocastra, Nussloch, Germany

**Table 10. Antibodies for immunohistochemistry**

### 3.1.6.3 Multimer

Multimer	HLA-molecule	Conjugation	Purchase/Origin
MPO <sub>5</sub>	HLA-B*0702	PE	Dirk H. Busch, TU Munich, Germany

**Table 11. Multimer**

### 3.1.7 BUFFERS

Reagent	Additives	Used for
10xTAE buffer	0.4mM Tris-HCl, pH 7.8	DNA gel electrophoresis
ACK lysis buffer	150mM NH <sub>4</sub> Cl 10mM KHCO <sub>3</sub> 0.1mM EDTA in H <sub>2</sub> O	Red blood cell lysis
Coating buffer	100mM NaHCO <sub>3</sub> 30mM Na <sub>2</sub> CO <sub>3</sub> in H <sub>2</sub> O, pH 9.5	ELISA
FACS buffer	PBS; 1% $\Delta$ FCS	Flow cytometry washing
Fixation buffer	1% paraformaldehyde	Flow cytometry
Washing buffer	PBS; 0,02% Tween 20	ELISA
Sodium acetate	pH 4.9-5.5	<sup>89</sup> Zr-labeling
Sodium bicarbonate	100mM Na bicarbonate pH 9 2M Na Carbonate 0.5M HEPES pH7	<sup>89</sup> Zr-labeling
Elution buffer	25mM Na acetate 5mg/ml gentisic acid pH 5.5	<sup>89</sup> Zr-labeling
Phosphate buffer	0.1M phosphate buffer pH 6.8	<sup>89</sup> Zr-labeling
$\Delta$ FCS	Inactivated FCS (20min at 58°C)	Media preparation, freezing of cells

ΔHS	Inactivated HS (20min at 58°C)	Flow cytometry, media preparation
Isolation buffer	PBS, 0.2% ΔFCS 2mM EDTA	Cell purification (MACS Isolation)
Retronectin-solution	PBS, 12μg/ml RetroNectin	Transduction

**Table 12. Buffers**

### 3.1.8 MEDIA

Medium	Composition
cRPMI	RPMI supplemented with 10% (v/v) FCS, Sodium pyruvate (1mM), L-Glutamine (2mM), non-essential amino-acids (10mM) and Penicilline/streptomycine (100IU/ml)
cDMEM	DMEM supplemented with 10% (v/v) FCS, Sodium pyruvate (1mM), L-Glutamine (2mM), non-essential amino-acids (10mM) and Penicilline/streptomycine (100IU/ml)
T-cell Medium	RPMI supplemented with 5% (v/v) ΔFCS, 5% (v/v) ΔHS, Sodium pyruvate (1mM), L-Glutamine (2mM), non-essential amino-acids (10mM), HEPES (10mM), penicilline/streptomycine (100IU/ml) and Gentamycine (16μg/ml).
Binding medium	PBS supplemented with 1% Bovine serum albumine (BSA)
Freezing medium	FCS supplemented with 10% DMSO
AIM-V	AIM-V (Invitrogen)

**Table 13. Media**



3.1.9 DNA VECTORS AND PRIMER

Vector	
pcDNA3.1-MLV	containg “gag- pol”
pALF10A1-GALV	containing “env”
pMP71	containing LTR of MPSV and a PRE of the woodchuck hepatitis virus (Engels, Cam et al. 2003) and used for transfer of TCR or HLA molecules

**Table 14.Vectors**

Primer	Sequence
TCRmu beta Forward	5'-GACCACGTGGAAGTCTTG-3'
TCRmu beta Reverse	5'CTCTCAGTCTGCTGGACAGG-3'
TCRhu beta Forward	5'CGAGTCTTACCAGCAAGGG-3'
TCRhu beta Reverse	5'-ATACAAGGTGGCCTTCCCTA-3'

**Table 15. Primers for detection of human and murine TCR sequences**

Probe	Sequence
TCRmu beta	5'FAM-ACACGCCGCTGTGCACCTCT-3'TAMRA
TCRhu beta	5'FAM-TCCTGTCTGCCACCATCCTCTATGA-3'TAMRA

**Table 16. Probes for detection of human and murine TCR sequences**

Primer	Sequence
A3-Forward	5'- TGGCCCAGAATAATTTACCACTCCCCC -3'
A3-Reverse	5'- ACTTCGTTGAGGTCTGTCTGGATAGCG -3'

**Table 17. Primer for detection of viral envelope**

3.1.10 RESTRICTION ENZYMES

Enzyme	Company
NotI (10000U/ml)	Thermo Fischer Scientific, Waltham, USA
EcoRI (10000U/ml)	Thermo Fischer Scientific, Waltham, USA
Sall (10000U/ml)	Thermo Fischer Scientific, Waltham, USA

Table 18. Restriction enzymes

3.1.11 PRIMARY CELLS AND CELL LINES

Cell line and use		Purchase/Origin
CD8+central memory T-cells (T <sub>CM</sub> )	Human primary cells used for transduction of TCR	Isolation from PBMCs by microbead-technology (Miltenyi)
EL4 cells	Mouse T-lymphoma cell line	ATCC
Jurkat76	Human T-lymphoma cell line containing CD8+	Kind gift from M.Heemskerk (Heemskerk, Hoogeboom et al. 2003)
ML2 cells	Human acute myeloid leukemia (AML) cell line	The CABRI consortium
murine B cell hybridoma H57-597	Production of TCR $\mu$ antibody	ATCC (HB-218)
NSO-IL15	Mouse myeloma cells transfected with the gene for human IL-15	Kind gift from S.R.Riddell (Wang, Berger et al. 2011)
Peripheral blood mononuclear cells (PBMC)	Human primary cells used for transduction of TCR	Isolation from the blood of healthy donors by density gradient centrifugation
T293 hamster embryonal kidney cells	Producer cell line for viral particles	ATCC

**Table 19. Primary cells and cell lines**

3.1.12 MOUSE MODELS

Mouse strain		Purchased from
NOD/MrkBomTac-Prkdc <sup>scid</sup>	NOD/SCID	Taconic (Germantown, NY, USA)
C.Cg-Rag2 <sup>tm1Fwa</sup> Il2rg <sup>tm1Sug</sup> /JicTac	NSG	Taconic (Germantown, NY, USA)
NOD.Cg-Prkdc <sup>scid</sup> Il2rg <sup>tm1Wjl</sup> /SzJ	BRG	Jackson Laboratory (Bar Harbor, Maine, USA).

**Table 20. Mouse strains**

3.1.13 SOFTWARE

Software
AIDA Image analyzer software version 4.21
Graph Pad prism Version 5.01
Inveon Research Workplace
Microsoft Office (Word, Excel, Powerpoint) 2010
Windows EndNote X7.4
BioDoc Analyze digital system (BioMetra)
StepOne Software v2.3
Flow Jo

**Table 21. Software**

## 4 METHODS

### 4.1 MOLECULAR BIOLOGY

#### 4.1.1 AGAROSE GEL ELECTROPHORESIS

For analysis of DNA fragments by gel electrophoresis, 1-1,7% agarose gels were prepared. Therefore, the respective amount of agarose (w/v) was melted by heating in 1xTAE buffer (Table 12) and ethidium bromide was added to a final concentration of 0.8µg/ml. Samples were mixed with the respective amount of 6x DNA-loading dye and loaded on the agarose gel. DNA marker 1kb or 100bp were used to interpret size of DNA of interest. DNA fragments were separated for 20-40min at 100-130V in an Electrophoresis chamber midi horizontal. Results were visualized and documented using BioDoc Analyze digital system.

##### 4.1.1.1 Gel extraction

For purification of DNA from agarose gels, respective gel containing the fragment were cut and DNA was purified using NucleoSpin Gel and PCR clean-up Kit according to manufacturer's instructions. Elution of DNA was performed using 30µl DEPC-H<sub>2</sub>O and concentration and quality was determined using NanoDrop ND-1000.

#### 4.1.2 RESTRICTION DIGEST

For further cloning of DNA into a DNA vector (pMP71), the purified PCR product or gel extracted DNA fragment (section 4.1.1) and the respective vector were digested with respective restriction-enzymes for 2h at 37°C. The reaction was terminated by incubation for 10min at 65°C. Following amounts were used:

Reagent	Volume
DNA Vector/PCR product	~15µg/30µl
10x buffer	10µl
Enzyme 1	2µl
Enzyme 2	2µl
DEPC H <sub>2</sub> O	Ad 100µl

**Table 22. Reaction mix for restriction digest**

After restriction reaction was performed, DNA was purified from small DNA fragments and restriction buffer by Agarose DNA electrophoresis (section 4.1.1) and gel extraction (section 4.1.1.1) before used for ligation (section 4.1.3).

#### 4.1.3 LIGATION

For ligation of digested PCR products into the respective DNA vector, ligation was performed using molar ratios of 1:5 and 1:3. The amount of PCR fragment was calculated using following formula:

$$m(\text{PCR fragment (ng)}) = \text{ratio} \times \text{size (insert (bp))} \times \frac{m(\text{DNA vector (ng)})}{\text{size (DNA vector (bp))}$$

The components were mixed as followed, incubated for 16h at 16°C and used afterwards for transformation into chemically competent E.coli (section 4.1.4).

Reagent	Volume
DNA Vector	100ng
PCR fragment	x ng
10x T4 ligase buffer	1µl
T4 ligase	1µl
DEPC H <sub>2</sub> O	Ad 10µl

**Table 23. Reaction mix for ligation**

#### 4.1.4 TRANSFORMATION OF CHEMICALLY COMPETENT E. COLI

Chemically competent E.coli bacteria (TOP10 or NEB5α) were thawed on ice. 2µl of ligation mixture (section 4.1.3) was added to 25µl of bacterial suspension, mixed carefully and incubated for 30min on ice. Heat shock was performed for 30sec at 42°C and following incubation for 2min on ice. 250µl S.O.C medium was added and bacteria were shaken for 60min at 300rpm in a Thermomixer. Different dilutions of bacterial suspensions were plated on LB-agar (pre-warmed to room temperature) plates containing antibiotics (100µg/ml Ampicillin or Kanamycin) and incubated over night at 37°C. Re-transformation of purified plasmids (section 4.1.5) was performed by adding 1µl of DNA to 25µl of bacterial suspension and incubation for 2min. After heat shock and incubation on ice for 2min, cells were shaken for 10min at 37°C in S.O.C medium and plated on LB-agar plates containing antibiotics as described.

#### 4.1.5 PLASMID PREPARATION FROM E. COLI - MINI-PREP AND MAXI PREP

To analyze transformation of bacteria with the respective DNA vector, single colonies of plated transformed E.coli (section 4.1.4) were inoculated in 5ml LB-medium supplemented with antibiotics (100µg/ml Ampicillin or Kanamycin) and incubated over night at 37°C and 265rpm in a Incubator shaker. Plasmids were purified from 1,5ml of the overnight E.coli culture using JetStar 2.0 Plasmid Purification Kit according to manufacturer's instructions. DNA vectors used for transfection (section 4.5.1) were re-transformed as described in section 4.1.4 and a 5ml starter culture (in LB Medium supplemented with antibiotics) from one colony was incubated for 6h. Afterwards, 500µl of the starter culture was used for

inoculation of a 250ml maxi culture. After overnight incubation at 37°C and 265rpm shaking, plasmids were purified using endotoxin-free plasmid DNA purification kit. DNA concentration and quality was determined using NanoDrop ND-100.

#### 4.1.6 ANALYTICAL DIGEST

After plasmid preparation (section 4.1.5) an analytical digest was performed to search for clones with expected digestion patterns. The following pipeting scheme was used:

Reagent	Volume
DNA Vector	1µl
10x buffer	1µl
Enzyme 1	0,5µl
Enzyme 2	0,5µl
DEPC H <sub>2</sub> O	Ad 10µl

**Table 24. Reaction mix for analytical digest**

#### 4.1.7 ISOLATION OF GENOMIC DNA FROM HUMAN CELLS

Genomic DNA (gDNA) was isolated using QiAamp DNA mini kit with slight modifications. Briefly, cell suspension was centrifuged at 500g for 5min and pellet was resuspended in 100µl ATL buffer prior to adding 20µl of Proteinase K. After incubation at 56°C for at least 5min, cells were incubated with 4µl RNase-A and incubated for 2min at room temperature. After adding 200µl of AL-buffer and incubation at 70°C for 10min, 200µl 100% Ethanol was added, the sample was mixed and loaded onto the DNA isolation column. After discarding the flow through, the column was washed with AW1 and AW2 buffer and DNA was eluted by adding 200µl of DEPC H<sub>2</sub>O for 5min followed by centrifugation at 6000g. Yield and quality of genomic DNA was determined by NanoDrop ND-100 measurement.

#### 4.1.8 DETECTION OF RETROVIRAL PARTICLES - DOWNGRADING TO SAFETY-LEVEL S1

##### 4.1.8.1 Isolation of viral RNA from conditioned medium

For downgrading of transduced cells (section 4.5.2 and section 4.5.3) from safety level S2 to S1, eventually remaining viral RNA was isolated from conditioned medium of transduced cells using QiAmp Viral RNA Mini Kit (Qiagen) following manufacturers recommendations. Viral RNA concentration was determined by NanoDrop ND-100 and stored at -20°C until further use for cDNA synthesis.

#### 4.1.8.2 cDNA synthesis of viral RNA

For synthesis of cDNA by Reverse Transcription PCR (RT-PCR), the AffinityScript Multiple Temperature Reverse Transcriptase was used according to manufacturer's instructions with slight modifications. 1µg was mixed with 2µl of A3-Reverse primer (10pM) (Table 17) and DEPC-H<sub>2</sub>O to a final volume of 12µl. After incubation for 5min at 65°C the sample was cooled to room temperature for 10min. Afterwards 4µl Affinity script buffer and 2µl DTT (0.1M) were added and the mixture was incubated for 2min at 42°C followed by adding 1µl dNTPs (Fermentase 2mmol/l), 0,5µl RNase Block (RNase Out, 40IU/ml) and 1µl AffinityScript Reverse Transcriptase. The mixture was incubated for 1h at 47,5°C followed by incubation for 15min at 70°C in a T-Gradient Thermocycler. The cDNA was stored at 20°C until further use for PCR (section 4.2.1) using the primer pair described in Table 17. Cells were downgraded to S1 if no amplified product is detectable in gel electrophoresis (section 4.1.1) compared to positive control containing cDNA of viral supernatant (section 4.5.1).

## 4.2 POLYMERASE CHAIN REACTION (PCR) METHODS

### 4.2.1 PCR

For amplification of selected genes out of different cell lines or plasmids, PCR reaction was performed using KOD Hot start polymerase kit (Merck).

Reagent	Volume
10x KOD buffer	10µl
dNTP mix (2mM)	10µl
MgSO <sub>4</sub> (25mM)	0,5µl
Primer forward (15mM)	3µl
Primer reverse (15mM)	3µl
DNA/cDNA	2µl
KOD polymerase	2µl
DEPC H <sub>2</sub> O	Ad 100µl

**Table 25. Reaction mix for PCR with KOD polymerase**

The reaction mixture was mixed, separated in 0.5ml reaction tubes and the PCR reaction was performed in a T-Gradient Thermocycler using following conditions:

Temperature	Time	
95°C	2min	
95°C	30sec	
55°C	30sec	30 cycles
72°C	60sec	
72°C	10min	
4°C	∞	

**Table 26. PCR program for KOD polymerase**

#### 4.2.2 QUANTITATIVE PCR (QPCR) OF GENOMIC DNA

qPCR was performed using real-time fluorogenic 5' nuclease PCR. Reactions were performed using Universal PCR Master mix (KAPA™ PROBE FAST Universal) using following pipeting scheme :

Reagent	Volume
KAPA Probe Fast	5µl
Probe (10µM)	0,25µl
Primer forward (10µM)	0,3µl
Primer reverse (10µM)	0,3µl
ROX high (50x)	0,2µl
DNA/cDNA	3,95µl

**Table 27. Reaction mix for qPCR**

Dilutions in the range of  $10^4$  to  $10^{10}$  DNA molecules of TCR with human or murinized constant beta chains in the pMP71 vector were used as a standard curve for number of molecule calculation. Numbers of murinized TCR molecules were normalized to amount of present human TCR molecules. qPCR reaction was performed in duplicates using StepOnePlus (Applied Biosystems) using following conditions:

Temperature	Time	
95°C	2min	
95°C	20sec	
60°C	20sec	40 cycles

**Table 28. PCR program for qPCR**

### 4.3 CELL CULTURE METHODS

All cell culture methods were performed under sterile conditions. Work with human blood samples and retroviruses were performed according to S2 safety guidelines. All cells were routinely tested for mycoplasma-infection.



#### 4.3.1 FREEZING AND THAWING OF CELLS

Prior freezing, cells were centrifuged at 500g for 5min and the pellet was resuspended in 1ml of freezing medium and transferred to a cryovial. To provide successful cell cryo-preservation and recovery, vials were kept in a Freezing container (filled with isopropyl alcohol) over night at -80°C and were transferred into liquid nitrogen for long-term storage. Cells were thawed quickly by warming the vial in a water bath and transfer the cells in 10ml of medium. After centrifugation at 500g for 5min, the supernatant was discarded and pellet was resuspended in the appropriate medium (section 3.1.8) and cultivated in an appropriate cell culture flask or plate.

#### 4.3.2 COUNTING OF CELLS

10µl of well mixed cell suspension was counted using a Neubauer chamber. The cell suspension was diluted in 4% trypane blue solution to exclude dead cells. In case of counting of cells directly isolated from blood, acidic acid (3%v/v) was added to trypane blue solution to lyse erythrocytes. Concentration of cells was determined using following formula:

$$c \left( \frac{\text{cells}}{\text{ml}} \right) = \frac{\text{number of alive cells each chamber square}}{\text{number of chamber squares}} * \text{dilution factor} * 10^4$$

#### 4.3.3 CULTIVATION OF CELL LINES

Cells were cultured in the respective medium, as described in Table 13. Cells in suspension were resuspended and diluted in respective medium every three to four days. To split adherent cells, medium was removed and cells were washed with PBS before adding Trypsin EDTA. Cells were incubated for 3 to 5min at 37°C and medium was added to stop the trypsin reaction. Afterwards, cells were resuspended and centrifuged. The pellet was again resuspended in the appropriate amount of medium and cells were seeded out in new cell culture flask. Semi-adherent T293 cells were loosened without washing the cells or the use of trypsin and split as described for adherent cells.

#### 4.4 PURIFICATION OF PRIMARY CELLS

##### 4.4.1 ISOLATION OF PERIPHERAL BLOOD MONONUCLEAR CELLS (PBMC)

Blood from healthy donors was collected after informed consent following requirements of the local ethical board and principles of the Helsinki Declaration. PBMC were isolated by density-gradient centrifugation. Therefore, blood was diluted 1:1 with RPMI and layered on 15ml Ficoll/Hypaque (Biochrom, Berlin, Germany) in a 50ml tube. Centrifugation was performed for 20min at 880g at room temperature without break. PBMC in the interface were carefully harvested, washed twice with RPMI, counted and used either for direct retroviral transduction (section 4.5.2) or for isolation and transduction of CD8<sup>+</sup> central memory T-cells ( $T_{CM}$ ) (section 4.4.2 and 4.5.2).

##### 4.4.2 PURIFICATION OF CD8<sup>+</sup> CD62L<sup>+</sup> CD45RA<sup>-</sup> $T_{CM}$ CELLS

Isolation of CD8<sup>+</sup>  $T_{CM}$  was performed in a two-step process: First, CD4<sup>+</sup> and CD45RA<sup>+</sup> cells were depleted followed by enrichment of CD62L<sup>+</sup> cells. For the depletion step, freshly isolated PBMC (section 4.4.1) were counted and  $3 \times 10^8$  cells were resuspended in 800 $\mu$ l isolation buffer. Cells were then incubated with 100 $\mu$ l of anti-CD4-FITC and 100 $\mu$ l anti-CD45RA-APC for 15min at 4°C during slow rotation. After incubation, cells were washed with isolation buffer and resuspended in 960 $\mu$ l isolation buffer, 320 $\mu$ l anti-FITC and 640 $\mu$ l anti-APC beads (Miltenyi Biotec). Cells were rotated for 15min at 4°C, washed and resuspended in 1500 $\mu$ l isolation buffer before loading 500 $\mu$ l each on three LD columns (Miltenyi Biotec) according to manufactures instructions. The CD45RA-CD4<sup>-</sup> fraction (flow through) was counted and resuspended in 100 $\mu$ l isolation buffer and 20 $\mu$ l anti-CD62L-PE. Incubation was performed at 4°C for 15min while rotating. Afterwards, cells were washed, resuspended in 160 $\mu$ l isolation buffer and 40 $\mu$ l anti-PE microbeads. After rotation for 15min at 4°C and a washing, the cell pellet was resuspended in 500 $\mu$ l isolation buffer and loaded onto a MS column (Miltenyi Biotec) according to manufacturer's instructions. Positively isolated CD62L<sup>+</sup> cells were eluted, counted and activated (section 4.4.3) for retroviral transduction (section 4.5.2). Phenotype and purity of isolated cells in all steps was analyzed by flow cytometry (section 4.6.1).

#### 4.4.3 ACTIVATION OF PRIMARY CELLS

Isolated PBMC were seeded out in a concentration of  $1 \times 10^6$  cells/ml in T-cell Medium (section 3.1.8) supplemented with 50ng/ml OKT3 and 30 IU/ml hIL-2 (Table 8). Isolated  $T_{CM}$  were activated using CD3/CD28 beads (Table 7) in a bead to cell ratio of 1:1 and 30IU/ml hIL2. Briefly, CD3/CD28 beads were mixed, 25 $\mu$ l per  $1 \times 10^6$  cells were washed with PBS and added to the cell suspension. Cells were seeded out in a concentration of  $1 \times 10^6$ /ml in a 24-well plate. For both activation protocols, cells were incubated for 2 to 3 days at 37°C before retroviral transduction was performed (section 4.5.2).

### 4.5 GENE TRANSFER TECHNIQUES

Gene transfer into primary cells or cell lines was performed using retroviral transduction. The work was performed according to S2 guidelines.

#### 4.5.1 PRODUCTION OF VIRUS PARTICLES

The T293 cell line (Table 19) was used as a producer for retroviral particles. Therefore,  $2 \times 10^5$  cells were seeded in 3ml cDMEM per well of a cell culture treated 6-well plate. On the next day, when cells were adherent, 9 $\mu$ l TransIT-293 Transfection reagent were gently mixed, added to 200 $\mu$ l DMEM and incubated for 20min at room temperature. Afterwards, 1 $\mu$ g DNA of the vector pcDNA3.1-MLV (containing “gag-pol”), pALF10A1-GALV (containing “env”) and pMP71 (containing the gene of interest) was added, mixed by pipetting and incubated for 30min at room temperature. Medium of T293 cells was changed carefully and 200 $\mu$ l of the Transfection mix was added dropwise to the well. After incubation for 48h at 37°C, supernatant was harvested and cells were removed by centrifugation followed by filtering through 0.45 $\mu$ m syringe filter.

#### 4.5.2 TRANSDUCTION OF ACTIVATED PBMC OR $T_{CM}$

Activated PBMC or  $T_{CM}$  (section 4.4.3) were transduced by centrifugation in retronectin-coated 24-well plates. Therefore, 400 $\mu$ l of RetroNectin-solution (12,5mg/ml in PBS) were added per well of a non-tissue culture treated 24 well plate, sealed by parafilm and incubated over night at 4°C. For blocking, RetroNectin was removed and plates were incubated with 500 $\mu$ l 2%BSA in PBS for 30min at 37°C. Wells were washed twice with PBS

2.5% HEPES and stored at 4°C until transduction was performed. Therefore, activated cells were harvested, counted and  $1 \times 10^6$  cells per well were seeded in RetroNectin coated plates in 1ml T-cell medium supplemented with 50IU/ml IL2, 1%HEPES and 4µg/ml protamine sulfate (calculated for  $V_{\text{end}}$  of 2ml). 1ml of cleared virus supernatant (section 4.5.1) was added to the cells and the plate was centrifuged for 90min at 880g and 32°C. Cells were incubated for 24h, washed and a second transduction was conducted. On the third day, cells were harvested, washed and incubated in T-cell medium supplemented with hIL-7 and hIL-15 (5ng/ml each) in T75 cell culture flasks in a concentration of  $1 \times 10^6$  cells/ml. After 3 to 4 days, transduction efficiency was determined by flow cytometry (section 4.6.1). Transduced cells were downgraded to Safety-level S1 prior to use for in vivo experiments by determination of virus-envelope in culture supernatant as described in section 4.1.8.

#### *4.5.3 TRANSDUCTION OF CELL LINES*

Cell lines were transduced in RetroNectin coated 24-well plates. Therefore  $3 \times 10^5$  cells per well were seeded in 1ml of respective medium and 1ml of retroviral supernatant was added. Protamine sulfate (4µg/ml) and 1% HEPES were added and plates were centrifuged for 90min at 880g and 32°C. After incubation for 24h at 37°C, cells were washed and cultured in respective medium in a T25 flask. Transduction efficiency was analyzed after 3 to 4 days by flow cytometry (section 4.6.1).

#### *4.5.4 CLONING OF CELLS BY LIMITING DILUTION*

To generate a stable cell line containing the retrovirally transduced construct, cells were cloned by limiting dilution either directly after transduction (section 4.5.3) or after cell sorting (section 4.6.4). Therefore, cells were counted, and 0.5 to 0.8 cells in 200µl of respective medium per well were seeded in a 96well U-bottom plate. After 7 to 14 days cells were harvested, expanded and tested for the respective transgene by flow cytometry (section 4.6.1). Stable transgene expression of the generated cell line was controlled monthly by flow cytometry (section 4.6.1).

## 4.6 FLOW CYTOMETRY AND FLOW CYTOMETRY BASED ASSAYS

For flow cytometry, cells were pelleted by centrifugation for 5min at 500g and 4°C. Flow cytometric analysis was performed using LSRII (BD Bioscience) or Cytomics FC500 (Beckman Coulter). Sorting of cells was performed either on FACS Aria (BD bioscience) or MoFlo high performance cell sorter (Dako).

### 4.6.1 STAINING OF SURFACE MOLECULES

$1 \times 10^5$  to  $1 \times 10^6$  cells were pelleted by centrifugation and washed once with FACS buffer (Table 12). Fc-Receptors were blocked by incubation with 50 $\mu$ l  $\Delta$ HS (Table 12) for 10min at 4°C. After washing with FACS buffer, cells were incubated with 1.5 $\mu$ l of each antibody (Table 9) and incubated for 20min at 4°C in the dark. For exclusion of dead cells, 0.5 $\mu$ l of 7AAD solution (0,5mg/ml in PBS) (Table 9) was added parallel to the antibodies. After incubation, cells were washed and fixed in 150-200 $\mu$ l 1%PFA.

### 4.6.2 HLA-MULTIMER STAINING OF T CELLS

For confirmation of the presence of the peptide-specific TCR on the surface, cells were stained with respective HLA-multimer (Table 11). Therefore,  $5 \times 10^5$  to  $1 \times 10^6$  cells were pelleted, washed and blocked with  $\Delta$ HS as described (section 4.6.1). 1.5 $\mu$ l of the HLA-multimer was diluted in 50 $\mu$ l FACS buffer and centrifuged for 5min at 5000g and 4°C. The supernatant was carefully removed and added to the washed cells for 20min at 4°C in the dark. Subsequently, staining of surface molecules and dead cells was performed as described in section 4.6.1.

### 4.6.3 FC-RECEPTOR BLOCKING EXPERIMENTS

For determination of unspecific binding of the aTCRmu antibody (section 5.4.4) ML2 or ML2-B7 cells were washed with PBS and incubated with different blocking reagents: 100 $\mu$ l  $\Delta$ HS, 5 $\mu$ l human FcR-block (eBioscience), 5 $\mu$ l aTCRmu or 5 $\mu$ l isotype control (Table 9) or PBS for 20min at 4°C. After washing with PBS, cells were incubated with 1,5 $\mu$ l fluorophore-labeled aTCRmu and 0,5 $\mu$ l 7-AAD for 20min at 4°C in the dark. Afterwards, cells were washed, fixed with 150 $\mu$ l 1%PFA and analyzed by flow cytometry. The mean fluorescence intensity (MFI) of

fluorophore- $\alpha$ TCR $\mu$  staining was compared to different blocking reagents by normalization to PBS incubation.

#### 4.6.4 FACS SORTING OF CELLS

Cell lines transduced with HLA-molecules linked to eGFP were enriched after transduction by FACS sorting. Therefore, cells were washed and resuspended in 1ml FACS buffer for sorting. Sorting of cells was conducted on the MoFloII or FACS Aria. GFP positive cells were collected in FCS and used for cloning by limiting dilution (section 4.5.4).

### 4.7 FUNCTIONAL ANALYSIS OF T CELLS

#### 4.7.1 24H CO-INCUBATION ASSAY

TCR transgenic PBMC or T<sub>CM</sub> were co-cultivated in triplicates with tumor cells in 96-U-bottom well plates using an effector to target ratio of 1:1 in 200 $\mu$ l T-cell medium, unless otherwise indicated. After 20h to 24h of incubation at 37°C, the supernatants were removed, stored at -20°C and used for IFN $\gamma$  ELISA assay (section 4.7.2).

#### 4.7.2 ENZYME LINKED IMMUNOSORBENT ASSAY (ELISA)

The amount of secreted IFN $\gamma$  by T cells after co-incubation with tumor cells (section 4.7.1) was determined by human IFN $\gamma$  ELISA Set using a slightly modified protocol. Nunc MaxiSorp ELISA plates were coated with ELISA coating buffer (Table 12), and anti-IFN $\gamma$  capture antibody, sealed and incubated over night at 4°C. Afterwards, plates were washed 3 times and unspecific binding sites were blocked by ELISA blocking buffer (Table 12) for 1h at room temperature. After 3 washing steps, 50 $\mu$ l of serial 1:2 dilutions of IFN $\gamma$  standard (1000pg/ml to 31,25ng/ml) were added in duplicates to each plate. 50 $\mu$ l of samples were added in triplicates and incubated for 1-2h at room temperature. After 5 washing steps, detection solution consisting of 1% milkpowder in PBS with biotinylated detection antibody (1:250) and Streptavidin-horseradish peroxidase (HRP) conjugate (1:250) was added and incubated for 1h at room temperature. Plates were washed 7 times before 100 $\mu$ l/well of substrate solution (TMB substrate Reagent Set, BD) was added. Reaction was incubated in the dark for 10-15min and stopped when standard was visible from strong to light blue by adding 50 $\mu$ l of

H<sub>2</sub>SO<sub>4</sub> (1M). Absorbance was measured at 450nm with 570nm as reference wavelength using an ELISA reader (Sunrise photometer – Tecan).

#### 4.7.3 FLOW CYTOMETRY BASED CYTOTOXICITY ASSAY

Cytotoxic activity of TCR-transduced effector cells was analyzed by flow cytometry after co-incubation with GFP positive tumor cells after 24h (section 4.7.1). Supernatant from triplicates was removed, cells were pooled, washed with FACS buffer and incubated with 50µl FACS buffer containing 0,5µl 7-AAD (final concentration 5ng/µl). After incubation for 20min at 4°C in the dark, cells were washed with FACS buffer, fixed with 1%PFA and analyzed by flow cytometry. The percentage of lysis was calculated by analysis of the percentage of eGFP positive, 7-AAD negative tumor cells.

### 4.8 PURIFICATION, CONJUGATION AND LABELING OF *ATCRMU*-IGG AND *ATCRMU*-F(AB')<sub>2</sub>

Antibody isolation and F(ab')<sub>2</sub> fragmentation was performed by Nahid Yusufi and Dr. Calogero D'Alessandria, Nuklearmedizinische Klinik u Poliklinik, Munich. Purification of aTCRmu-IgG was performed with support of Dr. Elisabeth Kremmer, Helmholtz Center Munich.

#### 4.8.1 *ATCRMU*-IGG PURIFICATION AND F(AB')<sub>2</sub> FRAGMENTATION

The murine B cell hybridoma cell line H57-597 (ATCC HB-218), producing the Armenian Hamster anti-murine TCR β chain antibody (aTCRmu-IgG), was cultured in RPMI with bovine IgG free serum at 37 °C in a humidified atmosphere of 5% CO<sub>2</sub>. The aTCRmu-IgG was affinity purified using Protein A Sepharose and was dialyzed overnight against PBS. F(ab')<sub>2</sub> fragments were generated by Pepsin digestion followed by Protein-A purification using F(ab')<sub>2</sub> Preparation Kit following manufacturer's instructions. Digestion to F(ab')<sub>2</sub> was confirmed by SDS-PAGE under reducing and non-reducing conditions followed by Coomassie staining. The aTCRmu-IgG and aTCRmu-F(ab')<sub>2</sub> were stored in PBS 0.05% sodium azide at 4°C and were stable over several months. The concentration of aTCRmu-IgG and aTCRmu-F(ab')<sub>2</sub> was determined by a nanophotometer according to the manufacturer's instructions for subsequent chelator conjugation and radiolabeling (section 4.8.2).

#### 4.8.2 DFO CONJUGATION AND $^{89}\text{Zr}$ LABELING OF ATCRMU-IGG AND ATCRMU-F(AB')<sub>2</sub>

For conjugation of aTCRmu-IgG and aTCRmu-F(ab')<sub>2</sub> the p-isothiocyanatobenzyl derivate of desferrioxamine (DFO-Bz-NCS) was used as a bifunctional chelator for Zirconium-89 ( $^{89}\text{Zr}$ ) ( $^{89}\text{Zr}$ -aTCRmu-IgG or  $^{89}\text{Zr}$ -aTCRmu-F(ab')<sub>2</sub>). Therefore, at least 2mg of the protein stock solution was dialyzed against 0.1M sodium bicarbonate (pH 9) using Amicon Ultra-15 Centrifugal Filter Units and DFO-Bz-NCS was dissolved in DMSO at a concentration of 5mM. The chelator was added successively in a 3-fold molar excess over the molar amount of the protein in a total volume of 500µl. After incubation for 30min at 37°C on a thermomixer, the immuno-conjugate was purified and eluted by size exclusion chromatography (Sephadex G-25 M, PD10 column) in 2.5mM sodium acetate (pH 4.9-5.5). The conjugation yield was determined by a nanophotometer. The labeling of aTCRmu-IgG-DFO and aTCRmu-F(ab')<sub>2</sub>-DFO with was performed based on the labeling protocol of (Perk, Vosjan et al. 2010) with slight modifications. Briefly, 37MBq  $^{89}\text{Zr}$  in 1M oxalic acid was adjusted with 2M sodium carbonate and 0.5M HEPES (pH 7) after addition of 100µg DFO-IgG or DFO-F(ab')<sub>2</sub> in sodium acetate in a total volume of 1mL. After incubation at 37°C for 30min the  $^{89}\text{Zr}$ -DFO-immunocomplex was purified by size exclusion chromatography (Sephadex G-25 M, PD10 column) in 25mM sodium acetate/5mg/ml gentisic acid (pH 5.5). Radiochemical purity was assessed by radio-ITLC using 20mM citric acid (pH 5) and by SE-HPLC (BioSep™ SEC-s3000 LC Column, Phenomenex) using 0.1M Phosphate buffer (pH 6.8) as mobile phase.

#### 4.8.3 DETERMINATION OF SPECIFIC BINDING OF $^{89}\text{Zr}$ -ATCRMU-IGG OR $^{89}\text{Zr}$ -ATCRMU-F(AB')<sub>2</sub> TO 2.5D6 TRANSDUCED T-CELLS (CELL TEST).

Determination of specific binding of  $^{89}\text{Zr}$ -aTCRmu-IgG or  $^{89}\text{Zr}$ -aTCRmu-F(ab')<sub>2</sub> to TCR2.5D6 transduced T-cells was performed in cooperation with Nahid Yusufi, department of nuclear medicine, Klinikum rechts der Isar.

$0.6 \times 10^6$  TCR-transduced and non-transduced effector T-cells were resuspended in 60µl binding medium (Table 13) and incubated with 40µl of different concentrations of  $^{89}\text{Zr}$ -aTCRmu-IgG or  $^{89}\text{Zr}$ -aTCRmu-F(ab')<sub>2</sub> to following final concentrations in a total volume of 200 µl:



Concentration $^{89}\text{Zr-aTCRmu-IgG/F(ab')}_2$	
$1.0 \times 10^{-08}$	M
$5.0 \times 10^{-09}$	M
$1.0 \times 10^{-09}$	M
$5.0 \times 10^{-10}$	M
$1.0 \times 10^{-10}$	M
$5.0 \times 10^{-11}$	M
$1.0 \times 10^{-11}$	M

**Table 29. Concentrations of  $^{89}\text{Zr}$ -labeled aTCRmu for determination of specific binding**

To determine unspecific binding, unlabeled aTCRmu-IgG/F(ab')<sub>2</sub> in a final concentration of  $1.0 \times 10^{-08}$  M was added for competitive binding.

Cells were incubated on ice for 2h and washed twice by adding cold binding medium and centrifugation. Bound activity on cell pellets as well as activity in collected supernatants was measured as counts per minute (CPM) in a gamma counter. Specific binding was calculated by subtraction of unspecific binding (bound activity of cells incubated with  $^{89}\text{Zr-aTCRmu-IgG/F(ab')}_2$  and unlabeled aTCRmu-IgG/F(ab')<sub>2</sub>) from total binding (bound activity on cells incubated with  $^{89}\text{Zr-aTCRmu-IgG/F(ab')}_2$  only). The dissociation constant  $K_d$  was obtained by plotting the specific binding versus the different concentrations of aTCRmu-IgG/F(ab')<sub>2</sub> and nonlinear regression analysis.

## 4.9 ANIMAL MODELS

Mice were maintained in our animal facility according to the institutional guidelines and approval by local authorities. At the age of 8-12 weeks they were used for experiments.

### 4.9.1 EL4 TUMOR MODEL

The murine T-lymphoma cell line EL4 or ML2-WT tumor cells were counted, resuspended in PBS at a concentration of  $7.5 \times 10^7$  cells/ml and 200µl were subcutaneously (s.c.) injected into BRG mice (Table 20). EL4 cells were injected into the right flank of the mouse, ML2-WT cells were injected into the left flank of the mouse. After 5 days, mice were used for PET/CT imaging as described in section 4.10.

#### 4.9.2 ML2 TUMOR MODEL

ML2-B7GFP or ML2-WT tumor cells were counted, resuspended in PBS at a concentration of  $5 \times 10^7$  cells/ml and 200  $\mu$ l were subcutaneously (s.c.) injected. ML2-B7 cells were injected into the right flank of the mouse, ML2-WT cells were injected into the left flank of the mouse. Tumor growing kinetic was assessed by caliper measurement and showed either as tumor size calculated by length x width of the tumor or as tumor volume calculated by following formula:

$$Tumor\ Volume\ [cm^3] = \frac{\pi}{6} * length * width^2$$

#### 4.9.3 ADOPTIVE T-CELL TRANSFER

T-cell transfer was either performed intratumorally (i.t.) or intravenously (i.v.). Intratumoral injection was performed using  $1 \times 10^7$  cells resuspended in 20  $\mu$ l PBS. For i.v. injection,  $1.5 \times 10^7$  cells in 200  $\mu$ l PBS were used for injection into the tail vein of tumor bearing mice. One week before adoptive transfer of  $T_{CM}$ , mice were injected 3 times weekly with irradiated (80Gy) hIL-15 producing NSO cells intraperitoneally (Wang, Berger et al. 2011).

#### 4.9.4 TOTAL BODY IRRADIATION (TBI) OF MICE

For enhancement of engraftment of  $T_{CM}$  in mice, low dose irradiation was performed using a Gulmay Irradiation Cabinet. Mice were placed in a specific cage allowing equal irradiation for every mouse by holding them in one layer. Irradiation was performed with 1Gy (indicated in figures and figure legends) with following standardized settings: 200kV, 15mA, Filter 5, Table Position 500.

### 4.10 PET/CT IMAGING

PET/CT imaging of mice was performed in cooperation with the preclinical imaging team (Dr.Sibylle Ziegler, Dr.Iina Laitinen, Sybille Reeder, Markus Mittelhäuser, Marco Lehmann) of the department of nuclear medicine, Klinikum rechts der Isar in Munich.

Mice were anesthetized using 1.5% isoflurane and imaged with the Inveon small animal PET/CT scanner after indicated time points post injection of the  $^{89}Zr$ -TCRmu-IgG or  $^{89}Zr$ -TCRmu-F(ab')<sub>2</sub> (0,7-1,5MBq corresponding to 10-20  $\mu$ g). For determination of metabolic

activity of tumors, PET/CT imaging was performed 15min after intravenous injection of [18-Fluor]2-Fluor-2-desoxy-D-glucose ( $^{18}\text{F}$ -FDG) (15MBq), which was freshly prepared in the department of nuclear medicine. After CT acquisition, static PET emission images were acquired for 30min (for  $^{89}\text{Zr}$ -aTCRmu-IgG/F(ab')<sub>2</sub>) or 20min (for  $^{18}\text{F}$ -FDG) in the same bed position. CT acquisition consisted of 120 projections acquired with exposure time of 200ms, x-ray voltage of 80kVp and anode current of 500 $\mu\text{A}$  for 220° rotation. PET images were reconstructed using OSEM-3D algorithm with reconstructed pixel size of 0.77mm. CT images were reconstructed using a modified Feldcamp algorithm (reconstructed pixel size 0.21 x 0.21 x 0.21mm). The PET and CT images were fused and analyzed using the Inveon Research Workplace. The data was normalized for decay and the tracer uptake was calculated as percentage of injected dose per gram of tissue (%ID/g, 1cc=1g) and shown in 3D maximal intensity projection (MIP) and axial PET/CT projection. For quantification of signals, a region of interest (ROI), based on the CT image, was drawn for tumors and mean values of 50%-100% of maximal uptake (%ID/g) were depicted. For quantification of total % injected dose (%ID) a ROI, based on CT image was drawn and mean values of uptake were normalized by multiplication to the volume of the drawn region.

#### 4.11 EX VIVO ANALYSIS

##### 4.11.1 BIODISTRIBUTION ANALYSIS

48 hours after  $^{89}\text{Zr}$ -aTCRmu-IgG/F(ab')<sub>2</sub> administration, the animals were sacrificed and the blood and organs were removed and weighted. Radioactivity of organs and standard (1% of injected activity in 5 replications) were counted with a gamma counter (Table 4). Uptake was expressed as the percentage of injected dose per gram (%ID/g) and calculated as the ratio to blood for comparison of the accumulation of  $^{89}\text{Zr}$ -TCRmu-IgG/ F(ab')<sub>2</sub> between the different experimental groups.

##### 4.11.2 AUTORADIOGRAPHY

To determine the tissue distribution of  $^{89}\text{Zr}$ -TCRmu-IgG/F(ab')<sub>2</sub> after PET/CT, 20 $\mu\text{m}$  sections of frozen organs were prepared in a cyrotome and slides were put on a phosphor imaging plate for 48hrs. Signal on the imaging plate was analyzed on a phosphorImager using AIDA Image analyzer software. Signal-intensity scaling was kept constant for all different organs.

#### *4.11.3 PREPARATION OF SINGLE CELL SUSPENSION OF ORGANS*

For ex vivo flow cytometric analysis, tumor and organs were singularized using 40 $\mu$ m cell strainer. After washing with FACS buffer, erythrocytes were lysed using ACK lysis buffer for 5min at room temperature and used for flow cytometric analysis (section 4.6.1) or qPCR analysis (section 4.2.2).

#### *4.11.4 HISTOLOGY AND IMMUNOHISTOCHEMISTRY*

Immunohistochemical stainings were performed in cooperation with Dr. Michaela Aichler, Helmholtz Center Munich as well as Dr. Katja Steiger and Dr. Melanie Straub, Institute of Pathology, Klinikum rechts der Isar. For co-localization of tissue slices with PET pictures, tumors were flagged by tissue ink for ventral and dorsal orientation during necropsy of mice. Thereafter they were excised, cut in axial plane, fixed in 10% formalin and embedded in paraffin with downward orientation of the axial cutting site. 2 $\mu$ m sections were cut and stained with haematoxylin & eosin (H/E.). Consecutive slides were used to detect T cells within tumor tissue. After heat-induced antigen retrieval (10mM citrate buffer, pH6) and protein and peroxidase blocking (3% hydrogen peroxide and 3% normal goat serum), immunohistochemistry was performed with a Dako autostainer (DAKO) using an anti CD3-antibody (Table 10). Antibody detection was performed using the Dako Envision-HRP rabbit labeled polymer visualized by diaminobenzidine (DAB). Anti-CD5 staining and anti-CD3 staining used for co-registration analysis shown in Figure 23 (Table 10) was performed on an automated immunostainer with an iVIEW DAB detection kit according to the company's protocols. Counterstaining was performed with haematoxylin. Slides were evaluated with an Olympus BX53 microscope by semiquantitative evaluation of T-cell infiltration in predefined regions depicted by colored codes as indicated. Co-localization of imaging and histological slices was performed by calculating the sum of total sections including a variation factor of tissue modification due to the technical procedure.

#### 4.12 STATISTICS

Data are presented as mean  $\pm$  standard deviations (s.d.). Statistical analysis of results was performed using GraphPad Prism software version 5.01 using a two tailed non-parametric test (Mann-Whitney test) as indicated in Figure legends.

## 5 RESULTS

### 5.1 PRINCIPLE OF THE APPLIED T-CELL TRACKING METHOD

Murinization of TCR domains has been proposed for general transgene optimization in order to reduce the risk for mispairing of introduced and endogenous TCR (Cohen, Zhao et al. 2006). The hamster anti-murine TCR antibody (clone H57-597) (aTCRmu) specifically recognizes murine TCR and engineered TCR constructs harboring a murine constant beta domain (Kubo, Born et al. 1989; Kuball, Hauptrock et al. 2009). In this study we evaluated this antibody for potential clinical application to track specifically human T cells engineered with a cancer specific TCR. Figure 1 shows the principle of the tracking method using the aTCRmu as a specific tracer for human TCR-transgenic T cells.

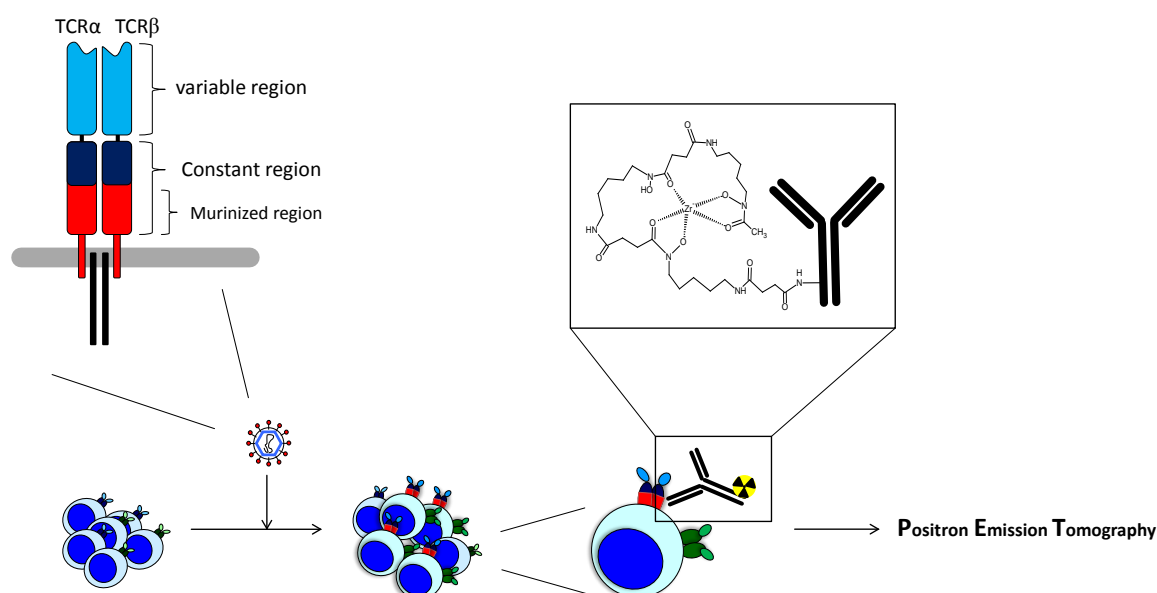


**Figure 1. Principle of T-cell tracking presented in this work.**

The anti-TCRmu antibody binds specifically to the murine beta domain introduced into the human-murine hybrid TCR as a general optimization strategy for expression enhancement. The TCR was introduced into human T cells by retroviral transduction. The antibody was conjugated to a bifunctional chelator for labeling with  $^{89}\text{Zr}$  and used as a tracer to monitor tumor-specific T cells in vivo by positron emission tomography (PET) imaging.

## 5.2 CHARACTERIZATION OF TCR2.5D6 TRANSDUCED T<sub>CM</sub>

### 5.2.1 CHARACTERIZATION OF TCR2.5D6 TRANSDUCED T<sub>CM</sub> IN VITRO

For development of a clinically implementable imaging strategy for TCR-transduced T cells, we used the TCR2.5D6, characterized extensively by Richard Klar et. al. (Klar, Schober et al. 2014). This TCR recognizes specifically a peptide (MPO<sub>5</sub>) derived from the hematopoietic differentiation antigen myeloperoxidase (MPO) in the context of HLA-B\*07:02 (HLA-B7). We isolated CD8<sup>+</sup> T<sub>CM</sub> from blood of healthy donors (Figure 2A) and retrovirally transduced the TCR2.5D6 into these cells. Expression of the exogenous TCR was analyzed by flow cytometry using the aTCRmu antibody (Figure 2B). Specific multimer staining confirmed the presence of the TCR on the surface of T<sub>CM</sub> (Figure 2C).

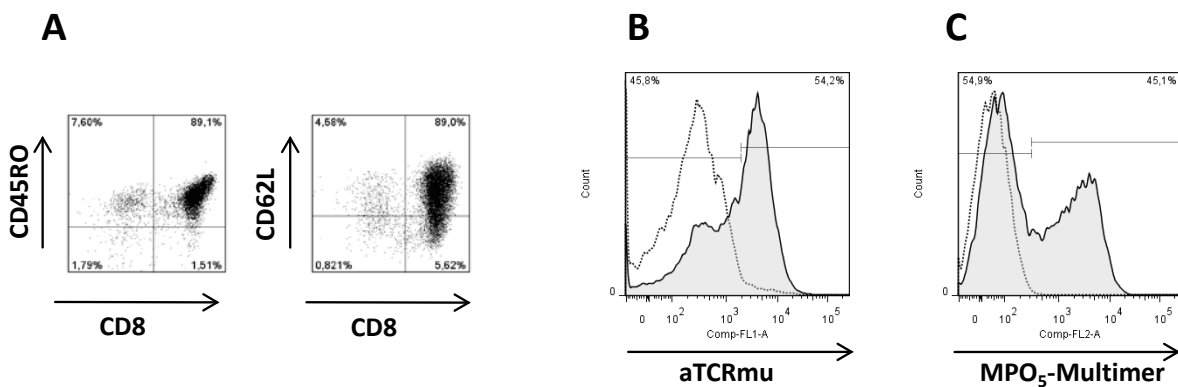


**Figure 2. Characterization of TCR2.5D6 transduced CD8<sup>+</sup> T<sub>CM</sub> cells.**

(A) Characterization of CD8<sup>+</sup>T<sub>CM</sub> cells isolated from blood of healthy donors by depletion of CD45RA<sup>+</sup> and CD4<sup>+</sup> cells and selection for CD62L<sup>+</sup> cells by magnetic bead technology. (B-C) Representative flow cytometric evaluation of TCR2.5D6 expression for transduced T<sub>CM</sub> (grey histogram) and non-transduced T<sub>CM</sub> (white histogram) analyzed by aTCRmu staining (B) and MPO<sub>5</sub>-multimer staining (C).

The acute myeloid leukemia (AML) cell line ML2 (ML2-WT) expressed endogenously MPO (Klar, Schober et al. 2014), but not HLA-B7 (Figure 3A). The cells were retrovirally transduced with the HLA-B7 linked to GFP and a stable cell line was generated by limiting dilution after GFP-based sorting (Figure 3B).

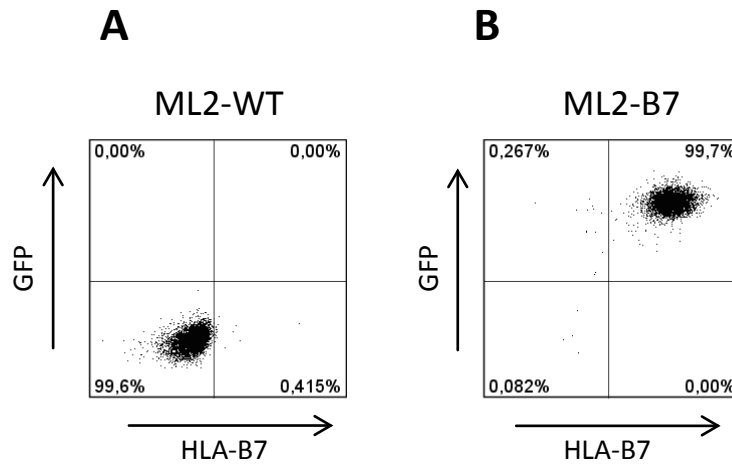


**Figure 3. Generation of a stable HLA-B7 expressing ML2 cell line.**

Expression of HLA-B7 and GFP of (A) ML2-WT cells and (B) after generation of a stable ML-2 cell line expressing HLA-B7 linked to GFP (ML2-B7). Representative dot-plots of ML2-WT and ML2-B7 cells analyzed by flow cytometry are shown.

We observed a high cytotoxic activity (Figure 4A) and IFN $\gamma$  production (Figure 4B) of TCR2.5D6-transduced T<sub>CM</sub> in 24h co-cultivation assays with ML2-B7 but not ML2-WT cells demonstrating specific MHC-dependent target cell recognition. Taken together, T<sub>CM</sub> isolated from blood of healthy donors and transduced with the MPO-specific TCR2.5D6 show strong anti-tumor activity against ML2-B7 in vitro. Therefore, this TCR was used as a model-TCR for the development of an in vivo imaging model to track specifically TCR-transgenic T cells by PET/CT imaging.

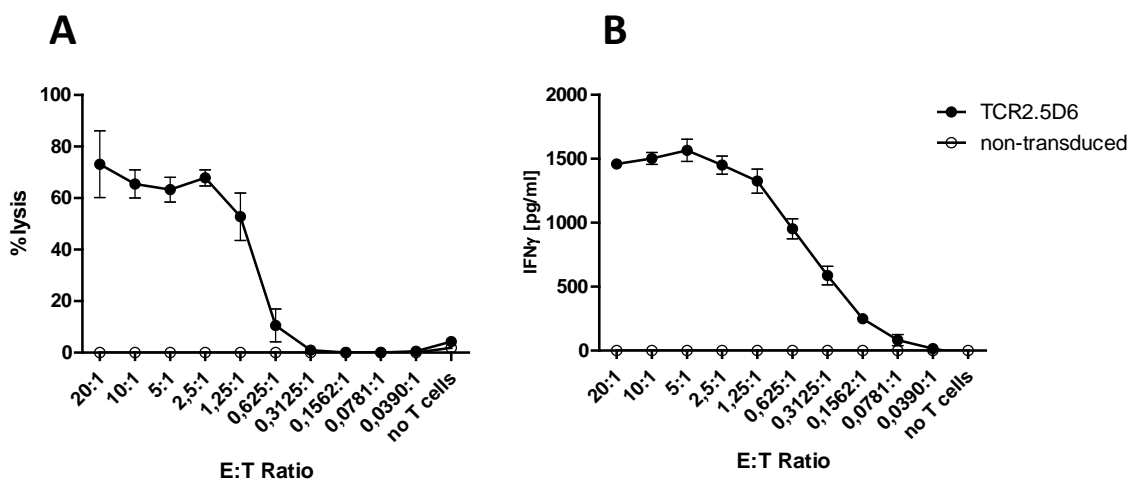


**Figure 4. Functionality of TCR2.5D6-transduced T<sub>CM</sub>.**

(A) Cytotoxic activity and (B) IFN $\gamma$  production of TCR2.5D6 transduced and non-transduced T<sub>CM</sub> cells in a 24h co-cultivation assay with ML2-B7 tumor cells.



### 5.3 CHARACTERIZATION OF THE ANTI-TCR $\mu$ -ANTIBODY AS TRACER FOR TCR-TRANSDUCE T-CELLS

#### 5.3.1 FUNCTIONALITY OF $T_{CM}$ AFTER LABELING WITH $^{89}\text{Zr}$ -ATCRMU-IGG OR $^{89}\text{Zr}$ -ATCRMU-F(AB')<sub>2</sub>

For the specific tracking of TCR2.5D6-transduced  $T_{CM}$ , we used the anti-TCR $\mu$ -antibody (aTCR $\mu$ -IgG) and its F(ab')<sub>2</sub> fragment (aTCR $\mu$ -F(ab')<sub>2</sub>), which bind specifically to the murinized constant beta domain of the introduced TCR. Therefore, we conjugated the aTCR $\mu$ -IgG and F(ab')<sub>2</sub> with a bispecific chelator (DFO) followed by labeling with  $^{89}\text{Zr}$ -Zirconium ( $^{89}\text{Zr}$ -aTCR $\mu$ -IgG and  $^{89}\text{Zr}$ -aTCR $\mu$ -F(ab')<sub>2</sub>) (the principle of the method is depicted in Figure 1). These molecules were used to mark specifically TCR2.5D6-transduced  $T_{CM}$  in vitro. Detailed characterization of  $^{89}\text{Zr}$ -aTCR $\mu$ -IgG and  $^{89}\text{Zr}$ -aTCR $\mu$ -F(ab')<sub>2</sub> regarding specific binding, stability after labeling and immunoreactivity was performed by Nahid Yusufi (data not shown).

Two potential mechanisms might be involved in the functional modification of T cells after labeling by  $^{89}\text{Zr}$ -aTCR $\mu$ -IgG and  $^{89}\text{Zr}$ -aTCR $\mu$ -F(ab')<sub>2</sub>. First, direct binding of the antibody to the TCR might induce differential cellular mechanisms as shown for other antibodies targeting T-cell marker such as CD3 or CD2 (Bromberg, Chavin et al. 1991; Guckel, Berek et al. 1991; Bemelmans, Abramowicz et al. 1994; Przepiorka, Phillips et al. 1998; Carpenter, Pavlovic et al. 2000; Chatenoud 2003; Li, Wang et al. 2005; Abraham, Karni et al. 2008; Shiheido, Chen et al. 2014). Ricarda Wagner characterized intensively the specific influence of aTCR $\mu$ -IgG and aTCR $\mu$ -F(ab')<sub>2</sub> binding on human  $T_{CM}$  in vitro and in vivo (data not shown). Another influence on functionality might derive from radiation damage through  $^{89}\text{Zr}$  which is bound to the aTCR $\mu$  antibody. To determine a potential functional impairment by exposure to  $^{89}\text{Zr}$  during labeling of  $T_{CM}$ , cells were labeled in vitro with different concentrations of  $^{89}\text{Zr}$ -aTCR $\mu$ -IgG/F(ab')<sub>2</sub> for 2h followed by removal of unbound  $^{89}\text{Zr}$ -aTCR $\mu$ -IgG/F(ab')<sub>2</sub>.  $^{89}\text{Zr}$ -aTCR $\mu$ -IgG/F(ab')<sub>2</sub> labeled  $T_{CM}$  were co-cultured for 24h with ML2-B7 or ML2-WT tumor cells transduced with an irrelevant HLA-molecule (ML2-B15). The amount of IFN $\gamma$  secretion of  $^{89}\text{Zr}$ -aTCR $\mu$ -IgG labeled TCR-transduced  $T_{CM}$  in response to target cells was not different when compared to TCR-transduced  $T_{CM}$  incubated with different concentrations of non-radioactively labeled aTCR $\mu$ -IgG or to non-labeled  $T_{CM}$  (Figure 5A). Similar results were obtained using  $^{89}\text{Zr}$ -aTCR $\mu$ -F(ab')<sub>2</sub> or non-radioactive aTCR $\mu$ -F(ab')<sub>2</sub> labeled  $T_{CM}$  (Figure 5B). To test influence of  $^{89}\text{Zr}$ -aTCR $\mu$ -IgG or  $^{89}\text{Zr}$ -

aTCRmu-F(ab')<sub>2</sub> labeling after a longer period, we analyzed IFN $\gamma$  secretion after co-cultivation with ML2-B7 or ML2-B15 cells 48h after labeling. We did not detect any difference in IFN $\gamma$  production between <sup>89</sup>Zr-aTCRmu-IgG/F(ab')<sub>2</sub>-labeled, non-radioactively aTCRmu-IgG/F(ab')<sub>2</sub> or non-labeled cells (Figure 5C-D). These data indicate no impairment of functionality, when cells are exposed to <sup>89</sup>Zr by labeling in vitro with <sup>89</sup>Zr-aTCRmu-IgG and <sup>89</sup>Zr-aTCRmu-F(ab')<sub>2</sub>. Furthermore, no unspecific IFN $\gamma$ -production upon co-cultivation with ML2-B15 cells was detected indicating no unspecific activation by <sup>89</sup>Zr-aTCRmu-IgG and <sup>89</sup>Zr-aTCRmu-F(ab')<sub>2</sub>. In conclusion, labeling of TCR-transgenic T<sub>CM</sub> with radioactive <sup>89</sup>Zr-aTCRmu-IgG or F(ab')<sub>2</sub> in vitro has no impact on T-cell function in response to specific target cells in this specific setting.

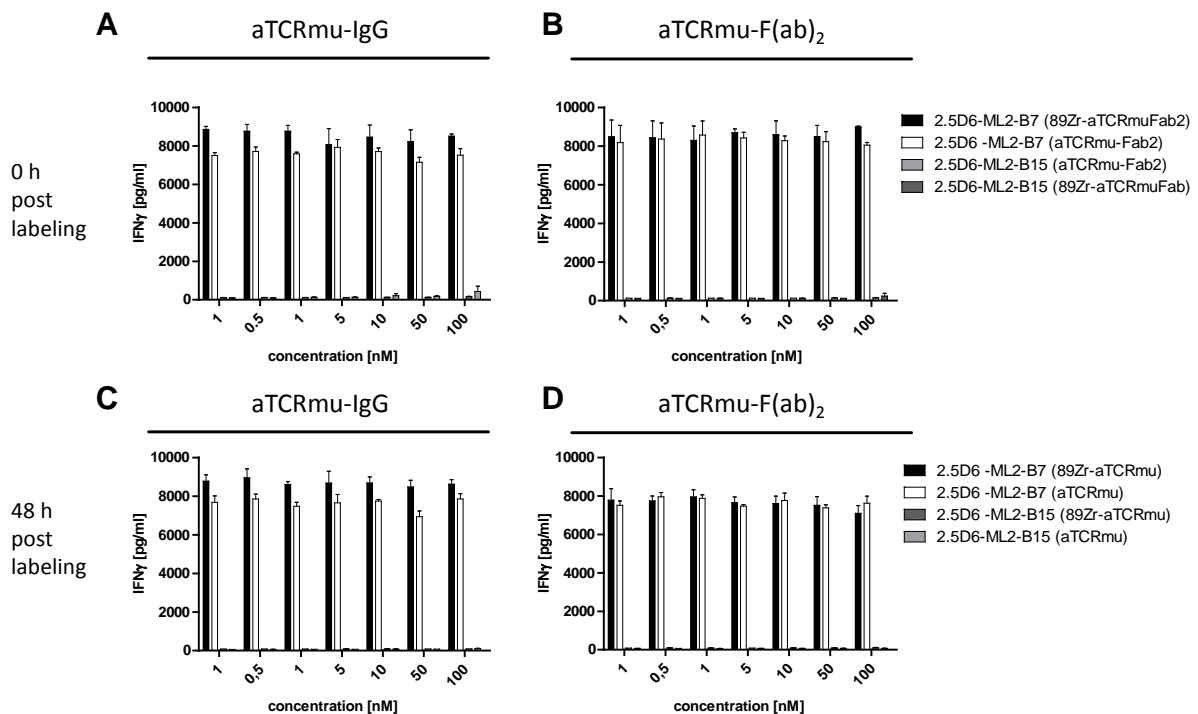


**Figure 5. Functionality of T<sub>CM</sub> after in vitro labeling with <sup>89</sup>Zr-aTCRmu-IgG or <sup>89</sup>Zr-aTCRmu-F(ab')<sub>2</sub>.**

(A-D) IFN $\gamma$  secretion of TCR2.5D6-transduced or non-transduced T<sub>CM</sub> in response to ML2-B7 or ML2-B15 tumor cells after 24h-co-cultivation is shown. Cells were co-cultured directly after labeling (0h) with indicated concentrations of (A) <sup>89</sup>Zr-aTCRmu-IgG and non-radioactive aTCRmu-IgG or (B) <sup>89</sup>Zr-aTCRmu-F(ab')<sub>2</sub> and non-radioactive aTCRmu-F(ab')<sub>2</sub>. To test functionality at a later time point, cells were co-cultured 48h after labeling with indicated concentrations of (C) <sup>89</sup>Zr-aTCRmu-IgG and non-radioactive aTCRmu-IgG or (D) <sup>89</sup>Zr-aTCRmu-F(ab')<sub>2</sub> and non-radioactive aTCRmu-F(ab')<sub>2</sub>. (A-D) Labeled 2.5D6TCR-transduced T-cells incubated with ML2-WT cells transduced with an irrelevant HLA-molecule (ML2-B15) served as control for induction of unspecific activation. Mean  $\pm$  s.d. of triplicates is depicted. The labeling of the cells was performed by Nahid Yusufi, department of nuclear medicine, Klinikum rechts der Isar.

## 5.4 IN VIVO PET/CT IMAGING

### 5.4.1 DEVELOPMENT OF AN EXPERIMENTAL WORKFLOW FOR CONFIRMATION OF IMAGING DATA

Based on the promising in vitro data, we aimed to establish an in vivo model to track specifically TCR-transgenic T cells migrating to the tumor. In order to validate and correctly interpret the imaging data generated by PET/CT, we developed a comprehensive set of ex vivo analyses to confirm on the one hand the specific radioactive signal and tracer accumulation and on the other hand the presence of T cells within the tumor or other organs on genomic as well as on protein level. Overview of experimental techniques used is depicted in Table 30.

AIM	Name	Method	Result /Outcome	
Confirmation of Tracer uptake	<b>Biodistribution</b>	Weight organs – measurement in g-counter	Percentage of injected dose per gram (%ID/g)	Organ/blood ratio
	<b>Autoradiography</b>	Determination of radioactivity on tissue sections	Spatial distribution of activity on tissue section	
Confirmation of presence of T cells	<b>Flow cytometry</b>	Analysis of single cell suspension prepared after biodistribution	% of total T cells and transduced T cells in organs	
	<b>Immunohistochemistry</b>	Staining for CD3 or CD5 positive cells	T cell distribution within tissue	
	<b>qPCR</b>	Determination of TCRmu in genomic DNA	Copies of murinized TCR within different tissues	

**Table 30. Experimental setup of ex vivo analysis for confirmation of imaging data.**

Directly after the last imaging time point, mice were sacrificed and organs were taken to confirm PET/CT imaging data by determination of tracer uptake using biodistribution and autoradiographic methods. Presence of T cells within the organs was determined by flow cytometry, immunohistochemistry and qPCR as indicated.

### 5.4.2 DEVELOPMENT OF A POSITIVE CONTROL MODEL FOR IN VIVO IMAGING USING EL4 CELLS

For validation of the experimental workflow, imaging settings and specificity of tracer, we developed a simple in vivo tumor model potentially to be used as a positive control model. The T-lymphoma cell line EL4 expresses constitutively murine TCR (Figure 6A) and we injected these cells subcutaneously into the right flank of BRG-mice. As a negative control, we injected the AML cell line ML2-WT subcutaneously into the left flank. The experimental overview is shown in Figure 6B. Of note, EL4 cells showed higher growing kinetics in mice compared to ML2-WT cells leading to different a tumor size at the day of imaging. PET/CT imaging was performed 24h and 48h post intravenous injection of <sup>89</sup>Zr-aTCRmu-IgG (Figure 6C) or <sup>89</sup>Zr-aTCRmu-F(ab')<sub>2</sub> (Figure 6D). PET/CT imaging of <sup>89</sup>Zr-aTCRmu-IgG revealed a clear

signal on the EL4 tumor, but also uptake in the ML2-WT tumor and spleen. A high PET signal was detected in the liver where metabolism and secretion of the antibody takes place (Johansson, Lovdal et al. 1996; Lobo, Hansen et al. 2004). Compared to 24h post injection, imaging 48h post injection showed a reduced background signal within the intestinal area and the blood (Figure 6C). PET/CT imaging of  $^{89}\text{Zr}$ -aTCRmu-F(ab')<sub>2</sub> showed a high signal on the EL4 tumor, but no uptake in the ML2-WT tumor. Compared to aTCRmu-IgG PET-imaging, we detected a high signal in the kidney due to differential secretion kinetics between F(ab')<sub>2</sub> and IgG based on their differences in size. Biodistribution analysis of organs 48h post injection confirmed the imaging data of  $^{89}\text{Zr}$ -aTCRmu-IgG (Figure 6E) and  $^{89}\text{Zr}$ -aTCRmu-F(ab')<sub>2</sub> (Figure 6F). Autoradiography of tumors, spleen and muscle sections revealed signals similar to the imaging and biodistribution data (Figure 6G-H). Taken together,  $^{89}\text{Zr}$ -aTCRmu-IgG and  $^{89}\text{Zr}$ -aTCRmu-F(ab')<sub>2</sub> PET/CT imaging showed a clear signal on the murine TCR expressing EL4 tumor. Ex vivo analysis by biodistribution and autoradiography confirmed in vivo PET/CT data. However,  $^{89}\text{Zr}$ -aTCRmu-IgG and  $^{89}\text{Zr}$ -aTCRmu-F(ab')<sub>2</sub> showed expected differences in body distribution kinetics as well binding characteristics in vivo.

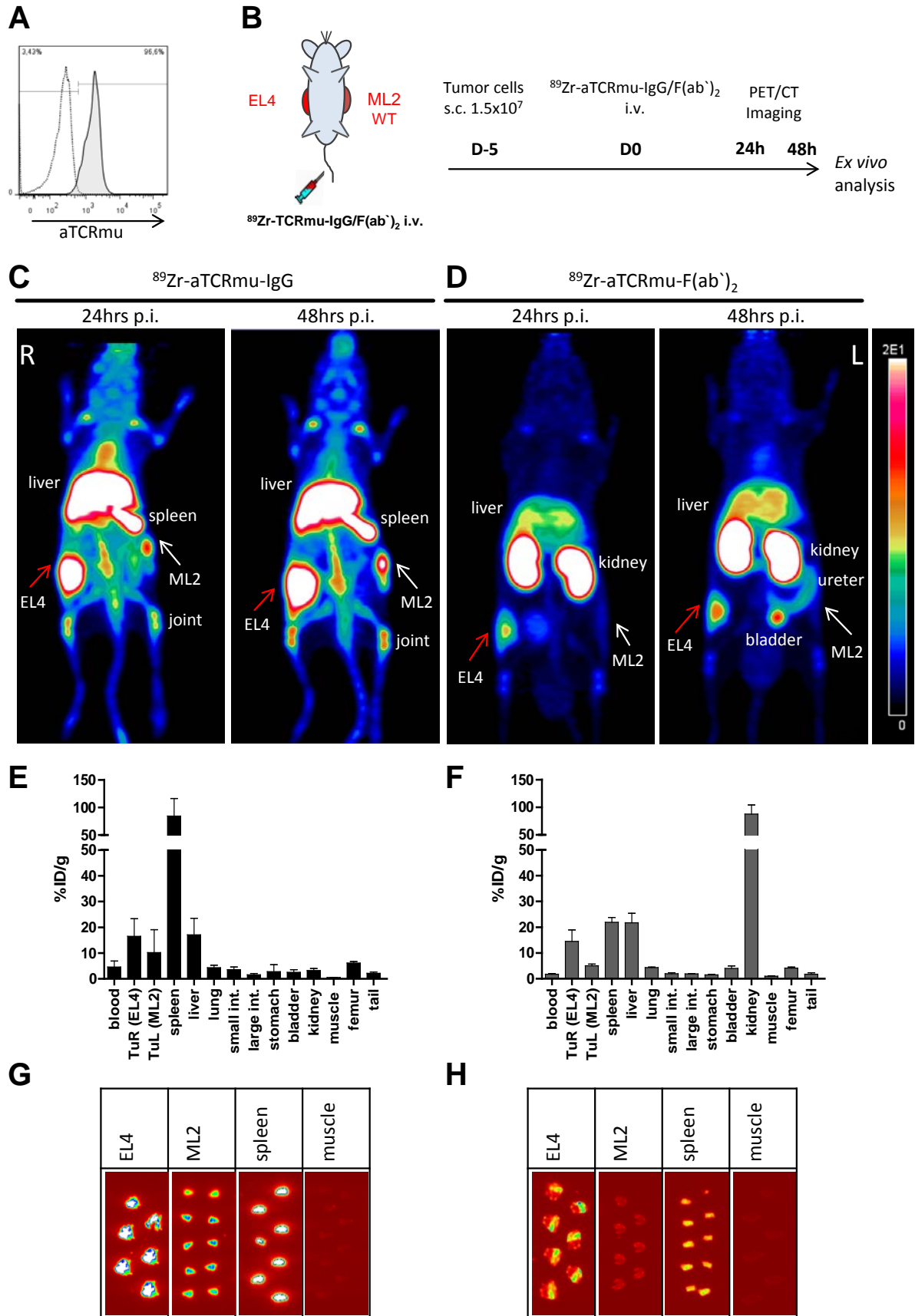


**Figure 6. PET/CT imaging and ex vivo analysis of murine TCR expressing EL4 cells.**

(A) Analysis of murine TCR expression by EL4 cells. Representative flow cytometry analysis of EL4 cells (grey histogram) compared to human PBMC (white histogram) stained with

aTCRmu-IgG are shown. (B) Experimental setup: murine EL4 T-lymphoma cells were injected subcutaneously into the right flank and ML2-WT into the left flank of BRG-mice. After tumor engraftment,  $^{89}\text{Zr}$ -aTCRmu-IgG/F(ab')<sub>2</sub> were injected intravenously (i.v.) and PET/CT imaging was performed 24h and 48h post injection. (C-D) 3D-PET (MIP) 24h and 48h post i.v. injection of (C)  $^{89}\text{Zr}$ -aTCRmu-IgG or (D)  $^{89}\text{Zr}$ -aTCRmu-F(ab')<sub>2</sub> is shown. Scale bar = 0-20% injected dose per gram (%ID/g). One representative of n=3 animals is shown. (E-F) Quantitative ex vivo biodistribution analysis shows uptake in indicated organs 48h post injection of (E)  $^{89}\text{Zr}$ -aTCRmu-IgG or (F)  $^{89}\text{Zr}$ -aTCRmu-F(ab')<sub>2</sub>. Mean  $\pm$  s.d. of %ID/g is depicted for n=3 animals. (G-H) Representative autoradiography analyses of ex vivo 20 $\mu\text{m}$  tumor sections prepared immediately after PET/CT imaging at 48h post injection of (G)  $^{89}\text{Zr}$ -aTCRmu-IgG or (H)  $^{89}\text{Zr}$ -aTCRmu-F(ab')<sub>2</sub>. Muscle probes were used as negative control. Representative tumors and organs for n=3 mice are shown.

#### 5.4.3 DEVELOPMENT OF AN IMAGING MODEL FOR HUMAN TCR-TRANSGENIC T CELLS

We then aimed to establish an in vivo model to track specifically human TCR-transgenic T cells on the tumor site. We first investigated the feasibility to visualize TCR2.5D6-transduced T-cells after intratumoral injection. Therefore, ML2-B7 cells were injected subcutaneously in the right flank and ML2-WT cells into the left flank of BRG-mice. After 10 days, when tumors were palpable (25.6  $\pm$  17.9mm<sup>2</sup>), TCR2.5D6 T<sub>CM</sub> were injected in the ML2-B7 tumor, non-transduced T<sub>CM</sub> were injected in the ML2-WT tumor and  $^{89}\text{Zr}$ -aTCRmu-IgG or  $^{89}\text{Zr}$ -aTCRmu-F(ab')<sub>2</sub> was subsequently injected intravenously. PBS injected into both tumor sites was used as a negative control (experimental overview is shown in Figure 7).

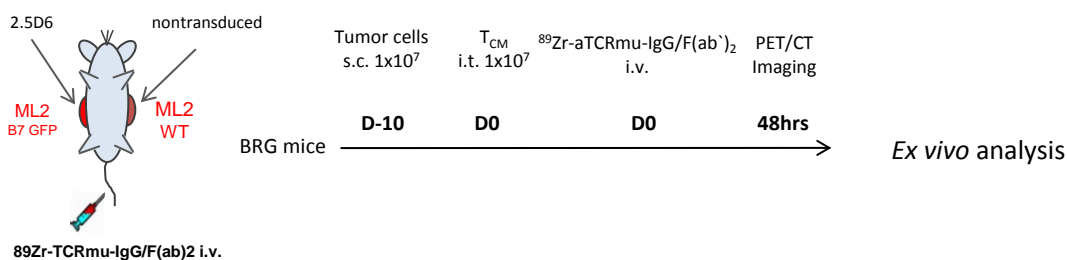


**Figure 7. Experimental setup of in vivo imaging model for human TCR transgenic T-cells.**

ML2-B7 cells were injected subcutaneously (s.c.) in the right flank and ML2-WT in the left flank of BRG-mice. After 10 days, 2.5D6-transduced T<sub>CM</sub> were injected directly in the ML2-B7 tumor and non-transduced T<sub>CM</sub> were injected in the ML2-WT tumor (i.t.) followed by intravenous application of  $^{89}\text{Zr}$ -aTCRmu-IgG or  $^{89}\text{Zr}$ -aTCRmu-F(ab')<sub>2</sub>. PET/CT imaging was performed 24h and 48h post injection of the tracer followed by ex vivo analysis to confirm imaging data.

#### 5.4.4 INTRATUMORAL DETECTION OF T-CELLS USING $^{89}\text{Zr}$ -ATCRMU-IGG

Using the model described in section 5.4.3, PET/CT imaging was performed 24h (Figure 8A) and 48h (Figure 8B) post  $^{89}\text{Zr}$ -aTCRmu-IgG injection. PET-Imaging analysis showed a higher signal on the ML2-B7 tumor in mice injected with TCR-transduced  $T_{\text{CM}}$ . Quantification of the signal by region of interest (ROI) analysis of tumors revealed a slightly higher percentage of injected dose per gram (%ID/g) at the tumor where TCR2.5D6-transduced  $T_{\text{CM}}$  were injected 24h post injection (Figure 8C), and this tendency increased 48h post injection (Figure 8D). 48h post  $^{89}\text{Zr}$ -aTCRmu-IgG injection, ex vivo biodistribution analysis (Figure 8E) and autoradiography (Figure 8F) of tumors, spleen and lung were performed and confirmed the imaging data by showing a signal enhancement at the tumor site where TCR2.5D6-transduced T cells were injected. However, enhanced signals were also detected in the ML2-WT tumor as well as in both tumors in the control mice, receiving PBS only injected into tumors. Of note, as this experiment represents a preliminary study using a limited number of mice, statistical analysis was not performed. In conclusion, these results and results from section 5.4.2 indicate both an unspecific binding of  $^{89}\text{Zr}$ -aTCRmu-IgG in vivo.

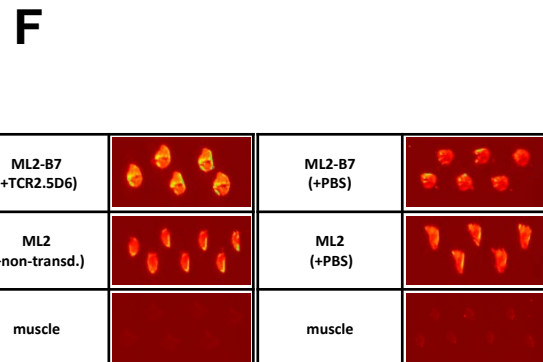
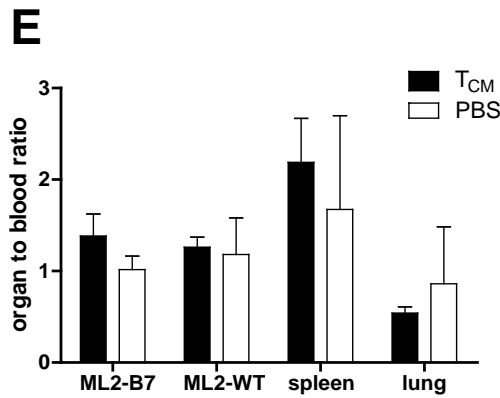
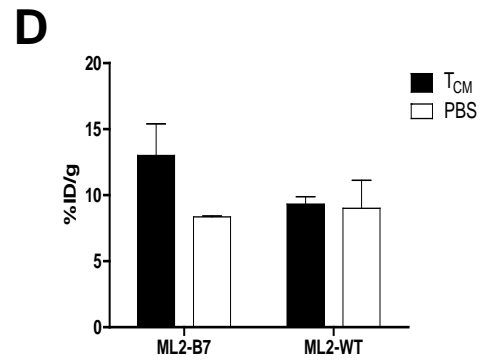
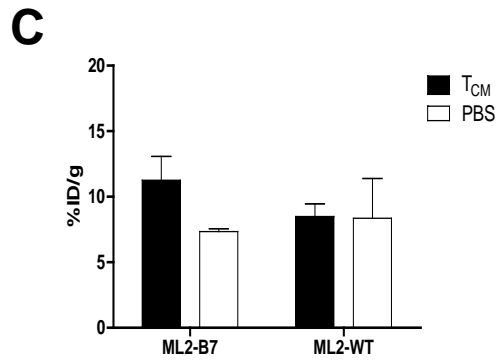
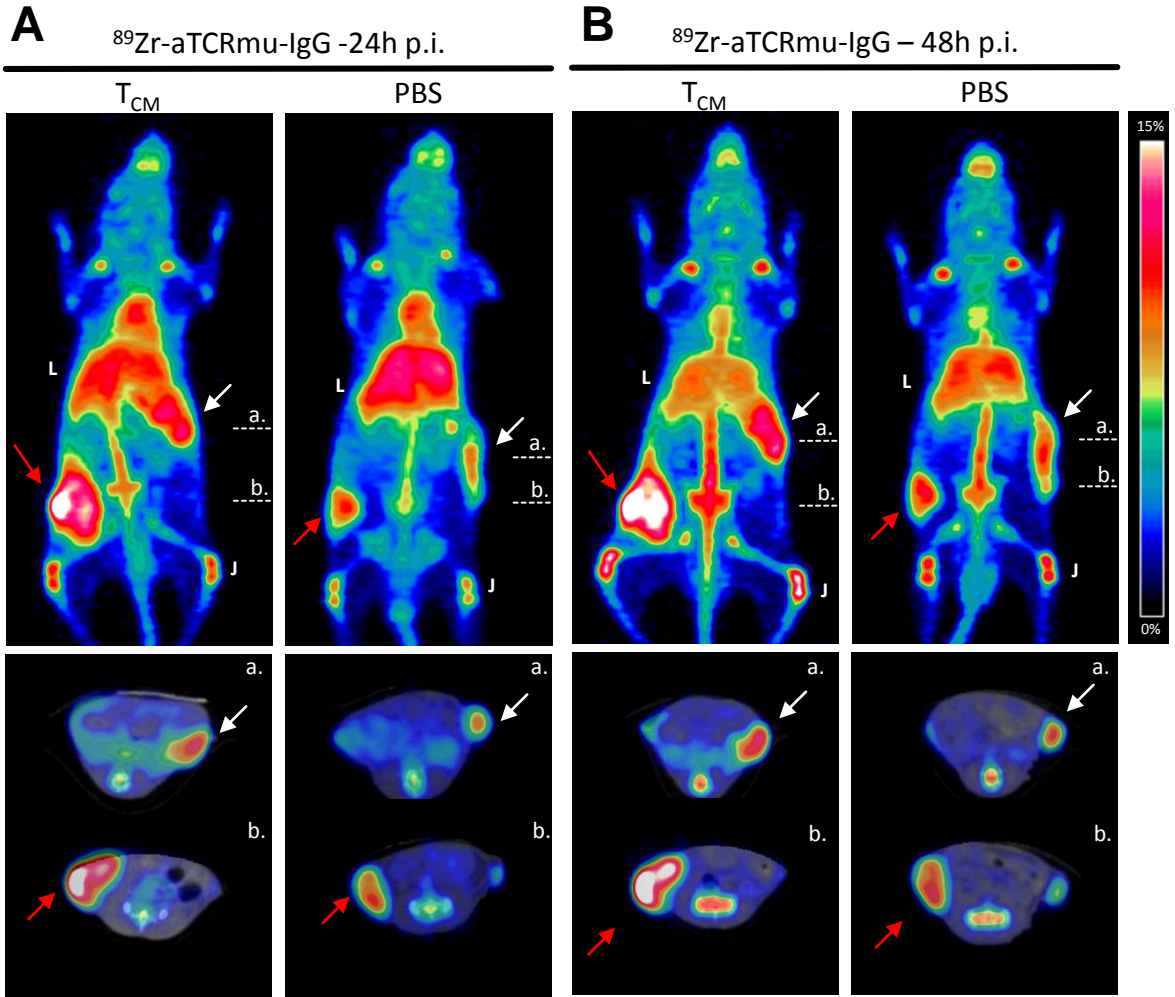




**Figure 8. Tracking of TCR2.5D6-transduced T<sub>CM</sub> after intratumoral injection by <sup>89</sup>Zr-aTCRmu-IgG.**

(A-B) 3D-PET (MIP) (upper part) and axial PET/CT (lower part) images (A) 24h and (B) 48h post intravenous injection of <sup>89</sup>Zr-aTCRmu-IgG of mice injected with T<sub>CM</sub> or PBS. TCR2.5D6-transduced T<sub>CM</sub> were injected in the right tumor (red arrow), non-transduced in the left tumor (white arrow) or PBS was injected into the right (red arrow) and left tumor (white arrow). Dotted lines, (a.) and (b.) indicate the respective position of axial PET/CT images. Scale bar = 0-15% %ID/g, L=Liver, J=Joints. (C-D) Quantitative ROI analysis of PET/CT images of ML2-B7 and ML2-WT tumors (C) 24h and (D) 48h post injection of <sup>89</sup>Zr-aTCRmu-IgG. Mean ± s.d. of %ID/g in defined ROI is depicted. One representative of n=3 for T<sub>CM</sub> and n=2 for PBS-treated animals is shown. (E) Quantitative analysis of organ to blood ratio 48h post injection of <sup>89</sup>Zr-aTCRmu-IgG after intratumoral injection of TCR2.5D6 T<sub>CM</sub>, non-transduced T<sub>CM</sub> or PBS. Mean ± s.d. of %ID/g in relation to blood is depicted for n=3 animals treated with T<sub>CM</sub> and n=2 treated with PBS. (F) Representative autoradiography analyses of ex vivo 20µm tumor sections prepared immediately after PET/CT imaging at 48h post injection and analyzed after 24h incubation. Muscle probes were used as negative control.

This unspecific binding of <sup>89</sup>Zr-aTCRmu-IgG to tumor cells detected in vivo by PET-imaging might be explained by binding of full antibody to Fc receptors as ML2 cells express CD32 and CD64 (FcγRI and FcγRII) but not CD16 (FcγRIII) as revealed by flow cytometry (Figure 9A). In fact, blockade of Fc-Receptors by human serum, commercially available FcR block, as well as aTCRmu-IgG or Isotype-IgG leads to a strong reduction of aTCRmu-IgG binding in vitro as shown by flow cytometric analysis (Figure 9B).

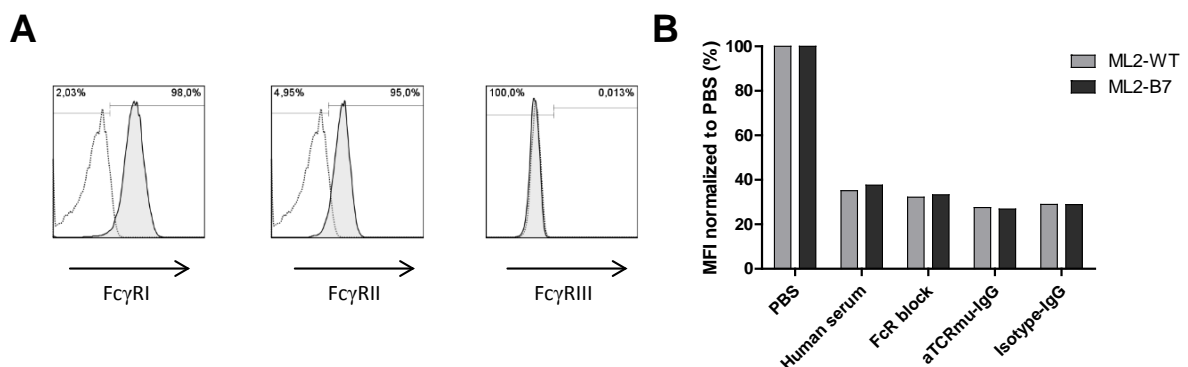


**Figure 9. Expression of Fc-receptors on ML2 cells.**

(A) Analysis of expression of FcγRI (CD32), FcγRII (CD64) and FcγRIII (CD16) by flow cytometry of ML2 cells (grey filled histogram) compared to isotype control (white histogram). (B) Quantitative evaluation of aTCRmu binding to ML2-WT or ML2-B7 cells by

flow cytometry after Fc-receptor blocking using human serum, human FcR-block, aTCRmu-IgG and Isotype-IgG. Mean fluorescence intensity (MFI) percentage of aTCRmu staining normalized to PBS treatment is shown.

#### 5.4.5 INTRATUMORAL DETECTION OF T CELLS USING $^{89}\text{Zr}$ -ATCRMU-F(AB')<sub>2</sub>

As unspecific binding of  $^{89}\text{Zr}$ -aTCRmu-IgG was shown to be mediated by Fc-Receptor binding, we hypothesized to reveal a specific signal using  $^{89}\text{Zr}$ -aTCRmu-F(ab')<sub>2</sub>. As aTCRmu-F(ab')<sub>2</sub> is of smaller size (110kDa) compared to a aTCRmu-IgG (150kDa), we investigated first the most appropriate time point for imaging post injection of  $^{89}\text{Zr}$ -aTCRmu-F(ab')<sub>2</sub>. We injected TCR2.5D6 T<sub>CM</sub> directly in the ML2-B7 tumor and non-transduced T<sub>CM</sub> in the ML2-WT tumor (experimental overview is depicted in Figure 7) and imaged mice 12h (Figure 10A-C), 24h (Figure 10D-F) and 48h (Figure 10G-I) post injection of  $^{89}\text{Zr}$ -aTCRmu-F(ab')<sub>2</sub>. After imaging, mice were euthanized and uptake in tumors was determined by biodistribution assay. 12h post injection of  $^{89}\text{Zr}$ -aTCRmu-F(ab')<sub>2</sub>, a low signal within the ML2-B7 tumor was detectable by PET/CT (Figure 10A), which was confirmed by ROI analysis of PET images (Figure 10B) and ex vivo biodistribution (Figure 10C). Higher specific activity and reduction of background signal has been observed after 24h (Figure 10D-F) and this was further improved 48h post injection (Figure 10G-I). Although statistical analysis was not performed due to limited number of animals, these observations indicate that 24h and 48h post injection are the best time points for PET/CT imaging with  $^{89}\text{Zr}$ -aTCRmu-F(ab')<sub>2</sub>. These time points were subsequently used for further studies.

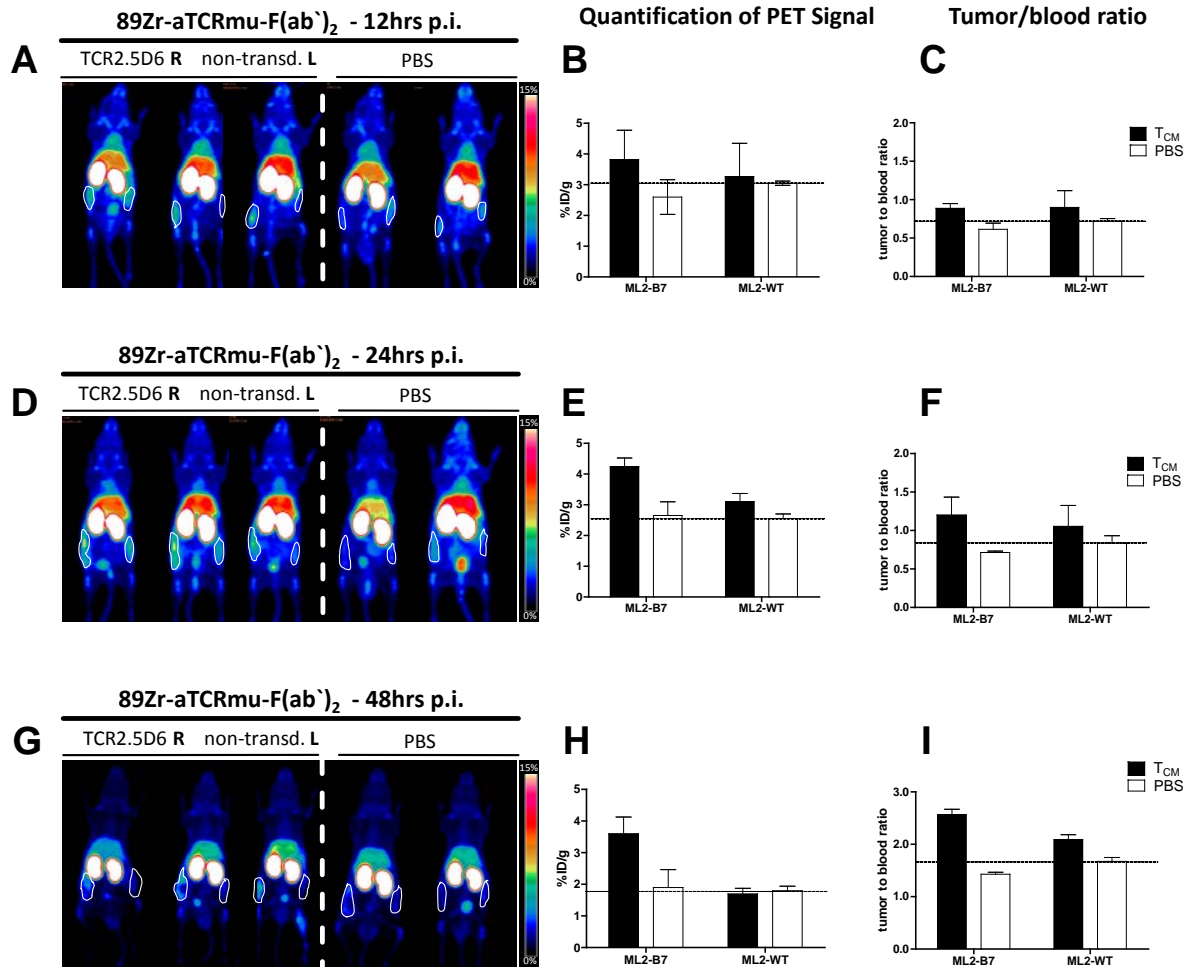


**Figure 10. Investigation of different imaging time points to detect TCR-transduced T<sub>CM</sub> after injection of <sup>89</sup>Zr-aTCRmu-F(ab')<sub>2</sub>.**

(A-I) TCR2.5D6-transduced T<sub>CM</sub> were injected into the ML2-B7 tumor and non-transduced T<sub>CM</sub> into ML2-WT tumors (experimental design see Figure 7). Mice injected with PBS into ML2-B7 and ML2-WT tumors were used as control. <sup>89</sup>Zr-aTCRmu-F(ab')<sub>2</sub> was subsequently injected i.v. and PET/CT imaging was performed (A-C) 12h, (D-F) 24h or (G-I) 48h post injection (p.i.). Representative 3D PET (MIP) images (A) 12h, (D) 24h or (G) 48h post injection of <sup>89</sup>Zr-aTCRmu-F(ab')<sub>2</sub> with marked tumors. Scale bar: 0-15%ID/g. Quantitative ROI analysis of ML2-B7 and ML2-WT tumors of PET images (B) 12h, (E) 24h or (H) 48h post injection of <sup>89</sup>Zr-aTCRmu-F(ab')<sub>2</sub> is shown. Mean ± s.d. of %ID/g in defined ROI is depicted. Tumor to blood ratio of %ID/g in ex vivo analysis (C) 12h, (F) 24h or (I) 48h post injection of <sup>89</sup>Zr-aTCRmu-F(ab')<sub>2</sub>. Mean ± s.d. of %ID/g ratio is depicted. Analysis has been performed with (A-C) T<sub>CM</sub> (n=5) and PBS (n=2), (D-F) T<sub>CM</sub> (n=6) and PBS (n=2), (G-I) T<sub>CM</sub> (n=3) and PBS (n=2). R=right, L=left, non-transd.= non-transduced.

PET/CT imaging of mice injected i.v. with  $^{89}\text{Zr}$ -aTCRmu-F(ab')<sub>2</sub> showed a specific signal on the tumor site of ML2-B7 where TCR2.5D6-transduced T<sub>CM</sub> were injected, but no signal on the ML2-WT tumor after 24hrs (Figure 11A) or 48h (Figure 11B). No signal has been detected in control mice injected with PBS. Quantification of the activity on the tumor site by ROI analysis revealed a higher %ID/g in the ML2-B7 tumor injected with TCR2.5D6-transduced T<sub>CM</sub> compared to the ML2-WT tumor injected with non-transduced T<sub>CM</sub> as well as PBS injected tumors (Figure 11C-D). Enhanced radioactivity was confirmed by ex vivo biodistribution analysis 48h post injection (Figure 11E) and autoradiographic detection of radioactivity on tumor sections (Figure 11F). Taken together, specific uptake of  $^{89}\text{Zr}$ -aTCRmu-F(ab')<sub>2</sub> was detected by PET/CT imaging 24h and 48h post injection on tumors containing TCR2.5D6 transduced T<sub>CM</sub>.

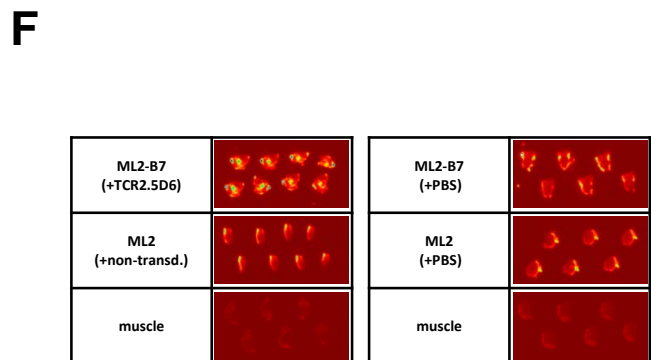
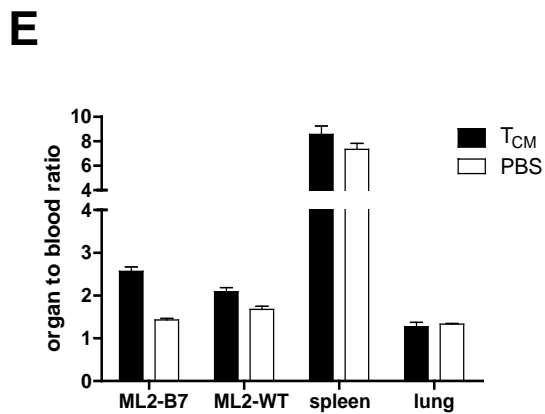
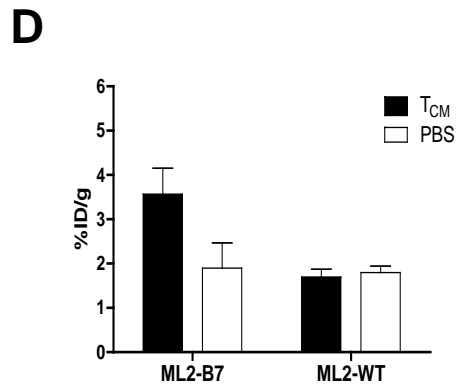
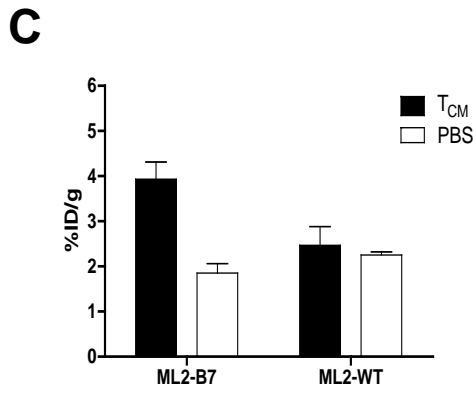
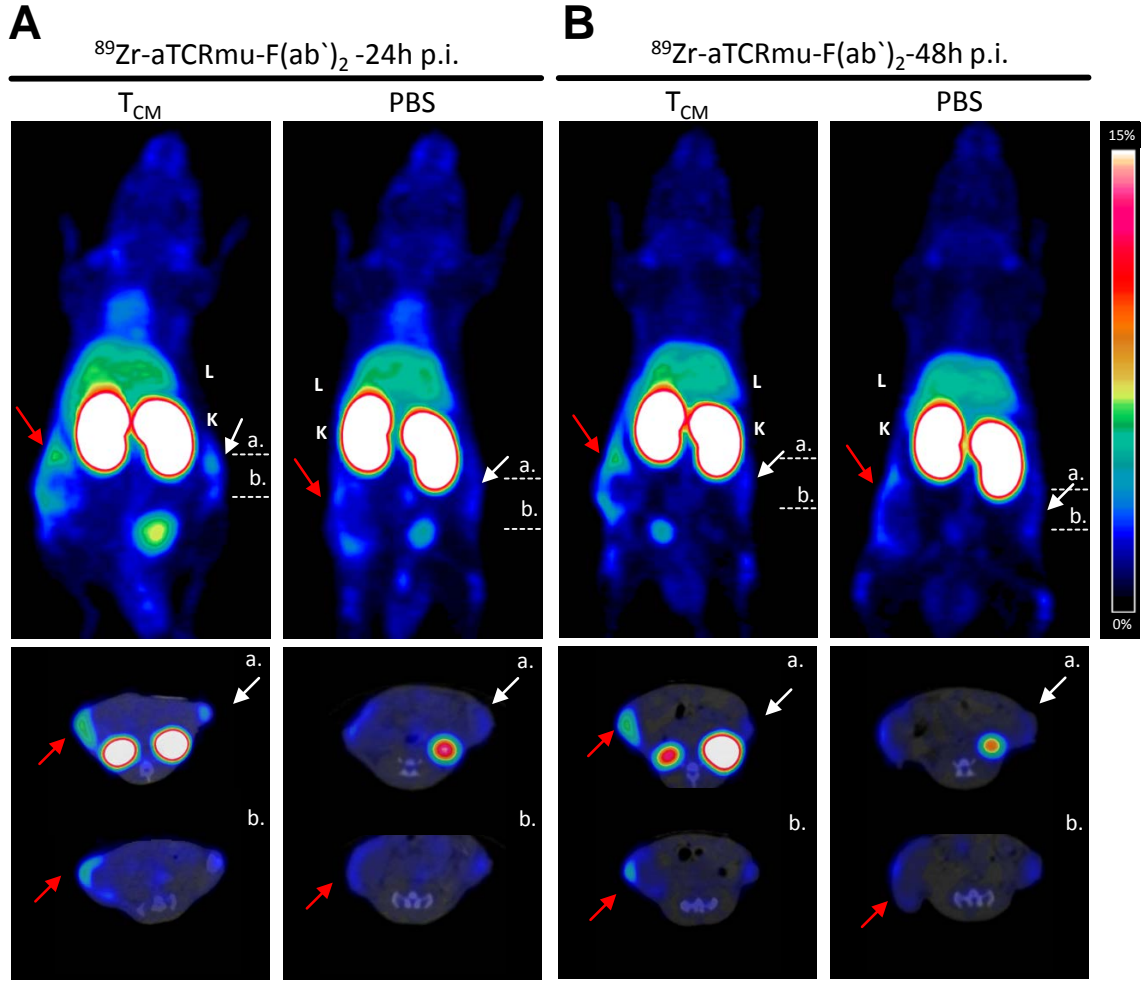


**Figure 11. Tracking of TCR2.5D6-transduced T<sub>CM</sub> injected directly into the tumor by <sup>89</sup>Zr-aTCRmu-F(ab')<sub>2</sub>.**

(A-B) Representative 3D-PET (MIP) and axial PET/CT images (A) 24h and (B) 48h after intravenous injection of <sup>89</sup>Zr-aTCRmu-F(ab')<sub>2</sub>. Red arrows indicate the position of ML2-B7 tumors injected with TCR2.5D6 transduced T<sub>CM</sub> and white arrows indicate the position of ML2-WT tumors injected with non-transduced T<sub>CM</sub>. Dotted lines, a. and b. show the position of axial PET/CT images. Scale bar = 0-15%ID/g; L=Liver; K=Kidney. (C-D) Quantitative analysis of PET/CT images (C) 24h and (D) 48h post injection of <sup>89</sup>Zr-aTCRmu-F(ab')<sub>2</sub>. Mean ± s.d. of %ID/g in defined ROI is depicted. (E) Quantitative evaluation of tumor or organ to blood ratios 48h post intravenous injection of <sup>89</sup>Zr-aTCRmu-F(ab')<sub>2</sub>. Mean ± s.d. of %ID/g ratio is depicted. (F) Representative autoradiographic data of 20μm sections of tumors injected with TCR2.5D6 or non-transduced T<sub>CM</sub> are shown. Muscle probes served as negative control. (A-F) Representative data of n=3 animals for T<sub>CM</sub> and n=2 animals for PBS are depicted.

**5.4.6 CONFIRMATION OF IN VIVO IMAGING OF INTRATUMORAL T CELLS TRACKED BY <sup>89</sup>ZR-ATCRMU-F(AB')<sub>2</sub>**

To determine the presence of injected T cells after imaging, we performed immunohistochemical staining and detected a high number of CD3-positive T cells around the injection site in ML2-B7 tumors (Figure 12A). The immunohistochemical analyses were validated by flow cytometry analyses of CD3, CD8, CD45 and aTCRmu staining (Figure 12B-C). To further confirm these observations we performed qPCR of genomic DNA (gDNA) extracted from ML2-B7 and ML2-WT tumors after imaging and detected copies of TCR2.5D6 in the ML2-B7 tumor but not in the ML2-WT tumor (Figure 12D).

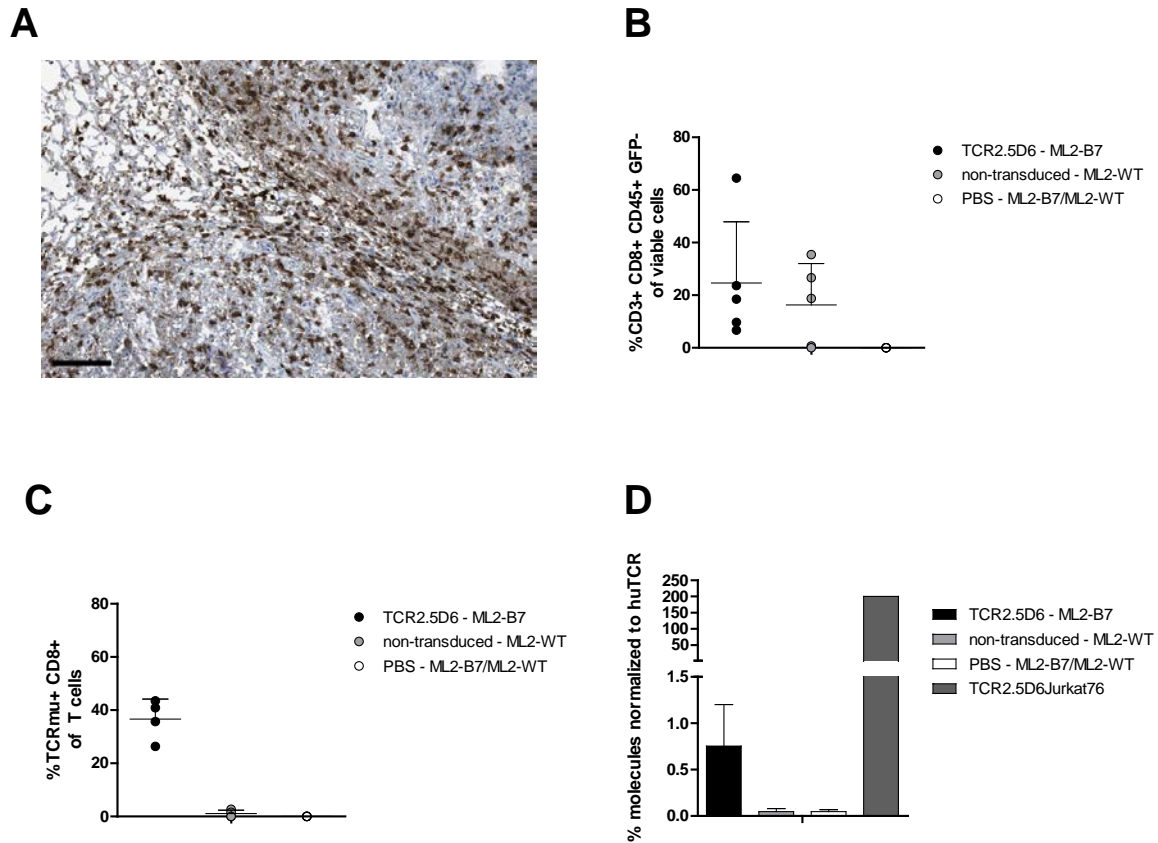


**Figure 12. Ex vivo detection of TCR2.5D6-transduced T-cells following direct injection into the tumors.**

(A) Immunohistochemical CD3 $\epsilon$  staining of a ML2-B7 tumor at the injection site, bar=200 $\mu$ m. (B-C) Flow cytometry analysis of single cell suspensions of tumors prepared after PET/CT imaging and cultivated for 3 days with hIL7/hIL15. The percentage of (B) viable T cells (hCD45+ GFP- hCD3+) and of (C) TCR2.5D6-transduced T<sub>CM</sub> (TCRmu+ hCD8+) of all viable T cells is shown. Mean  $\pm$  s.d. of TCR2.5D6-transduced T<sub>CM</sub> (n=4), non-transduced T<sub>CM</sub> (n=4) and PBS (n=4) is depicted. (D) qPCR of the murinized TCR beta constant gene sequences using gDNA isolated from single cell suspensions of tumors. gDNA of TCR2.5D6-transduced Jurkat76 was used as positive control. Percentage of TCRmu molecules normalized to the number of human TCR (huTCR) molecules is depicted.

#### 5.4.7 CHARACTERIZATION OF IN VIVO CYTOTOXIC ACTIVITY OF TCR2.5D6 TRANSDUCED T<sub>CM</sub>

With the aim to develop a more clinically relevant model, we optimized the tumor model of myeloid sarcoma by injecting T<sub>CM</sub> intravenously in tumor-bearing NSG-mice analog to a potential clinical setting of adoptive T-cell transfer. Compared to BRG-mice, NSG-mice were shown to exhibit higher engraftment rates of human T cells (Ali, Flutter et al. 2012). ML2-B7

and ML2-WT cells were injected subcutaneously in the right and left flanks, respectively. Tumor bearing mice were low dose irradiated and TCR-transgenic T<sub>CM</sub>, non-transduced T<sub>CM</sub> or PBS were transferred intravenously. Irradiated NSO-IL15 cells, which produce human IL-15, were injected in the peritoneum to support T-cell engraftment (Wang, Berger et al. 2011) (experimental overview is shown in Figure 13A). Tumor size was determined over 10 days by caliper measurement and revealed a significant reduction of the ML2-B7 tumor in mice injected with TCR2.5D6 T<sub>CM</sub>, but not in those mice treated by non-transduced T<sub>CM</sub> or PBS alone (Figure 13B). This in vivo cytotoxicity of TCR2.5D6-transduced T<sub>CM</sub> was first measurable four days post injection of TCR2.5D6-transgenic T<sub>CM</sub>. Ten days post injection of T<sub>CM</sub> cells, animals were euthanized due to the high tumor burden of the ML2-WT tumors on the other flank side which showed no modification in growing kinetics by adoptive transfer of TCR-transduced T<sub>CM</sub> or controls (Figure 13C). Ex vivo flow cytometry analyses of tissues showed a significant increase in total CD45+CD3+CD5+ T cells within the ML2-B7 tumor compared to ML2-WT tumor. In mice injected with non-transduced T<sub>CM</sub>, only few T cells were detected within the tumors. In contrast, T-cell infiltration was similar in spleen and lung irrespective if TCR2.5D6 T<sub>CM</sub> or non-transduced T<sub>CM</sub> were transferred (Figure 13D) indicating similar engraftment rates. Analysis of infiltrating T cells within the tumors showed that 29.8% ( $\pm 10.1\%$ ) of all T<sub>CM</sub> in the ML2-B7 tumor were positive for the aTCR $\mu$ , which was significantly higher when compared to ML2-WT tumor or animals treated with non-transduced T<sub>CM</sub> (Figure 13E). Taken together, TCR2.5D6-transduced T<sub>CM</sub> efficiently infiltrate and kill specifically the subcutaneously engrafted ML2-B7 tumor and are able to reduce the tumor mass within 6 days post adoptive transfer. ML2-WT tumors were not significantly affected or infiltrated by T<sub>CM</sub> indicating high specificity for TCR2.5D6-transduced T<sub>CM</sub>.



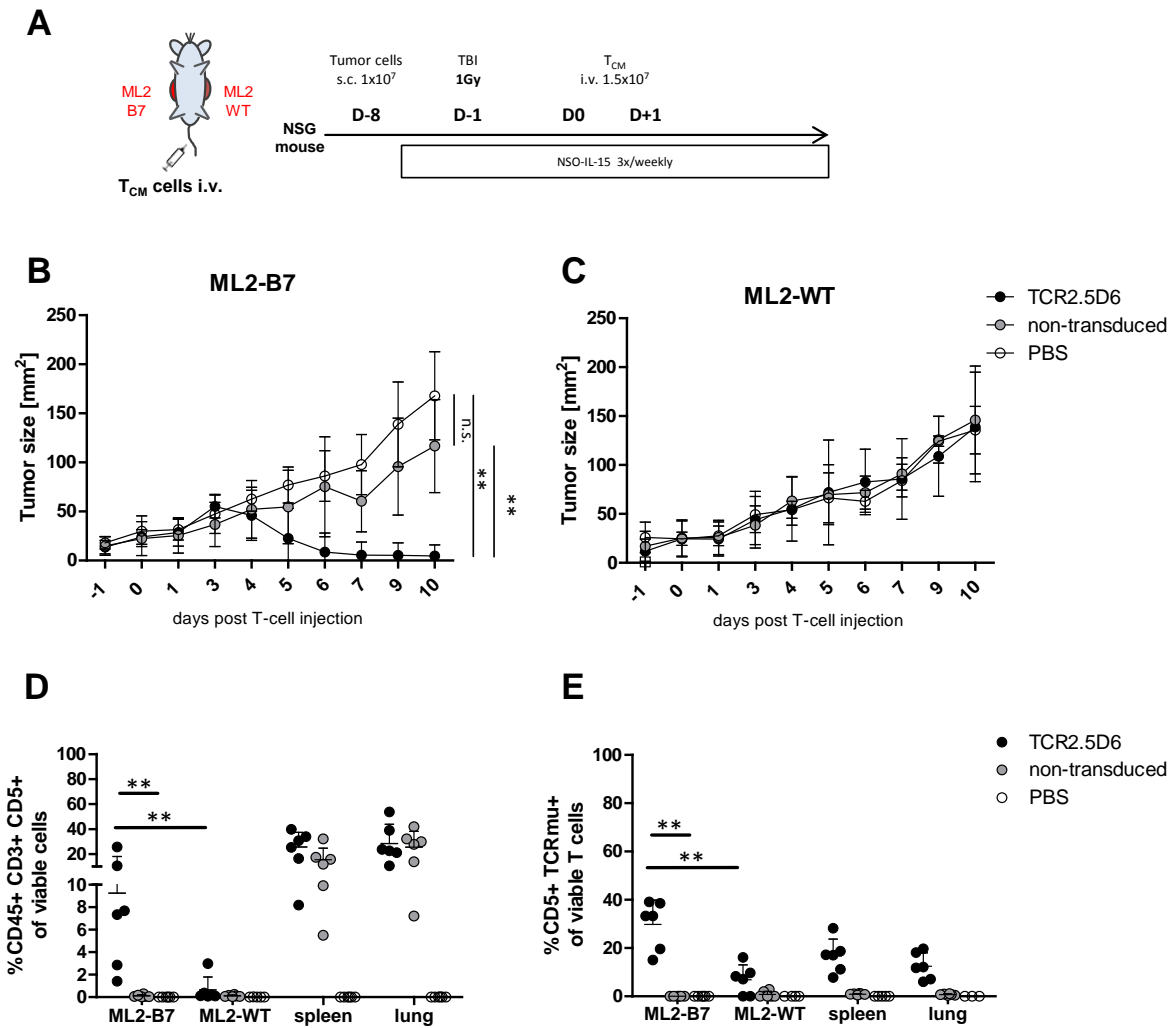


**Figure 13. Anti-tumor activity of TCR2.5D6-transduced T<sub>CM</sub> in vivo in a myeloid sarcoma model.**

(A) Overview of the experimental setting. NSG-mice were inoculated with  $1 \times 10^7$  ML2-B7 cells subcutaneously into the right and ML2-WT cells into the left flank followed by total body irradiation (TBI) and intravenous transfer of TCR2.5D6-transduced T<sub>CM</sub>, non-transduced T<sub>CM</sub> or PBS. Tumor size of (B) ML2-B7 and (C) ML2-WT at indicated days post T-cell injection is shown. Mean  $\pm$  s.d. of tumor size is indicated in mm<sup>2</sup> of  $n=6$  animals; Mann-Whitney test: \*\* $p < 0.01$ . (D-E) Flow cytometry analyses of single cell suspension derived from tumors and organs were performed at the end of the experiment (day 10). The percentage of (D) viable human T cells and of (E) TCR2.5D6-transduced T cells of viable T cells within the ML2-B7 or ML2-WT tumors, spleen and lung is shown. Mean  $\pm$  s.d. of viable T cells (%CD45+ GFP- CD3+ CD5+) or TCR-transduced T cells (%CD5+ TCRmu+) of viable T cells is depicted for  $n=6$  animals; Mann-Whitney Test: \*\* $p < 0.01$ .

#### 5.4.8 DETECTION OF INTRAVENOUSLY INJECTED T CELLS AT THE TUMOR SITE USING $^{89}\text{Zr}$ - $\text{aTCRMU-F}(\text{ab}')_2$

In order to simulate a potential clinical scenario for imaging of TCR-transgenic T cells, we injected TCR2.5D6-transduced  $\text{T}_{\text{CM}}$  into ML2-B7 and ML2-WT bearing NSG-mice as described in section 5.4.7. As previous experiments showed unspecific binding of  $^{89}\text{Zr}$ -aTCRmu-IgG (section 5.4.2 and section 5.4.4), we continued the tracking of TCR2.5D6-transduced  $\text{T}_{\text{CM}}$  using only  $^{89}\text{Zr}$ -aTCRmu-F(ab')<sub>2</sub>. The experimental setup is shown in Figure 14A. Two days after intravenous injection of  $\text{T}_{\text{CM}}$ ,  $^{89}\text{Zr}$ -aTCRmu-F(ab')<sub>2</sub> was injected intravenously and mice were imaged by PET/CT after 24h (Figure 14B) and 48h (Figure 14C). We detected a clear signal on the ML2-B7 tumor site in animals treated with TCR2.5D6  $\text{T}_{\text{CM}}$ , whereas no signal was observed on the ML2-WT tumors. No specific signal was detected neither in animals treated by non-transduced  $\text{T}_{\text{CM}}$  nor in control groups treated by PBS (Figure 14B-C). Quantification of PET signal 48h post  $^{89}\text{Zr}$ -aTCRmu-F(ab')<sub>2</sub> using ROI analysis confirmed these findings showing an enhanced %ID/g on the ML2-B7 tumor for mice injected with TCR2.5D6 transduced  $\text{T}_{\text{CM}}$  (Figure 14D). Determination of tumor size by caliper-measurement revealed a decrease in ML2-B7 tumor size in mice injected with TCR2.5D6-transduced  $\text{T}_{\text{CM}}$  indicating no impairment of  $\text{T}_{\text{CM}}$  functionality by in vivo labeling with  $^{89}\text{Zr}$ -TCRmu-F(ab')<sub>2</sub> (Figure 14E).

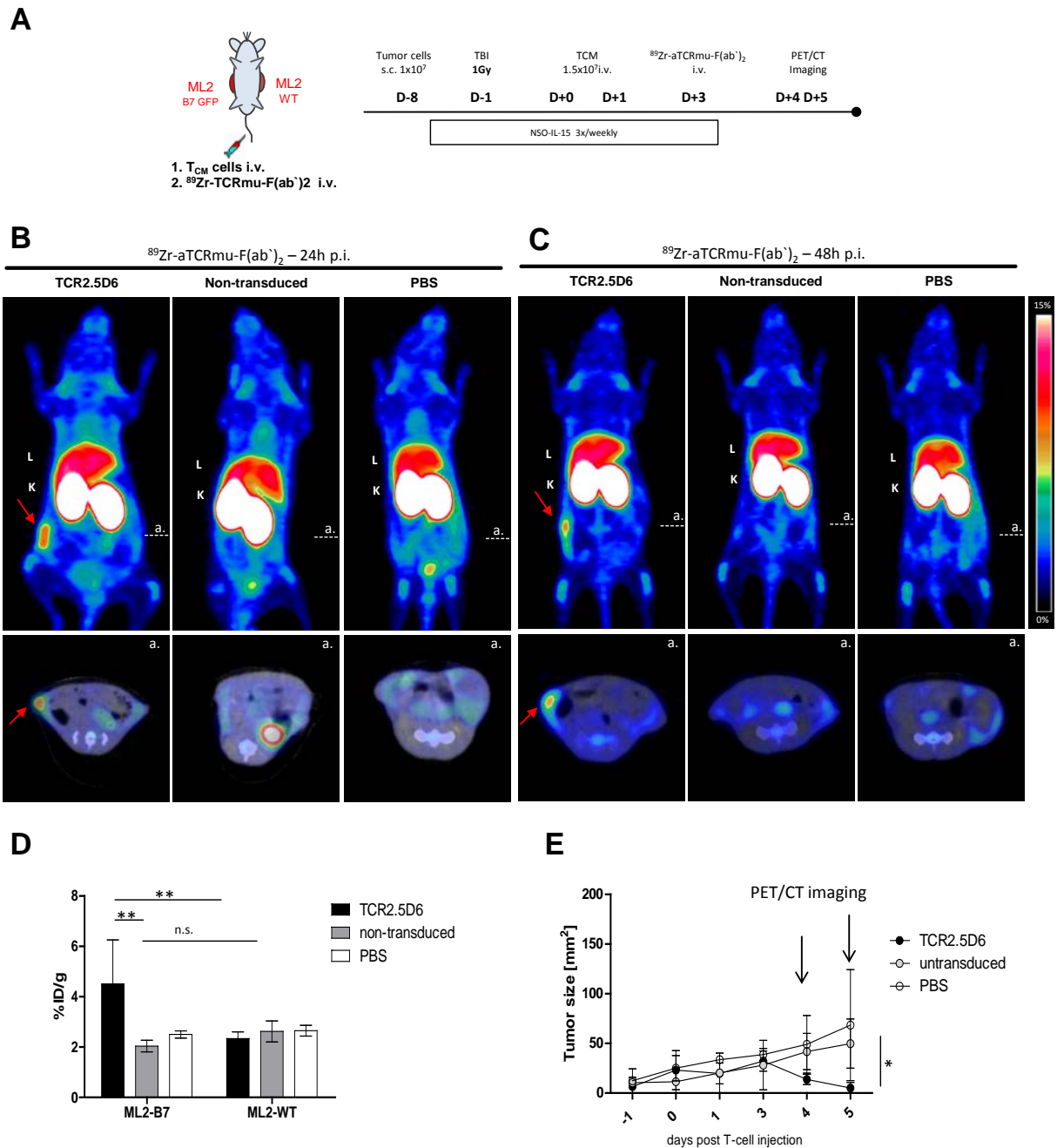


**Figure 14. Tracking of intravenously injected TCR2.5D6-transduced T<sub>CM</sub> within ML2-B7 tumors using <sup>89</sup>Zr-aTCRmu-F(ab')<sub>2</sub>.**

(A) Overview of the experimental setting: NSG-mice were inoculated with  $1 \times 10^7$  ML2-B7 cells subcutaneously into the right and ML2-WT cells into the left flank followed by total body irradiation (TBI) and intravenous transfer of  $1.5 \times 10^7$  TCR2.5D6-transduced T<sub>CM</sub>, non-transduced T<sub>CM</sub> or PBS on two subsequent days. Two days later, <sup>89</sup>Zr-aTCRmu-F(ab')<sub>2</sub> was injected intravenously and PET/CT imaging was performed after 24h and 48h. (B-C) Representative 3D PET (MIP) and axial PET/CT images (B) 24h and (C) 48h post injection of <sup>89</sup>Zr-aTCRmu-F(ab')<sub>2</sub>. Red arrows indicate the signal at the ML2-B7 tumors in animals injected with TCR2.5D6-transduced T<sub>CM</sub>. Dotted lines and a. show the position of axial PET/CT images. Scale bar = 0-15%ID/g; L=Liver; K=Kidney. (D) Quantitative analysis of PET/CT images of ML2-B7 and ML2-WT tumors 48h post injection of <sup>89</sup>Zr-aTCRmu-F(ab')<sub>2</sub>. Mean  $\pm$  s.d. of %ID/g of

defined ROI is depicted for n=5 animals treated with T<sub>CM</sub> and n=2 treated with PBS. Mann-Whitney test: \*\*p<0.01. (E) Size of ML2-B7 tumor at different time points post injection of T<sub>CM</sub> or PBS. PET imaging was performed on day 4 and 5 post injection of T<sub>CM</sub> or PBS indicated by arrows. Tumor size in mm<sup>2</sup> ± s.d. is depicted. Mann-Whitney test: \*p<0.1. (B-E) Representative data of one out of three experiments is shown.

Ex vivo biodistribution of tumor and organs showed an enhanced tumor to blood ratio on the ML2-B7 tumors of mice injected with TCR2.5D6-transduced T<sub>CM</sub> compared to the ML2-WT tumor. Mice infused with non-transduced T<sub>CM</sub> or PBS showed no elevated tumor to blood ratio (Figure 15A). We detected a higher activity in the spleen and lung of mice, which were infused with TCR2.5D6-transduced T<sub>CM</sub> (Figure 15A), whereas distribution in all other organs is similar (Figure 15B). Autoradiography of tumors and tissue sections (Figure 15C) confirmed these findings. Of note, activity in the lung was not detectable in autoradiography nor in PET/CT imaging indicating differences in sensitivity between the different ex vivo and in vivo detection-methods. Taken together, TCR2.5D6 transduced T<sub>CM</sub> were specifically tracked at the tumor site using <sup>89</sup>Zr-αTCRμ-F(ab')<sub>2</sub> in a clinically relevant murine model. Imaging data were confirmed by ex vivo biodistribution and autoradiography.

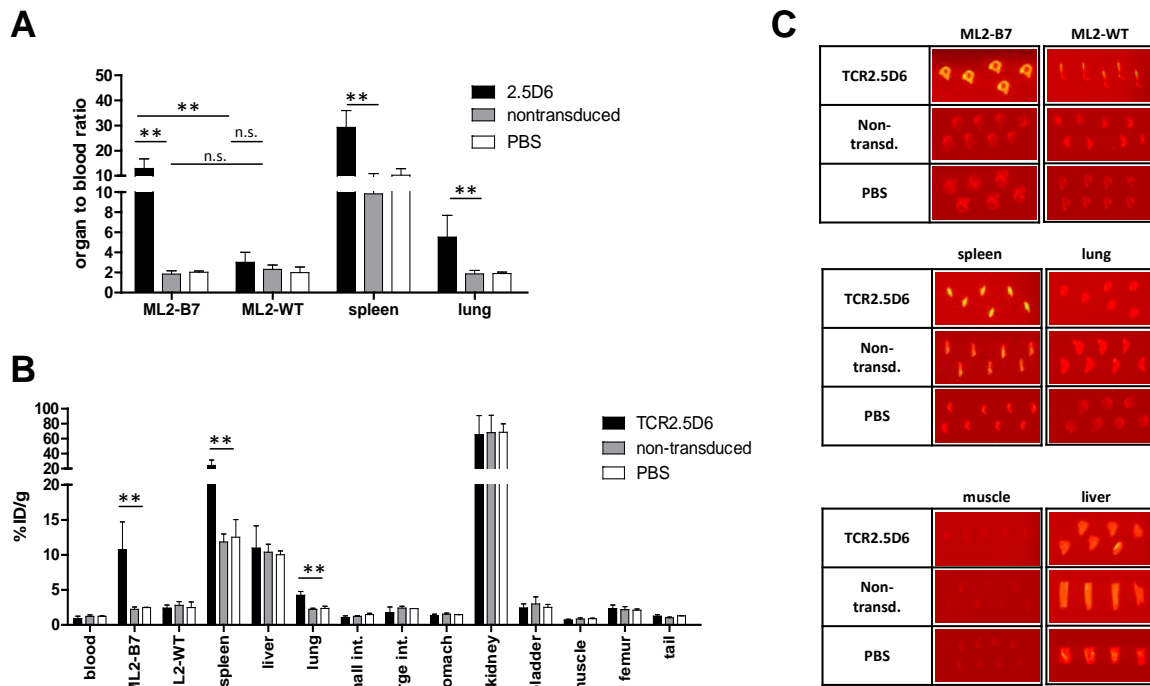


**Figure 15. Ex vivo analysis of tracer uptake confirming specific tracking of intravenously injected TCR2.5D6-transduced T<sub>CM</sub> within ML2-B7 tumors by <sup>89</sup>Zr-aTCRmu-F(ab')<sub>2</sub>.**

(A) Quantitative evaluation of tumor or organ to blood ratios 48h post injection of <sup>89</sup>Zr-aTCRmu-F(ab')<sub>2</sub>. Mean ± s.d. of %ID/g ratio is depicted for n=5 animals treated with T<sub>CM</sub> and n=2 treated with PBS. Mann-Whitney test: \*\*p<0.01. (B) Biodistribution of activity in indicated organs 48h post injection. Mean %ID/g ± s.d. is depicted for n=5 animals treated with T<sub>CM</sub> and n=2 treated with PBS. Mann-Whitney test: \*p<0.05. (C) Representative data of autoradiography are shown. (A-C) Representative data of one out of three experiments are shown.

#### 5.4.9 PRESENCE OF TCR2.5D6 TRANSDUCED T CELLS DETECTED BY <sup>89</sup>ZR-ATCRMU-F(AB')<sub>2</sub> WITHIN ML2-B7 TUMOR TISSUE

To analyze the specificity of this tracking method, ex vivo analyses were performed after the last imaging time point to confirm the presence of human TCR-transduced T<sub>CM</sub> in the ML2-B7 and ML2-WT tumors as well as different organs. Flow cytometry analyses of single cell suspension of tumors, spleen and lung of imaged mice revealed increased amount of T-cells in the ML2-B7 tumor, when mice were infused with TCR2.5D6-transduced T<sub>CM</sub> (Figure 16A). Increase of T-cell infiltration could be also detected in the ML2-WT tumor although to a lower extent. In all other compartments, the percentage of T cells was comparable irrespective if TCR2.5D6-transduced or non-transduced T<sub>CM</sub> were injected (Figure 16A)

indicating similar engraftment rates. Detailed analysis of human T cells for TCRmu expression showed that ML2-B7 tumors were specifically infiltrated by TCR2.5D6-transgenic T<sub>CM</sub> whereas these cells were not elevated in the ML2-WT tumor (Figure 16B) thus confirming the specific signal detected by PET/CT (Figure 14B-C). Of note, enhanced levels of TCR2.5D6-transduced T<sub>CM</sub> were detected in the lung. The gating strategy used for flow cytometry evaluation is shown in Figure 17.

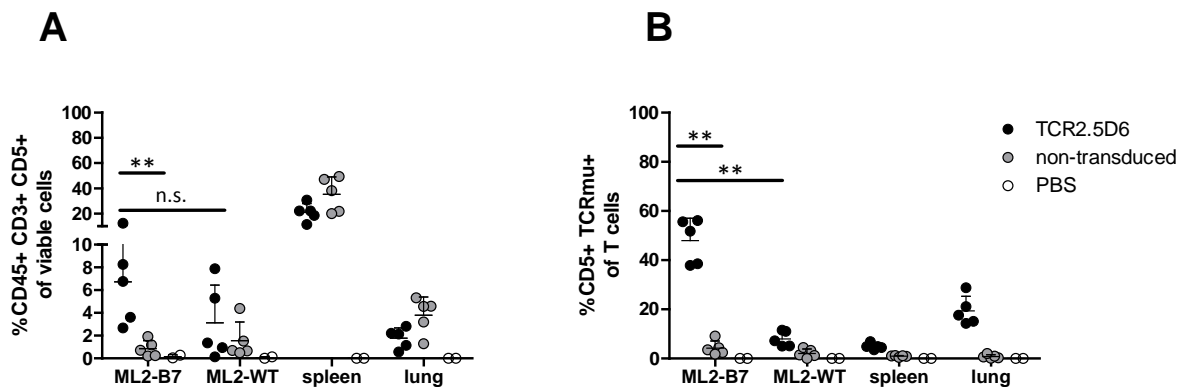


**Figure 16. Presence of aTCRmu positive T cells within ML2-B7 tumors analyzed ex vivo.**

(A-B) Flow cytometry ex vivo analyses of single cell suspensions from tumor and organs after the final imaging time point (48h post <sup>89</sup>Zr-aTCRmu-F(ab')<sub>2</sub> injection). The percentage of (A) viable T cells (%CD45+ GFP- CD3+ CD5+) and of (B) TCR2.5D6-transduced T cells (%CD5+ TCRmu+) of all viable T cells is shown. Mean ± s.d. of TCR2.5D6-transduced T cells (n=5), non-transduced T cells (n=5) and PBS (n=2) is depicted. (A-B) Mann-Whitney Test: \*\*p<0.01; n.s.=not significant

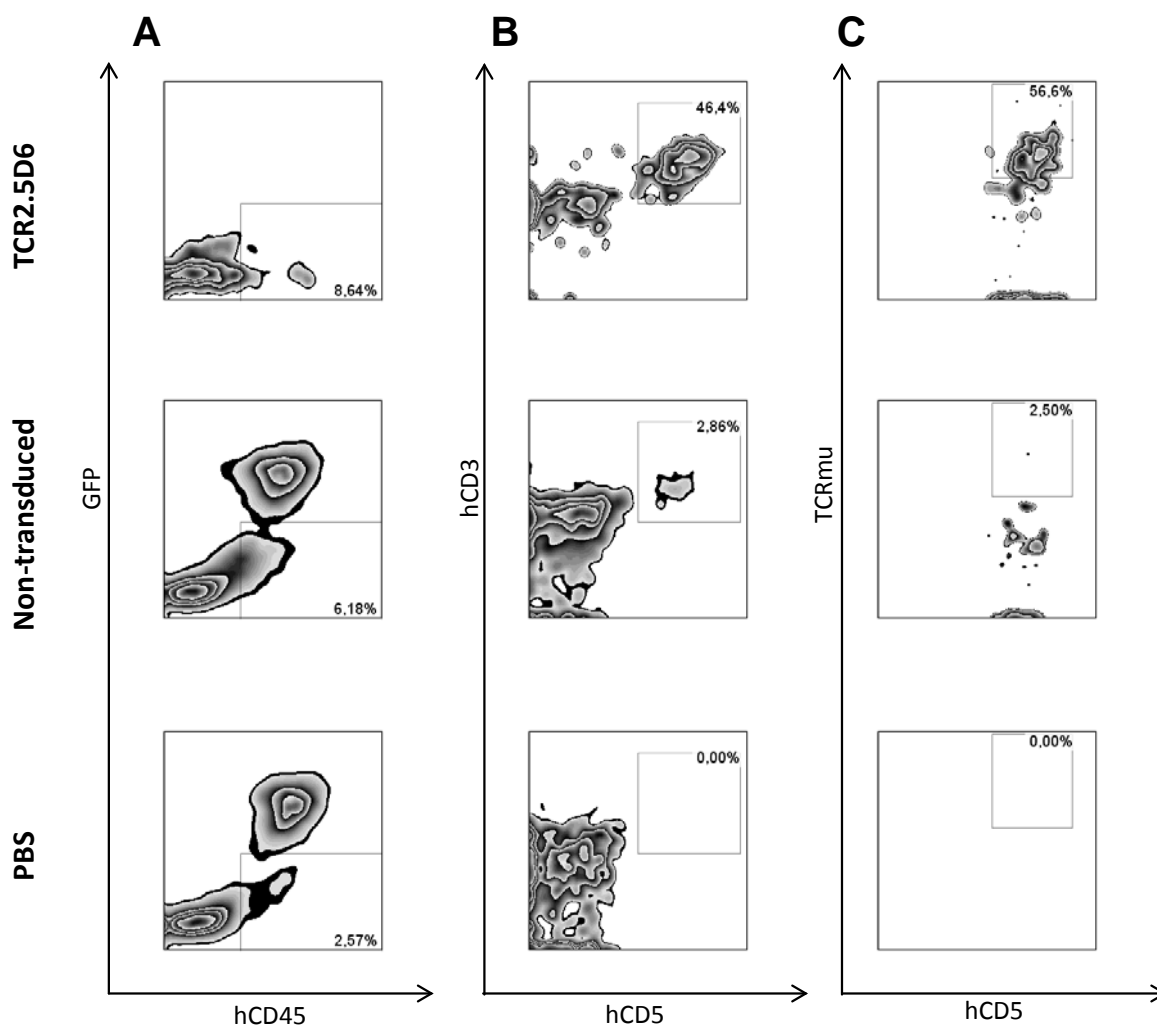


**Figure 17. Presence of TCR2.5D6 positive T cells in the tumor of i.v. injected mice.**

(A-C) Gating strategy shown on representative dot plots for ML2-B7GFP tumor of mice injected intravenously with TCR2.5D6 T<sub>CM</sub> (n=5), non-transduced T<sub>CM</sub> (n=5) or PBS (n=2). Cells were pre-gated for vital lymphocytes. Human T cells were further assessed by gating for (A) hCD45+GFP-followed by (B) hCD5+hCD3+ and (C) TCR2.5D6-transduced T cells were determined within the human T-cell population (hCD45+GFP-hCD5+hCD3+) by TCRmu+CD5+ cells.

To further confirm these observations we performed qPCR of gDNA extracted from single cell suspensions of ML2-B7 and ML2-WT tumors as well as spleen and lung after imaging. We detected copies of TCR2.5D6 in the ML2-B7 tumor, spleen and lung but not in the ML2-WT tumor (Figure 18A). Immunohistochemistry analyses of tumor sections showed necrotic areas within the ML2-B7 tumors but not within the ML2-WT tumors (Figure 18B). We detected high numbers of CD5+ and CD3+ T cells within the ML2-B7 tumors in the necrotic

as well as non-necrotic areas, whereas in ML2-WT tumors only few T cells were observed (Figure 18C).

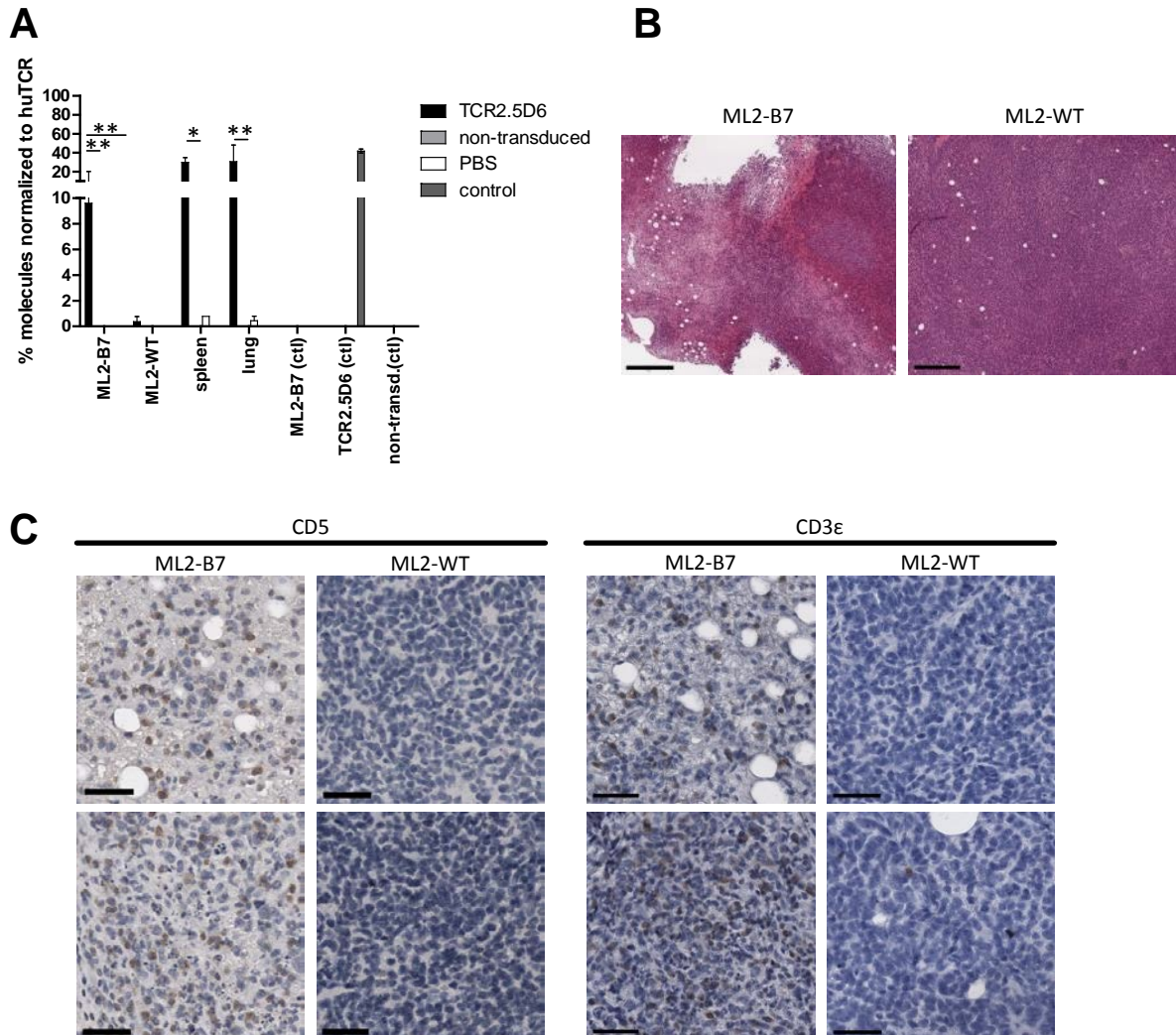


**Figure 18. Presence of aTCRmu positive T cells within ML2-B7 tumors analyzed ex vivo.**

(A) qPCR of the TCRmu gene using gDNA isolated from single cell suspensions of tumors and organs. gDNA of ML2-B7 and non-transduced  $T_{CM}$  were used as negative control, gDNA of freshly TCR2.5D6-transduced  $T_{CM}$  as positive control. Mean Percentage  $\pm$  s.d. of TCRmu molecules normalized to the number of human TCR (huTCR) molecules for TCR2.5D6-transduced T-cells (n=5), non-transduced T-cells (n=5), PBS (n=2) or controls (n=2) is depicted. Mann-Whitney Test: \* $p < 0.05$  \*\* $p < 0.01$  (B) H/E staining of ML2-B7 and ML2-WT tumors; bar=400 $\mu$ m. (C) Corresponding immunohistochemical CD5-staining and CD3 $\epsilon$ -staining of tumor-infiltrating T cells at two different areas of the ML2-B7 and ML2-WT tumor; bar=50 $\mu$ m. Immunohistochemistry and H/E staining were performed by Dr.Katja Steiger, Institut of Pathology, Klinikum rechts der Isar.



## 5.5 QUALITATIVE AND QUANTITATIVE EVALUATION OF T-CELL DISTRIBUTION BY $^{89}\text{Zr}$ -ATCRMU-F(AB')<sub>2</sub> PET-IMAGING

### 5.5.1 QUALITATIVE AND QUANTITATIVE EVALUATION OF $^{89}\text{Zr}$ -ATCRMU-F(AB')<sub>2</sub> SIGNALS IN ML2-B7 TUMORS

In depth analysis of all mice injected intravenously with TCR2.5D6 T<sub>CM</sub> (n=11) (section 5.4.8) revealed differences in distribution of  $^{89}\text{Zr}$ -aTCRmu-F(ab')<sub>2</sub> within ML2-B7 tumors. Based on this signal distribution and the tumor size at the day of imaging, we classified ML2-B7 tumors in three different groups (Figure 19A). Four mice showed a higher tumor burden and PET signal was detected mostly in the periphery around the ML2-B7 tumor (group I). Tumors of group II (n=4) showed medium tumor size and a high PET signal within the tumor-center. Mice classified in group III (n=3) demonstrated a small ML2-B7 tumor size with reduced signal intensities (Figure 19A). Although transduction rates of injected TCR2.5D6-transduced T<sub>CM</sub> were comparable (66,5% ±3,2%), the tumor volume differed in the groups at the days of T-cell injection (Figure 19B) with larger tumors in group I. Thus, this group represents treatment at a stage of advanced tumor size and tumor rejection by transgenic T-cells in an early phase at the day of imaging in comparison to groups II and III. These observations correlate to the tumor volume calculated by ROI analysis (Figure 20A) and the weight determined ex vivo at the day of imaging (Figure 20B). The total %ID in the tumor determined by ROI analysis was enhanced in tumors of group I compared to group II and III (Figure 20C). Analysis of %ID determined ex vivo revealed similar trends (Figure 20D). However, %ID/g was found to be the highest for tumors of group I and group II and reduced for group III tumors (Figure 20E). This observation correlates with the observed PET-signal density caused by different distribution patterns or T-cell hot spots. Taken together, using the  $^{89}\text{Zr}$ -aTCRmu-F(ab')<sub>2</sub> we classified groups which may reflect the dynamics of T-cell response against a tumor in vivo and resemble the different distribution patterns of T cells within these different rejection phases.

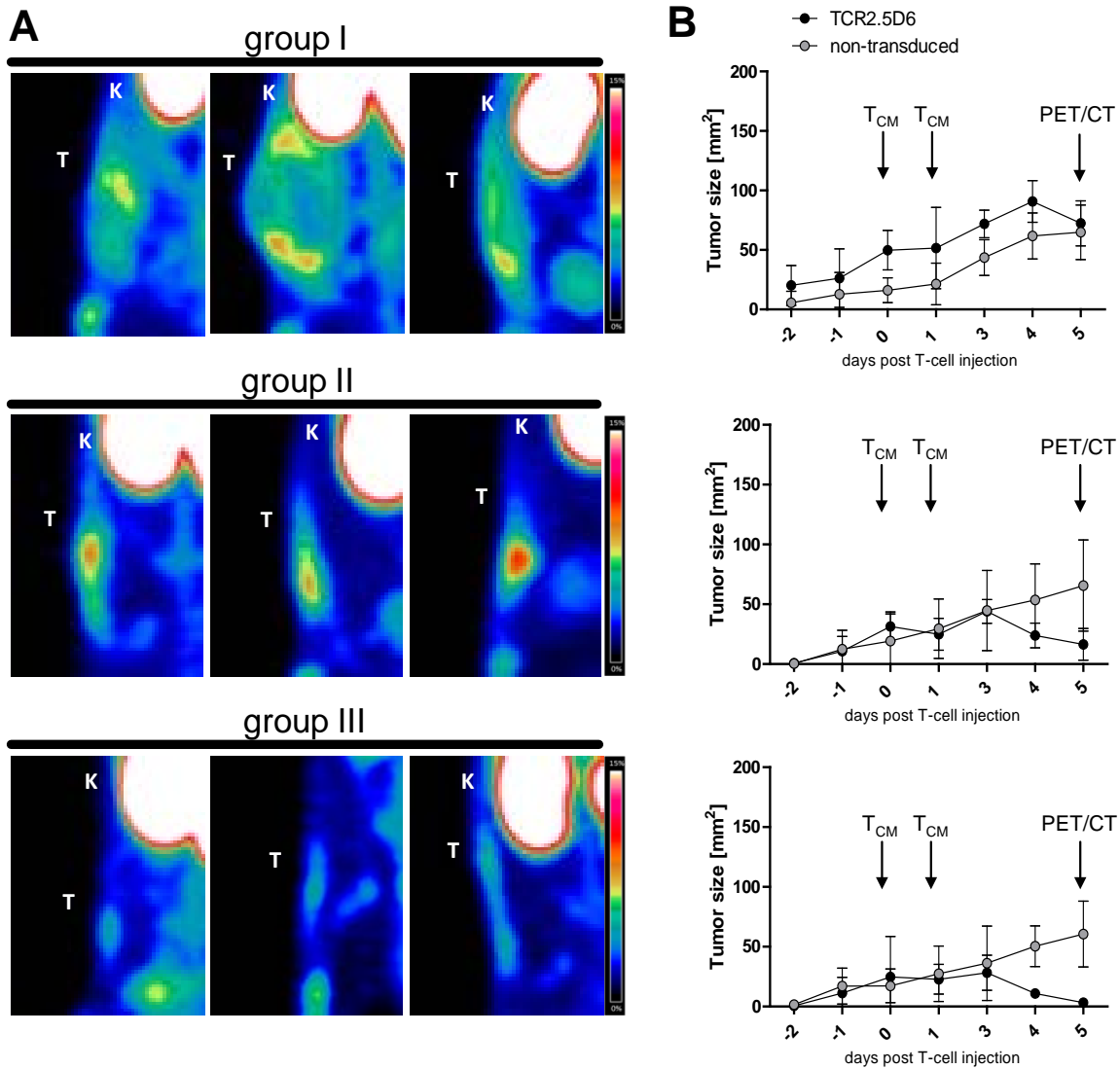


**Figure 19. Differential distribution of  $^{89}\text{Zr}$ -aTCRmu-F(ab')<sub>2</sub> signals within ML2-B7 tumors of mice injected with 2.5D6TCR-transgenic T<sub>CM</sub>.**

(A) Representative 3D-PET (MIP) pictures of ML2-B7 tumors 48h post intravenous injection of  $^{89}\text{Zr}$ -aTCRmu-F(ab')<sub>2</sub> are shown (experimental design in Figure 14A). Definition of tumor models in group I (n=4), group II (n=4) and group III (n=3) depending on PET signal distribution and tumor size are shown. Scale bar = 0-15%ID/g; T=Tumor; K=Kidney. (B) ML2-B7 tumor development in mice injected with TCR2.5D6-transduced T<sub>CM</sub> or non-transduced T<sub>CM</sub> according to the classification within group I, group II and group III. Tumor size in mm<sup>2</sup> at indicated days post T<sub>CM</sub> injection is depicted. Arrows indicate the days of T<sub>CM</sub> injection and PET/CT imaging. Data of 3 experiments are combined and include animals treated with TCR2.5D6 T<sub>CM</sub> (n=11) and non-transduced T<sub>CM</sub> (n=11).

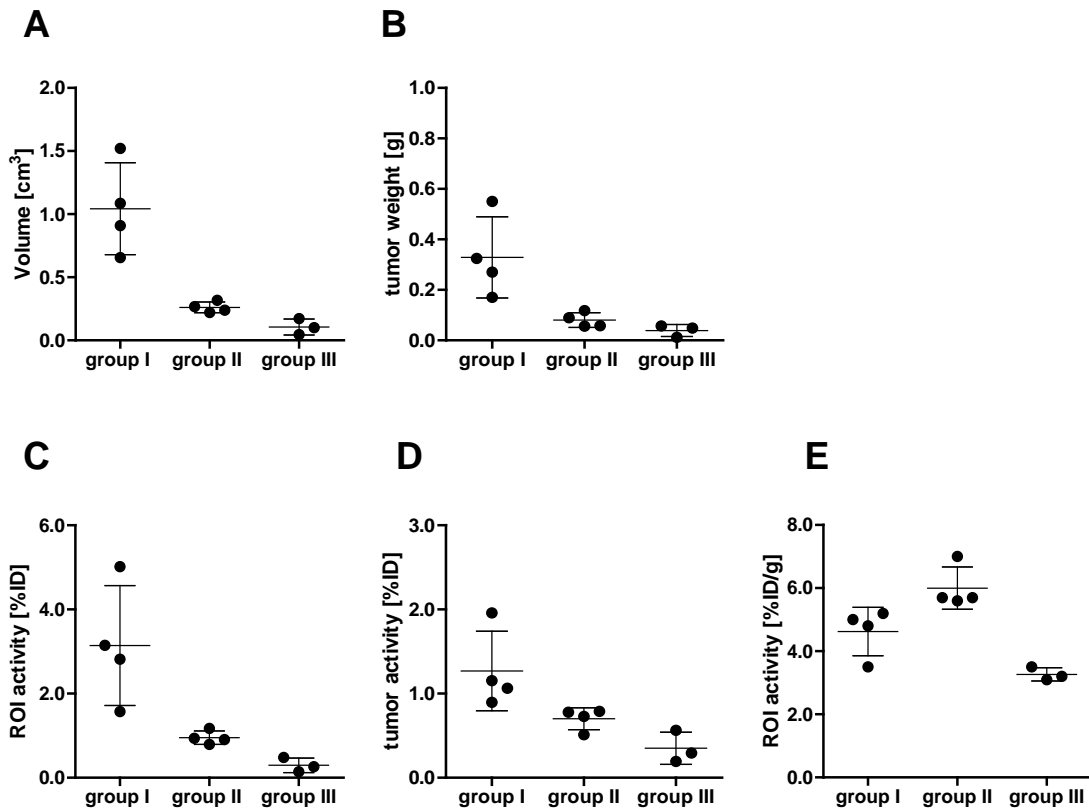


**Figure 20. Analysis of tumor volume and  $^{89}\text{Zr}$ -aTCRmu-F(ab')<sub>2</sub> uptake in ML2-B7 tumors according to the classification into group I-III.**

(A) Tumor volume determined by image based ROI analysis of PET/CT images 48h post injection of  $^{89}\text{Zr}$ -aTCRmu-F(ab')<sub>2</sub>. Mean  $\pm$  s.d. of cm<sup>3</sup> of defined ROI is shown. (B) Tumor weight of ML2-B7 tumors determined ex vivo after PET/CT imaging. Mean  $\pm$  s.d. of ML2-B7 tumor weight in grams is depicted. (C) Quantitative analysis of PET-signal of ML2-B7 tumors according to group classification. Mean  $\pm$  s.d. of %ID of defined ROI is depicted. (D) Determination of ex vivo uptake of ML2-B7 tumors. Mean  $\pm$  s.d. of %ID is depicted. (E) Quantitative analysis of PET/CT images of ML2-B7 tumors according to group classification. Mean  $\pm$  s.d. of %ID/g of defined ROI is depicted. (A-E) Data of 3 experiments are combined and include animals treated with TCR2.5D6 T<sub>CM</sub> (n=11).

### 5.5.2 HETEROGENEOUS T-CELL DISTRIBUTION DETECTED BY $^{89}\text{Zr}$ -ATCRMU-F(ab')<sub>2</sub> PET IMAGING

To confirm the results shown in section 5.5.1, we performed PET/CT imaging of TCR2.5D6-transduced and non-transduced T<sub>CM</sub> injected into NSG-mice bearing ML2-B7 and ML2-WT tumors of different sizes at the day of T<sub>CM</sub> injection. To resemble tumors of group I, mice were injected subcutaneously with ML2-B7 on the right flank and ML2-WT on the left flank 10 days before T<sub>CM</sub> injection. Mice of group II or group III were injected either on 8 or 6 days prior T<sub>CM</sub> treatment. TCR2.5D6-transduced or non-transduced T<sub>CM</sub> were injected intravenously on two consecutive days after low dose total body irradiation. To determine metabolic activity of tumors,  $^{18}\text{F}$ -FDG-PET/CT imaging was performed before  $^{89}\text{Zr}$ -aTCRmu-F(ab')<sub>2</sub> was injected intravenously. Overview of the experimental setup is shown in Figure 21A. Compared to group II and group III demonstrating a strong tumor rejection, mice of group I showed reduced tumor cytotoxicity resulting in a plateau of tumor growing kinetics at day 5 post T<sub>CM</sub> injection (Figure 21B). On the other site, ML2-B7 tumors of mice injected with non-transduced T<sub>CM</sub> did not show any change in tumor growth after T<sub>CM</sub> injection in all groups (Figure 21B). ML2-WT tumors showed the same growing rates for every group independent if TCR2.5D6 transgenic or non-transduced T<sub>CM</sub> were injected (Figure 21C). Figure 21D shows the direct comparison of ML2-B7 tumor growing kinetics of tumors for group I to group III. Comparison of tumor volume determined by caliper- and  $^{18}\text{F}$ -FDG measurements at the same day revealed comparable results (Figure 21E).

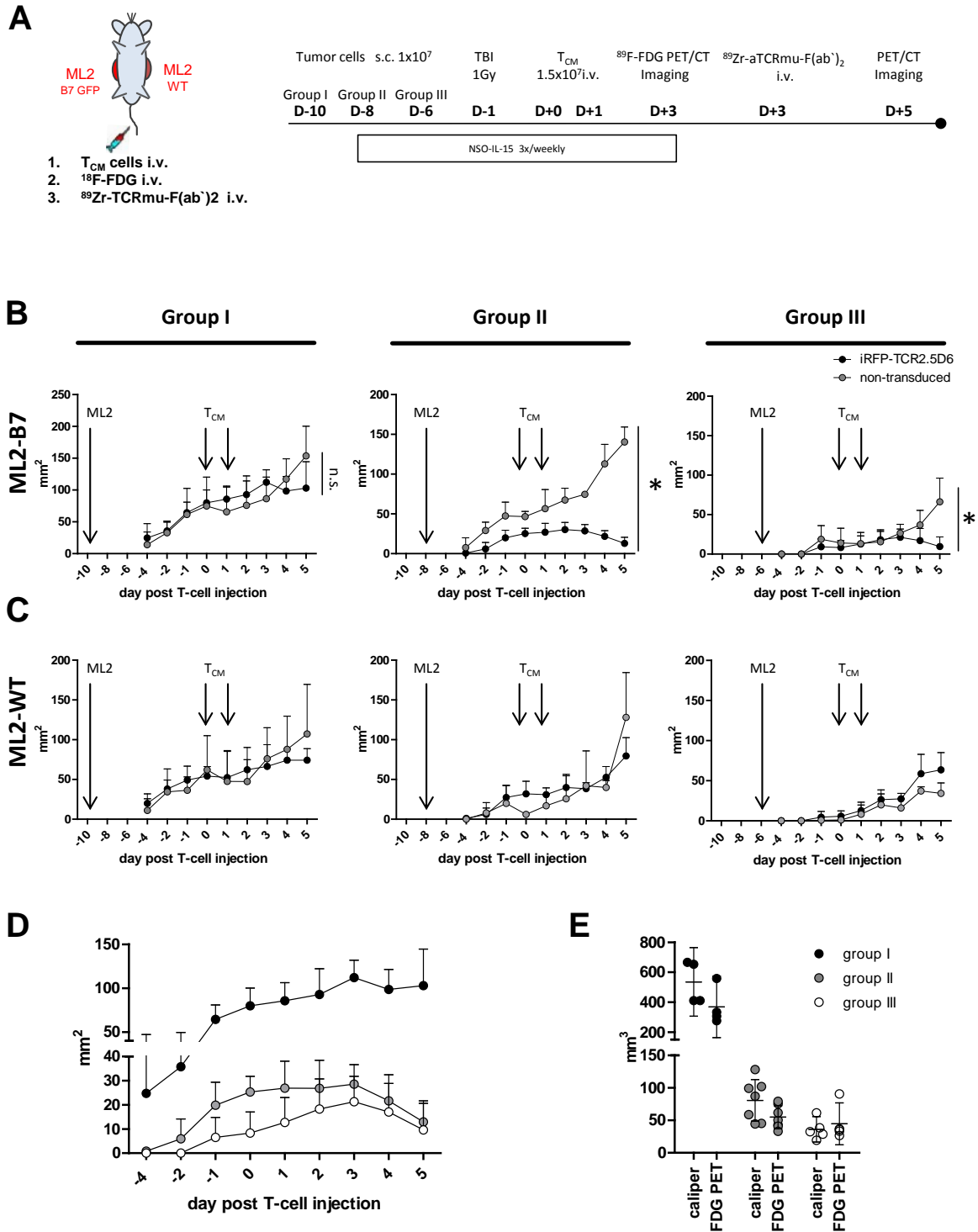


**Figure 21. Growing kinetics of ML2 tumors of different size before and after intravenous injection of TCR2.5D6-transduced or non-transduced  $T_{CM}$ .**

(A) Overview of the experimental setting: NSG-mice were inoculated with  $1 \times 10^7$  ML2-B7 cells subcutaneously into the right and ML2-WT cells into the left flank on different time points as indicated. Tumor bearing mice were total body irradiated (TBI) and intravenously injected with  $1.5 \times 10^7$  TCR2.5D6-transduced  $T_{CM}$  or non-transduced  $T_{CM}$  on two consecutive days. Two days later,  $^{18}F$ -FDG-PET/CT was performed followed by injection of  $^{89}Zr$ -aTCRmu-F(ab')<sub>2</sub>. PET/CT imaging was performed 48h post injection of  $^{89}Zr$ -aTCRmu-F(ab')<sub>2</sub>. (B-C) Tumor

volume of (B) ML2-B7 and (C) ML2-WT at indicated days post  $T_{CM}$  injection is shown for tumors of the 3 different groups. Mean  $\pm$  s.d. of tumor size is indicated in  $mm^2$ ; Mann-Whitney test: \* $p < 0.05$ ; n.s.= not significant (D) Tumor volume of ML2-B7 at indicated days post injection of TCR2.5D6 transduced  $T_{CM}$  is shown for tumors of the 3 different groups. Mean  $\pm$  s.d. of ML2-B7 tumor size in  $mm^2$  of mice injected with TCR2.5D6  $T_{CM}$  and classified into group I-III is depicted. (E) Tumor volume of ML2-B7 tumors classified in indicated groups at day 3 post T-cell injection. Mean  $\pm$  s.d. of  $mm^3$  either determined by caliper measurement or by  $^{18}F$ -FDG ROI determination is depicted. (B-E) Data are shown for  $n=4$  mice classified in group I,  $n=7$  classified in group II and  $n=5$  classified in group III and injected with TCR2.5D6 transduced  $T_{CM}$  and  $n=3$  mice injected with non-transduced  $T_{CM}$  and classified in group I, group II and group III .

PET imaging two days post  $T_{CM}$  injection showed a homogenous uptake of  $^{18}F$ -FDG within both ML2-WT and ML2-B7 tumors and no indication for necrotic areas were detectable by PET/CT imaging (Figure 22A). However,  $^{89}Zr$ -aTCRmu-F(ab')<sub>2</sub> imaging of mice injected with TCR2.5D6-transgenic  $T_{CM}$  revealed different signal distribution patterns within the different groups of tumors. Group I tumors showed a  $^{89}Zr$ -aTCRmu-F(ab')<sub>2</sub> signal distribution located on the tumor border combined with different local densities of T cells. Tumors of group II and group III showed a  $^{89}Zr$ -aTCRmu-F(ab')<sub>2</sub> signal at the tumor center, which is reduced for tumors of group III (Figure 22A). The total %ID in the tumor determined by image based ROI analysis was enhanced in tumors of group I compared to group II and III (Figure 22B) corresponding to tumor volume determined by caliper measurement at the day of imaging (Figure 22C). However, %ID/g quantification of the  $^{89}Zr$ -aTCRmu-F(ab')<sub>2</sub> signal by image based ROI analysis showed no significant differences in uptake for tumors of group I, group II or group III (Figure 22D), although a slightly reduced %ID/g for group III tumors was detectable.

Taken together, differences in signal distribution of T cells depending on tumor size and rejection phase as described in section 5.5.1 were confirmed. Furthermore,  $^{18}F$ -FDG-PET imaging revealed a homogenous uptake within the tumor indicating that necrosis is not involved in the observed differential distribution pattern shown by  $^{89}Zr$ -aTCRmu-F(ab')<sub>2</sub> imaging for tumors of group I. Furthermore, quantification of %ID revealed clear differences between groups whereas the %ID/g quantification method did not show any significant differences in uptake. These observations suggest that, within this setting, a combination of

different quantification analysis such as total %ID as well as weight adapted quantification (%ID/g) are important to represent T cell distribution within the tumor.

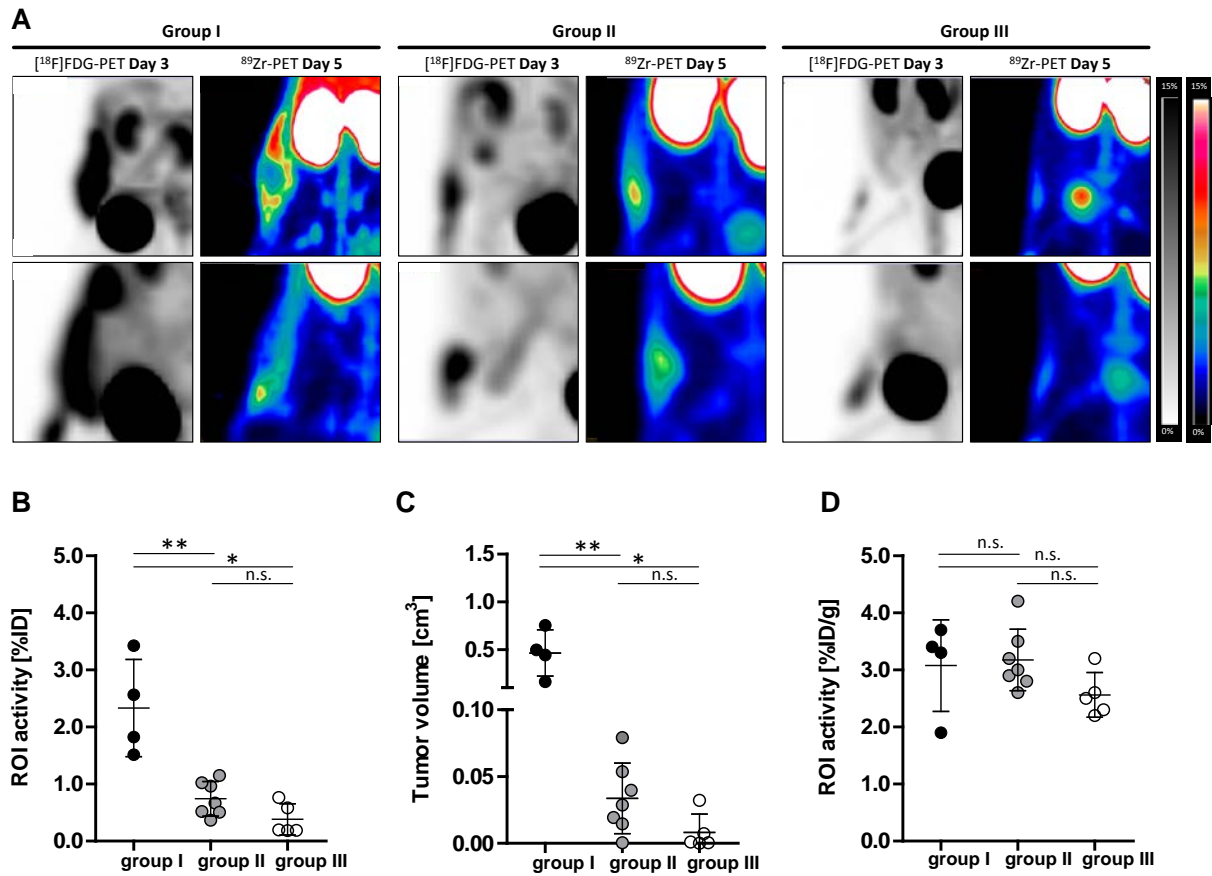


**Figure 22. Differential distribution of  $^{89}\text{Zr}$ -aTCRmu-F(ab')<sub>2</sub> signals within ML2-B7 tumors of mice injected with 2.5D6TCR-transgenic T<sub>CM</sub> in comparison to  $^{18}\text{F}$ -FDG imaging.**

(A) Representative 3D-PET (MIP) pictures of ML2-B7 tumors classified in group I-III and analyzed by  $^{18}\text{F}$ -FDG-PET (inverted gray scale panels) three days after injection of TCR2.5D6-T<sub>CM</sub> and  $^{89}\text{Zr}$ -aTCRmu-F(ab')<sub>2</sub> (colored panels) five days after injection of TCR2.5D6-T<sub>CM</sub> (experimental design is shown in Figure 21A). Representative data of two animals derived from group I (n=4), group II (n=7) and group III (n=5) are shown. Scale bar = 0-15%ID/g for  $^{18}\text{F}$ -FDG and  $^{89}\text{Zr}$ -aTCRmu-F(ab')<sub>2</sub>. T=tumor, B=bladder, K=kidney. (B) Image based quantitative analysis of PET-signal of ML2-B7 tumors according to group classification. Mean  $\pm$  s.d. of %ID of defined ROI is depicted. (C) ML2-B7 tumor volume at the day of  $^{89}\text{Zr}$ -aTCRmu-F(ab')<sub>2</sub> imaging according to group classification. Mean  $\pm$  s.d. of cm<sup>3</sup> determined by caliper measurement is shown. (D) Quantitative analysis of PET-signal of ML2-B7 tumors according to group classification. Mean  $\pm$  s.d. of %ID/g of defined ROI is depicted. (B-D) Mann-Whitney test: \*p<0.05; \*\*p<0.01; n.s.= not significant

### 5.5.3 MAPPING OF T-CELL DISTRIBUTION AT THE TUMOR SITE BY $^{89}\text{Zr}$ -ATCRMU-F(AB')<sub>2</sub> PET IMAGING

The differential distribution patterns detected by PET/CT imaging were validated by immunohistochemistry of tumor sections on different axial levels (Figure 23). We detected intra- and inter-sectional heterogeneity of CD3-positive T-cell infiltrations within the tumors of group I validating the previous observations from PET/CT imaging. For deeper correlation analysis, these tumor sections were co-localized to the respective axial imaging levels (Figure 23A-B). The intra-sectional T-cell heterogeneity was mapped by semiquantitative analysis of T-cell infiltration within predefined areas and showed correlation of distribution patterns to respective PET-imaging levels (Figure 23B-D).

Analysis of group II tumors showed a strong and uniform T-cell distribution within the tumor detected by immunohistochemistry and immunohistochemistry-based semi-quantitative analysis of the T-cell infiltration. This uniform distribution correlates again to PET images at respective axial level (Figure 23A-D).

Taken together, using  $^{89}\text{Zr}$ -aTCRmu-F(ab')<sub>2</sub> PET/CT imaging enables to map the differential distribution of T-cell infiltrations within the tumor and thereby classification of different tumor rejection phases reflecting the dynamics of T-cell response of TCR-transgenic T cells in this model.



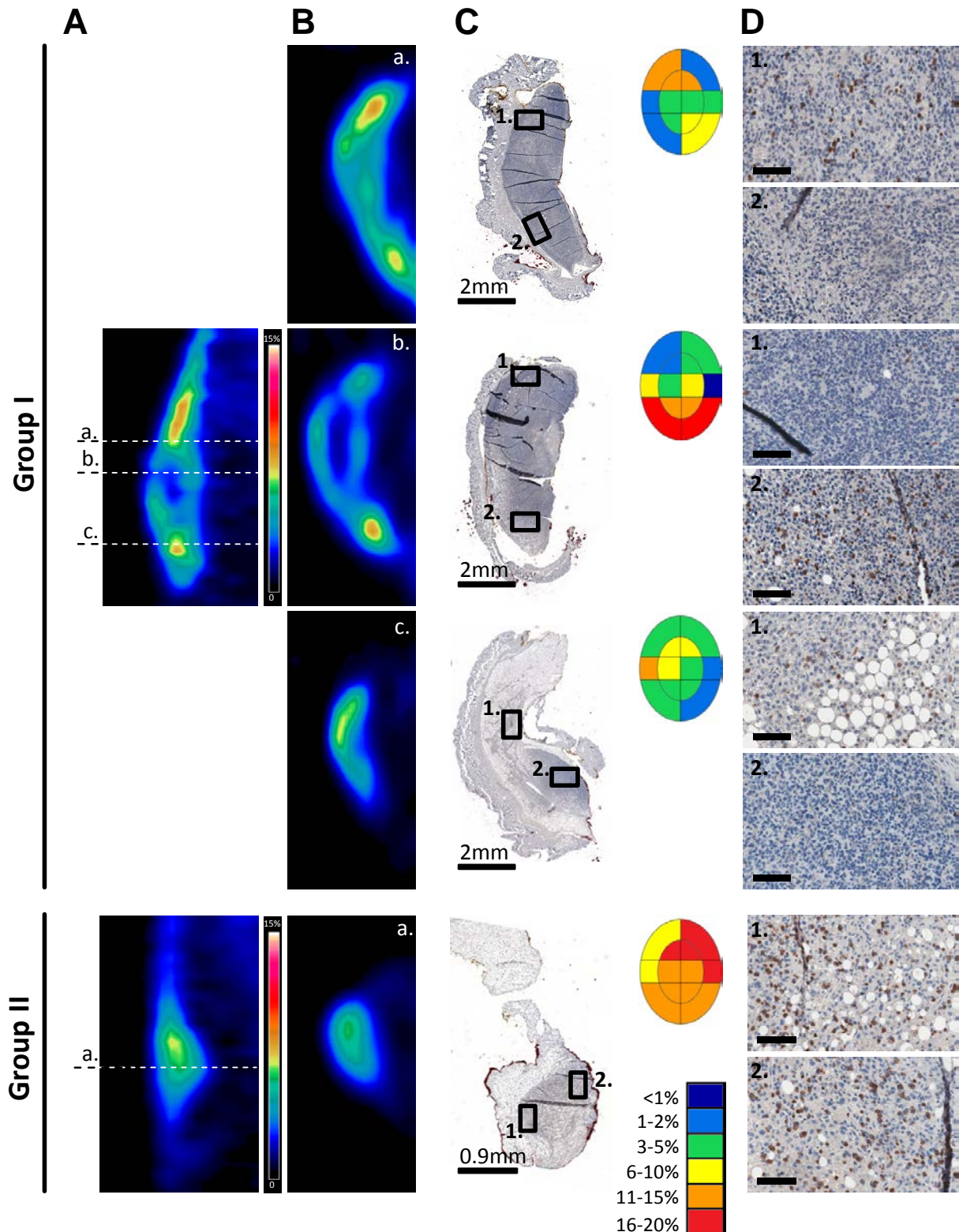


**Figure 23.** T-cell imaging by PET/CT using  $^{89}\text{Zr}$ -aTCR $\mu$ -F(ab') $_2$  facilitates mapping of T cells within ML2-B7 tumors of mice injected with TCR2.5D6-transgenic  $T_{\text{CM}}$ .

(A) Coronal PET image of a representative ML2-B7 tumor of mice injected with TCR2.5D6 transgenic  $T_{\text{CM}}$  classified into group I (upper part) or group II (lower part). Dotted lines, a., b., and c. show the position of corresponding axial PET images depicted in (B). Scale bar = 0-

15%ID/g. (C) Heterogeneous CD3<sup>+</sup> T-cell infiltration within ML2-B7 tumor sections corresponding to the respective axial PET images. Immunohistochemistry of CD3<sup>+</sup> T cells within ML2-B7 tumor sections is depicted. Differential CD3-positive T-cell distribution within respective tissue section was mapped by plotting the percentage of T-cell infiltration in pre-defined areas using a colored code as shown in the figure. Bar=2mm or 0.9mm as indicated in the figure. (D) Magnification of ML2-B7 tumor areas showing differential intra-sectional heterogeneity of T-cell infiltration. Localization of magnification areas is indicated by indicated numbers corresponding to marked areas of tumor sections shown in (C). Bar=100 $\mu$ m. (C-D) Immunohistochemistry and immunohistochemistry-based semi-quantitative T-cell quantification were performed by Dr. Katja Steiger and Dr. Melanie Straub, Institute of pathology, Klinikum rechts der Isar.

## 6 DISCUSSION

### 6.1 MONITORING OF TCR TRANSGENIC T-CELLS BY IMMUNO-PET

Imaging of T-cells currently becomes an important focus of research as adoptive T-cell therapies emerge to an effective novel treatment option in diverse malignant diseases (Morgan, Dudley et al. 2006; Johnson, Morgan et al. 2009; Robbins, Morgan et al. 2011; Robbins, Kassim et al. 2015). Clinically applicable imaging technologies for TCR-modified T cells are considered to be critical for an improved comprehension of pharmacodynamics and pharmacokinetics in the clinical context of immunotherapy. Moreover, development of clinically applicable imaging modalities may help to understand efficacy and toxicity of these novel therapeutic approaches. Monitoring of the in vivo behaviour of such genetically modified T cells in preclinical models are important to understand mechanisms of effective tumor rejection or evasion as well as mechanisms involved in potential adverse effects. Indeed, some TCR have demonstrated high toxicity with even fatal outcome in early clinical trials (Linette, Stadtmauer et al. 2013; Morgan, Chinnasamy et al. 2013). The reasons for observed and suspected autoreactivity can be diverse. Many tumor-associated antigens are not restrictedly expressed in the tumor complicating the isolated elimination of tumor cells (Cheever, Allison et al. 2009). Furthermore, in case of TCR-transgenic T cells, introduced TCR chains can form mixed heterodimers with the endogenous TCR and these mispaired TCR have been shown to bear autoreactive capacity (Bendle, Linnemann et al. 2010). Recently, it has been proposed to reduce the expression of endogenous TCR chains and to achieve a site directed integration of transferable TCR chains by the usage of zinc finger nucleases (Provasi, Genovese et al. 2012) or by using TALEN-mediated editing of the endogenous TCR combined with lentiviral transduction of the TCR (Berdien, Mock et al. 2014). However, these technologies require a multistep procedure of gene transfer and cell sorting including long-term T cell culturing, which is highly demanding for clinical application. As another option to reduce mispairing and enhance expression of introduced TCR, exchange of human constant TCR domains by the murine counterparts and introduction of a second disulfide bond were developed (Cohen, Zhao et al. 2006; Cohen, Li et al. 2007; Kuball, Dossett et al. 2007). We also optimized the TCR2.5D6 by codon optimization, murinization of the constant domains and introduction of a second disulfid bond (Klar, Schober et al. 2014). This TCR 2.5D6 was

retrovirally transduced into T<sub>CM</sub> and used for the development of a specific in vivo imaging model for transgenic T-cells.

The establishment of imaging modalities for specific tracking of T cells modified by a specific immunoreceptor, e.g. CAR or TCR, are intensively investigated (Roszik, Rabinovich et al. 2011; Griessinger, Maurer et al. 2015; McCracken, Vatakis et al. 2015). To monitor real time survival, distribution and anti-tumor responses of T cells in vivo, non-invasive in vivo imaging is the model of choice. Imaging modalities which are broadly applicable and do not have an impact on engraftment, viability, proliferation, cellular function or malignant transformation of the tracked cells are mostly desirable. Several approaches use direct labeling of T cells as <sup>64</sup>Cu-PTSM labeling (Adonai, Nguyen et al. 2002; Griessinger, Kehlbach et al. 2014), labeling with <sup>18</sup>F-FDG (Eriksson, Sadeghi et al. 2011), <sup>99m</sup>Tc-HMPAO or <sup>111</sup>In-oxiquinolone (Botti, Negri et al. 1997) or labeling with gold-nanoparticles coupled to <sup>64</sup>Cu (Bhatnagar, Li et al. 2013). However, direct labeling results often in an impact on viability, proliferation or cytotoxic function of T cells (Botti, Negri et al. 1997; Griessinger, Kehlbach et al. 2014). Moreover, for <sup>64</sup>Cu-PTSM labeling was shown that the amount of double strand breaks in T cells correlates with the radioactive dose used (Griessinger, Kehlbach et al. 2014). In addition, longitudinal tracking of labeled T cells is challenging due to label dilution by proliferation of the cells. Thus, this method might be not ideal for understanding the therapeutic efficacy as T-cell engraftment mainly requires a longer time period and changes of in vivo biodistribution might be detectable at later time points. Furthermore, false positive results from labeled dead cells cannot be excluded. Reporter-gene imaging circumvents the dilution of the tracer and therefore allows serial imaging but needs genetic manipulation of T cells resulting in enhanced mutational risk. Recently, a novel highly attractive approach has been published using hdCK3mut as additional transgene for tracking of TCR-transgenic T cells (McCracken, Vatakis et al. 2015). This approach is independent of the construct and may be similarly applied for CAR- and TCR-modified effector cells. Moreover, long-term functionality of transgenic effector cells has been demonstrated in vitro. However, the functional properties of T cells with and without the additional reporter gene have not been directly compared in this study. A very low cell number of TCR-hdCK3mut-positive T cells was detected after HSC engraftment and authors could not clarify if this might be due to influence of the reporter gene or due to negative thymic selection and therefore it remains unknown if constitutive expression of hdCK3mut in cells does lead to impaired T cell function or not. In this work all

cell types originating from transduced HSC will express the reporter gene and therefore macrophages or myeloid derived suppressor cells cannot be distinguished from T cells at the tumor site. Another disadvantage of reporter-gene imaging is the role of the metabolic stage of cells which influences the reporter-gene expression and therefore the accumulation of PET probe within the cell (Shu, Guo et al. 2005). This leads to loss of imaging sensitivity. The PET reporter probe used for detection of hdCK3mut positive T cells ( $^{18}\text{F}$ -FMAU) is a thymidine analog and will be phosphorylated by thymidine kinases which can cause background in replicating organs such as tumors (Tehrani, Muzik et al. 2007; Jadvar, Yap et al. 2012). Indeed, our  $^{89}\text{Zr}$ -F(ab')<sub>2</sub> PET-imaging showed a much higher signal to noise ratio compared to this work (Table 32). Moreover, hdCK3mut is a mutated gene being potentially immunogenic in vivo. These problems are also present for other reporter genes as HSV1-tk (Dubey, Su et al. 2003; Koehne, Doubrovin et al. 2003; Kim, Dubey et al. 2004; Dobrenkov, Olszewska et al. 2008; Dotti, Tian et al. 2009; Shu, Radu et al. 2009; Yaghoubi, Jensen et al. 2009). The human norepinephrine receptor (hNET) (Doubrovin, Doubrovina et al. 2007) or human sodium-iodine symporter (hNIS) (Penheiter, Russell et al. 2012) are from human origin and might be not immunogenic. However, high background in organs with physiological expression of the defined gene may be prominent. Furthermore, the size of the transgene may limit the applicability of this approach, as hNET or hNIS consists of around 2000bp on the genomic level. Linked to a TCR, these constructs will be not easy to introduce into a human T cell using retro-or lentiviral vector systems. However, alternative systems such as transposon-based vectors might improve expression of such fusion-genes of big size (Huang, Guo et al. 2008; Manuri, Wilson et al. 2010; Nakazawa, Huye et al. 2011).

In vivo tracking of T cells by PET imaging using specific antibodies (Immuno-PET) might be an alternative option for specific and longitudinal imaging of adoptively transferred T-cells. T-cell targets such as CD4 and CD8 were previously used for in vivo monitoring by Immuno-PET and are discussed in detail in section 6.2. However, for monitoring adoptive T-cell therapies there is evident need to distinguish between TCR-engineered and non-transduced transferred T-cells in vivo. One recent study used an antibody specifically binding to murine T-cell populations with monospecificity (cOVA-TCR-Tg-TH1 cells or Tag2-TCRtg-Tcells) (Griessinger, Maurer et al. 2015). However, as these antibodies target one specific TCR, this tracking method is not generally applicable. Furthermore, the cells were labeled in vitro before intravenous injection and therefore, imaging was shown only for 24h and 48h post

injection which might be too short for monitoring of immunotherapies in vivo. We used the approach to track TCR-transgenic T cells by directly targeting the transgene. Therefore, we used the murinized constant domains introduced as a general optimization strategy as specific target. The aTCRmu antibody (Kubo, Born et al. 1989) and its F(ab')<sub>2</sub> fragment bind specifically to the murine constant TCR beta domain of the TCR. Therefore, this approach can be applied for any TCR independent of the defined specificity in case that the distinct murine epitope is present. For proof of concept, we used T<sub>CM</sub> transduced with TCR2.5D6 specifically recognizing a peptide derived from MPO (Klar, Schober et al. 2014) in a novel myeloid sarcoma model. We showed specific binding of the TCRmu antibody to 2.5D6TCR-transduced T<sub>CM</sub> confirmed by multimer binding. As a model tumor target, we used the AML cell line ML2, which expresses MPO endogenously. We additionally transduced this cell line with HLAB\*07:02 (ML2-B7), the restriction element required for recognition by TCR2.5D6. We observed high cytotoxic reactivity of TCR2.5D6-transduced T<sub>CM</sub> against this cell line in vitro as well as in vivo. These results suggest this model highly suitable for the monitoring of TCR-transgenic T-cells during tumor rejection by non-invasive imaging.

The in vivo specificity of the aTCRmu antibody was verified on EL4-tumors, a murine T-lymphoma cell line which expresses endogenously murine TCRs. Specific tracking of human TCR2.5D6-transgenic T<sub>CM</sub> injected directly into the tumor or systemically by intravenous injection was shown in a xenogenic mouse model with subcutaneously established myeloid sarcomas. Using this method we were able to observe a clear signal discrimination at the tumor site by PET imaging confirmed by ex vivo analysis with an over tenfold increase in the tumor to blood ratio.

## 6.2 FUNCTIONALITY OF T CELLS AFTER TCRMU-LABELING AND DEVELOPMENT OF TCRMU-F(AB')<sub>2</sub>

The usage of the primary transgene for labeling allows omission of additional reporter genes or ex vivo labeling of T cells. However, in the setting of Immuno-PET imaging, definition of the target for T-cell tracking needs to be evolved very carefully, as the in vivo application of several antibodies showed depletion or loss of functionality for T cells shown for anti-CD2 or anti-CD3 antibodies (Bromberg, Chavin et al. 1991; Guckel, Berek et al. 1991; Bemelmans, Abramowicz et al. 1994; Przepiorka, Phillips et al. 1998; Carpenter, Pavlovic et al. 2000; Chatenoud 2003; Li, Wang et al. 2005; Abraham, Karni et al. 2008; Shiheido, Chen et al. 2014). CD8 and CD4 were used as targets for endogenous T-cell tracking in vivo using <sup>111</sup>In-,

<sup>89</sup>Zr- or <sup>64</sup>Cu-labeled antibodies or antibody fragments (Kanwar, Gao et al. 2008; Tavare, McCracken et al. 2014; Tavare, Escuin-Ordinas et al. 2015; Tavare, McCracken et al. 2015). However, functional impact of labeling was not addressed in these studies. The aTCRmu-IgG has been already demonstrated to modulate murine T-cell function in vitro and in vivo (Kubo, Born et al. 1989; Nishimura, Eto et al. 1994; Drobyski and Majewski 1996; Kummer, Zengerle et al. 2001). We similarly observed functional modulation and partial depletion of human TCR-transgenic T cells by the aTCRmu-IgG but not by the F(ab')<sub>2</sub> fragment in vitro and in vivo (work from Ricarda Wagner, data not shown). In contrast, another study reported about functional modulation of T cells by the F(ab')<sub>2</sub> fragment (Henrickson, Reid et al. 1995). Differences in purity or dosages may contribute to these discrepancies. In fact, an over tenfold higher amount of F(ab')<sub>2</sub> was used for in vivo application in this study. Nevertheless, this needs to be carefully evaluated in future studies. Such properties may be useful for directed effector-cell depletion especially if unacceptable toxicity is mediated by TCR-transgenic T cells and could be analyzed for the use of a potential suicide mechanism. However, functional modulation and partial depletion of T cells alone are not enough for reasonable suicide mechanism as this effect might be too slow in case of severe toxicities. Therefore, a conjugation with a toxin to create an active immunotoxin as shown for anti-CD3 antibodies (Neville, Scharff et al. 1992; Weetall, Digan et al. 2002) and others (Flavell, Warnes et al. 2000; van Oosterhout, van Emst et al. 2000) might be a possibility and need to be further evaluated. An alternative or additive possibility for depletion of TCR-transgenic T cells by the antibody is the usage of toxic radiotracers (McDevitt, Finn et al. 1999; Gordon, Witzig et al. 2004; Gorin, Guilloux et al. 2014). However, a potential role of antibody-dependent cytotoxicity (ADCC) or complement dependent cytotoxicity (CDC) as shown to be a major mechanism of depletory antibodies (van Meerten, van Rijn et al. 2006) was so far not investigated in detail by our studies. For isolated imaging purposes, however, functional modulation of TCR-transgenic T cells is disadvantageous suggesting the aTCRmu-F(ab')<sub>2</sub> to be favorable for our purposes.

Using the <sup>89</sup>Zr-aTCRmu-IgG for in vivo imaging, we additionally detected a high background binding to the ML2-WT and ML2-B7 cells. We detected FcR-expression on the tumor cells and demonstrated that blocking of these receptors leads to a strongly reduced binding of the aTCRmu-IgG in vitro. These observations suggest an unspecific binding of the aTCRmu-IgG to ML2 cells. Therefore, we hypothesized that F(ab')<sub>2</sub> fragment of the aTCRmu-antibody,

which is depleted from the Fc-portion, might reduce unspecific binding as well as functional impairment of the transgenic T cells. As the F(ab')<sub>2</sub> fragment of the aTCRmu antibody has been previously proposed to be suitable for microscopic T-cell imaging (Crites, Chen et al. 2012), we produced the F(ab')<sub>2</sub> fragment by pepsin digestion and protein-A purification and labeled it with <sup>89</sup>Zr for in vivo imaging. Using the <sup>89</sup>Zr-aTCRmu-F(ab')<sub>2</sub>, we did not detect any unspecific binding to non-transduced T<sub>CM</sub>, ML2-WT, ML2-B7 or to other organs in PET/CT imaging, as shown for mice receiving non-transduced T<sub>CM</sub> or PBS. The labeling with the <sup>89</sup>Zr-aTCRmu-F(ab')<sub>2</sub> provided a distinct and clear signal at the ML2-B7 tumor site of mice injected with TCR2.5D6-transduced T<sub>CM</sub> and this was validated by biodistribution and autoradiography. Furthermore, we confirmed the presence of specific T-cells by flow cytometry and qPCR.

### 6.3 <sup>89</sup>ZIRCONIUM - AN IDEAL RADIONUCLIDE FOR T-CELL IMAGING?

In addition to the targeting device, choice of the nuclear tracer is of particular importance with the need to combine safety and quality properties. We used <sup>89</sup>Zr for radioactive labeling of the aTCRmu-IgG and F(ab')<sub>2</sub> fragments. <sup>89</sup>Zr is one of the most promising metallo-radionuclides for developing new immuno-PET agents for in vivo imaging of cancer and several <sup>89</sup>Zr-labeled antibodies entered already pre-clinical and clinical studies (Borjesson, Jauw et al. 2006; Perk, Visser et al. 2006; Borjesson, Jauw et al. 2009; van de Watering, Rijpkema et al. 2014). The physical decay properties of <sup>89</sup>Zr (Table 2) are ideally suited for usage in the design of full antibody or F(ab')<sub>2</sub> fragment-based radiotracers which present slow blood clearance and extended in vivo circulation times for optimal biodistribution (Verel, Visser et al. 2003). In fact, specific signals were more distinct after 48h compared to 24h suggesting an optimal match between half-life of the tracer and biodistribution of full antibodies or F(ab')<sub>2</sub> fragments at this time point. However, later time points up to 6 days may still provide significant information and need to be investigated. Compared to other radionuclides as e.g. <sup>64</sup>Cu having a shorter half-life (Table 2), this might be an important advantage resulting in highly specific signals. In addition, <sup>89</sup>Zr labeling may have advantages in comparison to radionuclides as e.g. <sup>124</sup>Iodine due to a low organ background activity and improved intracellular retention contributing to high specificity (Cheal, Punzalan et al. 2014). Tonic TCR internalization might even contribute to tracer accumulation as previously shown for an antibody also targeting a defined T-cell population (Griessinger, Maurer et al. 2015).



Moreover,  $^{89}\text{Zr}$  may show much lower cellular toxicity due to the lower emitted  $\gamma$ -energy (0.9 MeV) in comparison to  $^{64}\text{Cu}$  (1.34 MeV) (Lewis, Laforest et al. 2001; Verel, Visser et al. 2003). Indeed, a dose dependent decrease in viability and increase of double strand breaks of T cells after the labeling procedure was observed for different  $^{64}\text{Cu}$ -labeled tracer (Griessinger, Kehlbach et al. 2014; Griessinger, Maurer et al. 2015). We have shown that labeling by  $^{89}\text{Zr}$  does not alter T-cell function in vitro. In this experiment, we labeled the cells by  $^{89}\text{Zr}$ -aTCRmu-IgG and  $^{89}\text{Zr}$ -aTCRmu-F(ab')<sub>2</sub> followed by a washing step to exclude the dose-dependent immuno-modulatory effect derived from the antibody binding itself as discussed in section 6.2. After labeling the transgenic cells by  $^{89}\text{Zr}$ -aTCRmu-IgG and  $^{89}\text{Zr}$ -aTCRmu-F(ab')<sub>2</sub> we did not detect any differences in IFN $\gamma$  production after co-incubation with ML2-B7 cells. In addition, we did not detect any unspecific activation after labeling the cells with  $^{89}\text{Zr}$ -aTCRmu-IgG or F(ab')<sub>2</sub>. Furthermore, our data indicate no alteration of T cell function in vivo, as tracking of T-cells by  $^{89}\text{Zr}$ -aTCRmu-F(ab')<sub>2</sub> does not lead to changes in tumor rejection kinetics. This result is in line with recently published data demonstrating no impact of direct labeling by  $^{89}\text{Zr}$  on functionality and viability of cytotoxic T cells in vivo (Sato, Wu et al. 2015). Internalization of the  $^{89}\text{Zr}$ -aTCRmu-IgG and F(ab')<sub>2</sub> and tracer retention within the T cell, as was shown for  $^{68}\text{Cu}$ -labeled antibody (Griessinger, Maurer et al. 2015) needs to be evaluated. Moreover, effect of  $^{89}\text{Zr}$  needs to be further evaluated in detail by analysis of apoptosis, proliferation as well as DNA-damage upon incubation with  $^{89}\text{Zr}$ -aTCRmu-IgG and F(ab')<sub>2</sub>. Furthermore, in vivo stability of the tracer itself needs to be evaluated in future studies.

$^{89}\text{Zr}$  based Immuno-PET was shown to reveal high-resolution images and good signal-to-noise ratios and is therefore promising for a clinical translation. However, in current clinical trials, the mean effective dose for patients undergoing  $^{89}\text{Zr}$ -based Immuno-PET is higher compared to  $^{111}\text{In}$  or  $^{99\text{m}}\text{Tc}$ -based tracers (Buijs, Oyen et al. 1998; Borjesson, Jauw et al. 2009). In contrast, developments of new PET/CT scanner have already reduced the dose needed to obtain high-quality images (Bruno, Washington et al. 2005; Gaykema, Brouwers et al. 2013). The ongoing development of new  $^{89}\text{Zr}$ -labeled antibodies will rapidly expand the application to a valuable method in medical imaging (van de Watering, Rijpkema et al. 2014).

#### 6.4 CONFIRMATION OF IMAGING DATA BY EX VIVO ANALYSIS

Specific signals detected by PET/CT were intensively validated ex vivo by biodistribution and autoradiography as well as the detection of TCR-engineered T<sub>CM</sub> by flow cytometry and qPCR. These analyses confirmed the high signal-to-noise ratio provided by PET/CT. We detected ex vivo enhanced activity in spleen and lung but in no other organs corresponding to higher amounts of TCR $\mu$  positive T cells detected by flow cytometry and qPCR. Within the spleen we observed high amounts of T cells, but the percentage of transgenic CD5+TCR $\mu$ + cells was comparably low, confirming the spleen as organ in which human T cells easily engraft (Wang, Berger et al. 2011). The percentage of CD5+TCR $\mu$ + cells was relatively high within the lung although only limited numbers of total human T cells were detected. Previous studies have shown the preferential retention of specifically activated CD8+ effector T cells in the non-inflamed lung by innate signals. However, cytokine secretion has been only observed when the cognate antigen was additionally present (Galkina, Thatte et al. 2005). We have not observed any pulmonary distress in treated animals indicating that there is no clinical impact regarding the presence of these specific T cells in the murine lung. Interestingly, the low amount of T cells in the lung, determined by flow cytometry, was detectable by ex vivo biodistribution analysis but not by autoradiography or PET imaging. Autoradiography shows only a partial picture of the whole tumor as not all slices of the tumor were analyzed by this method. Furthermore, it might not reach the sensitivity as obtained by biodistribution analysis. Correlation of the PET signal with the amount of labeled cells within a determined region of interest is focus of further studies.

#### 6.5 DIFFERENTIAL DISTRIBUTION OF TCR-TRANSGENIC T-CELLS DURING TUMOR REJECTION

Due to the diverse advantages described in section 6.2 and 6.3, we focused on the <sup>89</sup>Zr-aTCR $\mu$ -F(ab')<sub>2</sub> fragment for PET/CT imaging and developed a more clinically relevant model of myeloid sarcoma. We therefore used NSG-mice, showing higher engraftment rates of human cells compared to BRG-mice (Ali, Flutter et al. 2012). Furthermore, TCR transgenic T<sub>CM</sub> were injected intravenously into tumor bearing mice corresponding to clinical application of adoptive T-cell transfer. Prior to T-cell infusion, a low dose total body irradiation was performed as it was previously demonstrated that low dose irradiation has beneficial effects on immunotherapy by influencing the tumor-microenvironment towards efficient T-cell infiltration (Klug, Prakash et al. 2013). It was also shown that hIL-15 leads to

higher engraftment and persistence of human T cells in NSG-mice (Wang, Berger et al. 2011). Therefore we treated mice three times weekly with irradiated IL-15 producing cells. After T-cell infusion, we detected a strong reduction in tumor size already four days after TCR2.5D6-transgenic  $T_{CM}$  were injected. The infusion of  $^{89}\text{Zr}$ -aTCRmu-F(ab')<sub>2</sub> in this model revealed a highly distinct and specific signal of transgenic T cells at the tumor site. By analysis of all experimental imaging data of this model, we observed different signal-distribution patterns within ML2-B7 tumors depending on the tumor size at the time point of imaging. Higher tumor size at the day of T cell injection revealed T-cell distributions with different densities around the tumor mass. Mice bearing smaller tumors at the day of T-cell injection showed a stronger tumor rejection and distribution of the T cells on high density within the tumor center. In a third group in which tumors were very small on the day of T-cell injection, tumors were mostly totally rejected. We hypothesize that in this group reduced PET signal is originating from the contraction phase of the transgenic T cells after completion of tumor lysis comparable to the typical course of T-cell response in defended viral infections (Murali-Krishna, Altman et al. 1998; Badovinac, Porter et al. 2002). Furthermore, these results indicate that differences in the size of the tumor have an important influence on the capacity of TCR-transduced  $T_{CM}$  to control tumor growth. Quantification of the total uptake within the tumor correlates to qualitative imaging data and ex vivo biodistribution analyses. On the other side, analysis of the weight adapted uptake did not show significant differences between the three groups. Although visual analysis of data might be the prioritized analysis of imaging based techniques, quantification of the signal is still a very important issue to verify the data. Our analysis showed that quantification of the total injected dose reveals a clearer representation of the uptake of T cells. In case of weight-adapted calculations, weight or volume of the tumor itself interferes with the signal deriving from T-cell infiltrates and therefore the sole use might be not appropriate evaluation for such settings of cell infiltrations within an organ. Development of algorithms for analysis of heterogeneous signal patterns and diffusion which allow clearer determination of T-cell infiltration within tumor or other organs is of high interest and will be focus of further studies.

Differential distribution of TCR-transgenic T cells within tumors of different size detected by PET imaging were confirmed in a repeated experiment showing reproducible data. By the use of  $^{18}\text{F}$ -FDG imaging we could clearly show that differences in PET signal intensity and distribution within tumors are not deriving from necrotic areas within the tumors but

differences in the T-cell infiltration. Of particular interest, we showed not only visualization of T cells at the tumor site but concretely mapped the T-cell infiltration within the tumor by PET/CT imaging validated by immunohistochemistry-based semi-quantitative analysis. One key limiting factor for immunotherapy is the lack of infiltration of T cells within the tumor (Melero, Rouzaut et al. 2014) and several studies have shown that the presence of intratumoral T cells, especially CD8+ T cells is associated with a better clinical outcome in many different tumor types such as melanoma, head and neck cancer, breast, bladder, colorectal, lung cancer and others as reviewed in (Fridman, Pages et al. 2012). For example, for colorectal cancer it was shown that in patients whose tumor did not recur, the density of the immune infiltrates by CD8+ CD45RO+ and Granzyme B+ cells was predominantly high, in the tumor core and invasive margin, whereas patients whose tumors did recur had low immune reactions in both regions of the primary tumor (Galon, Costes et al. 2006; Mlecnik, Tosolini et al. 2011). One important role in the infiltration capacity of T cells might play the tumor microenvironment (TME) which can mediate strong immunosuppression (Joyce and Fearon 2015). Furthermore, the tumor vasculature can also play an important role in the restriction of T cell infiltration (Buckanovich, Facciabene et al. 2008; Joyce and Fearon 2015). The underlying mechanisms of these distribution patterns between the different groups in the described model need to be further evaluated by analysis of the interaction of T cells with the tumor microenvironment i.e. vascularization of the tumors, expression of PD-1 on the T-cells and PDL-1 on the tumor cells, cytokine and chemokine expression, presence of myeloid suppressor cells (MDSCs), cancer associated fibroblasts (CAFs) or tumor associated macrophages (TAMs) (Bayne, Beatty et al. 2012; Lesokhin, Hohl et al. 2012; Feig, Jones et al. 2013; Zhu, Knolhoff et al. 2014).

The comprehensive analysis of  $^{89}\text{Zr}$ -aTCRmu-F(ab')<sub>2</sub> PET-imaging and ex vivo data may provide information about the stage of tumor rejection and profoundness of tumor-infiltration by T cells. Our results match to previously published data using microscopic two-photon imaging, a technology with much higher sensitivity but without the potential for clinical translation (Boissonnas, Fetler et al. 2007). Our data indicate that this noninvasive  $^{89}\text{Zr}$ -aTCRmu-F(ab')<sub>2</sub>-based immuno-imaging technology may reach a sensitivity which provides deeper insights in pharmacodynamics of transgenic T cells in vivo as we were able to map the T-cell infiltration within different stages of tumor rejection. The technology may be useful for the timely identification of T-cell infiltration versus exclusion from the tumor

and trapping on the margin. Determination of these patterns might evolve as an important tool for the identification of responders versus non-responders and might be used as a biomarker which potentially facilitates consecutive modification and optimization of immunotherapeutic approaches.

## 6.6 POTENTIAL CLINICAL TRANSLATION OF THE PRESENTED T-CELL TRACKING METHODOLOGY

With regard to a clinical translation of the presented T-cell tracking method, potential immunogenicity of a partially murinized TCR may be critical. Antibody development against the variable domains of a murine TCR has been previously observed in treated patients. However, this response was neither associated to the persistence of transgenic cells nor response to therapy (Davis, Theoret et al. 2010). Reduction of murine gene segments sparing the relevant epitope may further reduce this risk of immunogenicity. One study showed that the replacement of only nine amino-acids from the human constant chain with the murine counterparts is sufficient to conserve improved expression of introduced TCR by supporting preferential pairing of the introduced TCR chains (Sommermeyer and Uckert 2010), therefore a reduction of murine parts might be feasible. However, the use of minimal murinization leads to the loss of the epitope. Therefore, the exact amino-acids composing the epitope need to be mapped in further studies. The known sequence could be then introduced into a minimally murinized TCR sequence revealing a construct containing the advantage of improved TCR expression and presence of the TCR $\mu$  binding epitope with minimal necessary murine parts for in vivo imaging. Humanization of the aTCR $\mu$ -F(ab')<sub>2</sub> itself may additionally decrease immunogenicity. Engineering of alternative antibody fragments or variants (Evazalipour, D'Huyvetter et al. 2014; Tavare, McCracken et al. 2014; Tavare, McCracken et al. 2015) may further be used to modify pharmacokinetic and represents therefore a reasonable optimization of this method towards clinical application. For clinical translation, the high <sup>89</sup>Zr-F(ab')<sub>2</sub> uptake in liver and especially in kidney needs to be addressed. This high has been previously published (Hoeben, Kaanders et al. 2010; Oude Munnink, de Vries et al. 2012; Sham, Kievit et al. 2014) and likely results from fragment reabsorption by the renal tubular cells (Hoeben, Kaanders et al. 2010) as well as the retention of radioactivity in the liver or kidney (Arano 1998). Nevertheless, the use of <sup>89</sup>Zr may have still advantages compared to other radionuclids. For example, <sup>89</sup>Zr-labeled anti-HER2 Fab showed better in vivo stability and higher tumor uptake compared to the same

Fab labeled with  $^{124}\text{I}$  (Mendler, Gehring et al. 2015). The use of smaller constructs or other antibody-derived devices which may provide rapid tissue penetration and high target retention. In addition, rapid blood clearance may be more suitable and may reduce liver uptake, although clearance by the kidneys may be enhanced (Holliger and Hudson 2005). However due to the shorter blood half-life, these molecules are also secreted faster (Goldenberg 2002). Kidney uptake can be reduced by amino-acid preloading of renal tubular cells by glycine-lysine or gelatin-based plasma expander solutions (van Eerd, Vegt et al. 2006). Addition of metabolizable linkages, which facilitate the excretion of radio-metabolites from renal cells, might be another optimization strategy (Arano 1998). A possible influence of infusion with unlabeled  $\text{F(ab')}_2$  fragments as a cold renal blocking agent, similarly to rituximab infusion before  $^{90}\text{Y}$ -ibritumomab-tiuxetan therapy or cold antibodies before  $^{131}\text{I}$ -tositumomab therapy (Kaminski, Tuck et al. 2005; Samaniego, Berkova et al. 2014), needs to be evaluated. In addition, capturing of free  $^{89}\text{Zr}$  by continuous infusion with deferoxamine might also result in reduced background (Abou, Ku et al. 2011).

In the clinically relevant setting of intravenously transferred T cells (Figure 14, Figure 19, Figure 22), we detected an absolute uptake of 3%ID/g to 6%ID/g dependent on the differential distribution of T cells according to the classified groups. Ex vivo biodistribution analyses revealed an uptake of 10.7%ID/g in the ML2B7 tumor (ML2WT tumor: 2.4%ID/g) in those animals injected intravenously with TCR-transduced T cells in comparison to 2.2%ID/g detected in ML2B7 tumors of those animals treated with non-transduced T cells. The inferior imaging-based quantification in comparison to ex vivo gamma-counter biodistribution analysis has been previously described deriving from yield less absolute values (especially in smaller sample sizes) due to detector performance, dead time and partial volume effects (Mannheim, Judenhofer et al. 2012). Qualitatively, we reached a clear visual delineation of the T-cell signal in PET. The difference between quantifying absolute uptake in cell tracking approaches to e.g. receptor binding is also issue of normalization for the accurate tissue volume. As we have demonstrated T-cell distribution is not even throughout the tumor, so especially in larger tumors the calculated volume delineated on CT data will be too large, accounting for an underestimation of the ID/g by image quantification.

If the sensitivity of this  $^{89}\text{Zr}$ -aTCRmu- $\text{F(ab')}_2$  imaging technology is high enough to enable clinical application of human T-cell imaging is difficult to estimate as there are so far no clinical experiences with imaging of T cells by Immuno-PET. Thus, quantification values of our

approach can be either compared to other preclinical approaches of PET-based T-cell imaging or to other clinical approaches quantifying cell activity by PET. In comparison to the preclinical work of others investigating a murine OT-1-model of adoptive T-cell transfer (Tavare, Escuin-Ordinas et al. 2016), we are reporting a higher uptake and enhanced tumor to blood ratio (ex vivo biodistribution  $\sim 8\%ID/g$  vs  $10.7\%ID/g$  in our studies, tumor to blood ratio 4.5 vs 12.8 in our studies). Other publications investigated the uptake of  $^{64}Cu$ -aCD8 antibody fragments and detected  $25\text{--}75\%ID/g$  in the spleen (Tavare, McCracken et al. 2014; Tavare, McCracken et al. 2015). However, these studies did not address imaging of defined T-cell populations after adoptive T-cell transfer but instead targeted endogenous T-cell populations. In our experiments, we observed an uptake of  $24.3\%ID/g$  in the spleen while only 21% of all cells were human T cells and 5% transgenic for the respective TCR. Therefore, although the amount of human transgenic cells within the murine spleen is much smaller ( $\sim 1\%$ ), we still detect them with a high organ-to-background ratio and show specific uptake in the same range or even higher as previously presented (Tavare, McCracken et al. 2014; Griessinger, Maurer et al. 2015; Tavare, McCracken et al. 2015; Tavare, Escuin-Ordinas et al. 2016). A comparative overview of reported uptake in recent pre-clinical studies of T-cell imaging and our work is listed in Table 31 and Table 32.

One of the examples of preclinical imaging that has changed diagnostic PET- and even therapeutic options,  $^{68}Ga$ -labelled Somatostatin-Receptor imaging, initially showed much lower normalized activity, ranging from  $0.27\text{--}0.74\%ID/ml$  in vivo (relying on PET image based quantification) (Smith-Jones, Stolz et al. 1994) and ex vivo biodistribution revealing values around 4% and  $7\%ID/g$  for  $^{68}Ga$ -DOTATOC and  $^{68}Ga$ -DOTANOC respectively (Stelter, Amthauer et al. 2008). These data pioneered the development of two of the most common diagnostic PET-tracers for Somatostatin-Receptor Imaging in neuroendocrine tumors, routinely and widely used since over 10 years. Antibody-derived constructs have certainly different pharmacokinetic properties in comparison to small peptide or peptidomimic molecules. However, development of smaller antibody-derived imaging devices may further improve this approach. Another example is PET imaging of HSV-tk transduced T cells showing an uptake of  $0.92\%ID/g$  of  $^{18}F$ -FIAU in vivo within the tumor (Koehne, Doubrovin et al. 2003). In a first clinical trial, HSV-tk transduced autologous cytotoxic T cells were transferred to a glioblastoma patient.  $^{18}F$ -FHBG imaging revealed a tumor to brain background ratio of 4.82 compared to a control patient without T cell infusions showing a tumor to background ratio

of 1.54 (Yaghoubi, Jensen et al. 2009). This again shows the clinical relevance of specific uptake within a range of even lower than 1%ID/g. The  $^{89}\text{Zr}$ -labeled chimeric monoclonal antibody cU36, which binds to CD44v6 expressed on squamous cell carcinoma of head and neck (HNSCC) and several other solid tumors showed in a preclinical study a tumor to blood ratio of 2.1 in HNSCC-tumor bearing nude mice (Verel, Visser et al. 2003), whereas the tumor to blood ratios in our studies were 12.8.  $^{89}\text{Zr}$ -cU36 was used in clinical trials for tumor imaging in HNSCC patients and detected 100% of the primary tumors and 72-73% of other positive sides or lymph node metastasis and was shown to be safe and well tolerated by the patients (Borjesson, Jauw et al. 2006; Borjesson, Jauw et al. 2009). Recently, first results of a clinical trial of  $^{89}\text{Zr}$ -Df-IAB2M (anti-prostate specific membrane antigen PSMA-minibody) were presented (Pandit-Taskar, O'Donoghue et al. 2015) describing targeting of bone and soft tissue lesions. Pre-clinical in vivo analysis showed ex vivo uptake of 12.12%ID/g in PSMA-positive tumors, vs. 2.36%ID/g for PSMA-negative tumors and in vivo tumor uptake was reported to be 9.17%ID/g (Viola-Villegas, Sevak et al. 2014). However, in contrast to our studies, tumors consisted mainly of targeted cells.

The number of effector cells infused in our experiments was high ( $1 \times 10^9/\text{kg}$ ) but comparable cell numbers were applied in previous clinical trials using genetically modified T-cells (Morgan, Dudley et al. 2006; Johnson, Morgan et al. 2009; Robbins, Morgan et al. 2011; Chodon, Comin-Anduix et al. 2014). Previous studies in humans suggested that T-cell engraftment may be more relevant than the absolute number of transferred T cells (Maude, Frey et al. 2014). As  $T_{\text{CM}}$  engraftment in humans can be expected to be superior as compared to NSG-mice, this preclinical model may even underestimate the potential of this approach in the clinical setting and therefore it can be expected that uptake would be also higher. Indeed, preliminary data indicate that higher numbers of engrafted cells show a higher accumulation and consequently higher PET signal (work from Nahid Yusufi, data not shown).



Reference	Method	Uptake (%ID/g)			Cell number
Description		Tumor (control)	Spleen (control)	Lymph node (control)	% of cells in organ (flow cytometry)
Mall et.al. • <sup>89</sup> Zr aTCRmu F(ab) <sub>2</sub> • <u>Imaging of transferred human TCR transgenic T cells</u>	In vivo (ROI analysis)	4.5 (2.0)	n.d.	n.d.	
	Ex vivo (biodistribution)	10.74 (2.2)	24.3 (11.8)	n.d.	Tumor: 3.5% TCR+ T cells
Griessinger et.al., PNAS 2015 • <sup>64</sup> Cu aTCR mAb • <u>Imaging of transferred murine monoclonal T cells (in vitro labeling of cells)</u>	In vivo (ROI analysis)	n.d.	n.d.	12.4 (9.1)	
	Ex vivo (biodistribution)	no ex vivo data shown			
Tavare et.al., PNAS 2014 • <sup>64</sup> Cu aCD8 minibody • <u>Imaging of murine endogenous CD8+ T cells</u>	In vivo (ROI analysis)	no in vivo data shown			
	Ex vivo (biodistribution)	n.d.	75 (15)	27 (2.7)	
Tavare et.al., JNM 2015 • <sup>89</sup> Zr aCD8/CD4 cys-diabody • <u>Imaging of murine endogenous CD4+/CD8+ T cells</u> • <u>Imaging of murine CD4+/CD8+ cells in a transplantation model</u>	In vivo (ROI analysis)	no in vivo data shown			
	Ex vivo (biodistribution) WT mice - CD8	n.d.	41 (12)	47 (14)	
	Ex vivo (biodistribution) 8wk post stem cell transfer-CD8	n.d.	28 (no ctl*)	18 (no ctl*)	Spleen:~6% CD8+ T cells Lymph node:~20% CD8+ T cells
Tavare et.al., Cancer Research 2016 • <sup>89</sup> Zr aCD8 cys-diabody • <u>Imaging of murine endogenous CD8+ T cells</u> • <u>Imaging of transferred murine OT-1 T cells</u>	In vivo (ROI analysis)	no in vivo data shown			
	Ex vivo (Biodistribution) WT mice	n.d.	~23 (~6)	~40 (~9)	
	Ex vivo (Biodistribution) OT-1 transfer	~7.5 (~6.5)	~18 (~4)	~15 (~8)	Tumor: ~40% CD8+ T cells
	Ex vivo (Biodistribution) WT mice +aCD137	~16 (~7)	~40(~20)	~40 (~28)	Tumor: ~40% CD8+ T cells
	Ex vivo (Biodistribution) WT mice +aPDL1	~11 (no ctl#)	~25 (no ctl#)	~21 (no ctl#)	Tumor: ~20% CD8+ T cells

**Table 31. Uptake in tumor or different organs compared to recently published antibody-based studies.**

\*In this experiment, no negative control group i.e. CD8 blocking is shown.

#In this experiment, no negative control group i.e. without antiPDL1 is shown for ex vivo uptake

Reference	Method	Uptake (RATIO tumor/muscle or tumor/blood)			Comment
Description		Tumor (control)	Spleen (control)	Lymph node (control)	
Mall et.al. • <sup>89</sup> Zr aTCRmu F(ab) <sub>2</sub> • <u>Imaging of transferred human TCR transgenic T cells</u>	In vivo (ROI analysis)	not performed			
	Ex vivo (biodistribution)	15.1(2.7)	35.3 (14.7)	n.d.	organ/muscle ratio
	Ex vivo (biodistribution)	12.9 (1.8)	29.3 (9.8)	n.d.	organ/blood ratio
McCracken et.al., JCI 2015 • <sup>18</sup> F-FMAU • <u>Imaging of transferred human hdCK3mut+ TCR+ T cells</u> • <u>human hdCK3mut+ cells post stem cell transfer</u>	In vivo (ROI analysis) i.v. T cell injection	~1.8 (~1.4)	n.d.	n.d.	organ/muscle ratio
	In vivo (ROI analysis) 16wk post human stem cell transfer	~1.6 (~1.3)	n.d.	n.d.	organ/muscle ratio
	Ex vivo uptake	No ex vivo uptake shown			

**Table 32. Uptake in tumor or different organs compared to recently published reporter-gene-based studies.**

## 6.7 CONCLUSION AND OUTLOOK

We have established a novel imaging technology which can be specifically applied for TCR-transgenic T cells harboring a murinized TCR constant beta domain using the F(ab')<sub>2</sub> fragment of the antibody H57-597 resulting in highly specific PET/CT signals at the tumor site

in a myeloid sarcoma model. The data were validated by ex vivo analysis of radioactivity as well as detection of TCR transgenic T cells by flow cytometry and qPCR. Furthermore, we were able to map differential T cell distribution patterns by Immuno-PET depending on tumor size and rejection phase. By correlation of the PET images to immunohistochemistry and immunohistochemistry-based semi-quantitative determination of T-cell infiltration we confirmed the heterogeneous T-cell distribution within the ML2-B7 tumor. Determination and mapping of T-cell infiltration by Immuno-PET in correlation with immunohistochemistry is providing important information about different T-cell distribution patterns and tumor rejection phase relevant for monitoring and optimization of immunotherapeutic approaches. Such a technology might serve as a biomarker system for the identification of responders versus non-responders and therefore might play a role in decision making processes for immunotherapies.

In order to transfer this novel imaging approach into the clinic, more pharmacodynamic and pharmacokinetic analyses are still necessary. Furthermore, the presented  $^{89}\text{Zr}$ -labeled- $\text{F(ab')}_2$  technology might be expanded to other targets, such as a pan-T-cell marker which might be applicable for imaging of T-cell distributions during other immunotherapies such as vaccination or checkpoint-inhibitor therapy. On the other side, optimization of the tracer in order to provide rapid blood clearance, but high tissue penetration and high target retention would be a further important improvement for introduction into a clinical setting.

## 7 REFERENCES

- Abou, D. S., T. Ku, et al. (2011). "In vivo biodistribution and accumulation of 89Zr in mice." Nucl Med Biol **38**(5): 675-681.
- Abraham, M., A. Karni, et al. (2008). "In vitro induction of regulatory T cells by anti-CD3 antibody in humans." J Autoimmun **30**(1-2): 21-28.
- Adonai, N., K. N. Nguyen, et al. (2002). "Ex vivo cell labeling with 64Cu-pyruvaldehyde-bis(N4-methylthiosemicarbazone) for imaging cell trafficking in mice with positron-emission tomography." Proc Natl Acad Sci U S A **99**(5): 3030-3035.
- Ahmadzadeh, M., L. A. Johnson, et al. (2009). "Tumor antigen-specific CD8 T cells infiltrating the tumor express high levels of PD-1 and are functionally impaired." Blood **114**(8): 1537-1544.
- Ali, N., B. Flutter, et al. (2012). "Xenogeneic graft-versus-host-disease in NOD-scid IL-2R $\gamma$ manull mice display a T-effector memory phenotype." PLoS One **7**(8): e44219.
- Ansell, S. M., A. M. Lesokhin, et al. (2015). "PD-1 blockade with nivolumab in relapsed or refractory Hodgkin's lymphoma." N Engl J Med **372**(4): 311-319.
- Arano, Y. (1998). "Strategies to reduce renal radioactivity levels of antibody fragments." Q J Nucl Med **42**(4): 262-270.
- Atkins, M. B., M. T. Lotze, et al. (1999). "High-dose recombinant interleukin 2 therapy for patients with metastatic melanoma: analysis of 270 patients treated between 1985 and 1993." J Clin Oncol **17**(7): 2105-2116.
- Badovinac, V. P., B. B. Porter, et al. (2002). "Programmed contraction of CD8(+) T cells after infection." Nat Immunol **3**(7): 619-626.
- Bayne, L. J., G. L. Beatty, et al. (2012). "Tumor-derived granulocyte-macrophage colony-stimulating factor regulates myeloid inflammation and T cell immunity in pancreatic cancer." Cancer Cell **21**(6): 822-835.
- Bemelmans, M. H., D. Abramowicz, et al. (1994). "In vivo T cell activation by anti-CD3 monoclonal antibody induces soluble TNF receptor release in mice. Effects of pentoxifylline, methylprednisolone, anti-TNF, and anti-IFN-gamma antibodies." J Immunol **153**(2): 499-506.
- Bendle, G. M., C. Linnemann, et al. (2010). "Lethal graft-versus-host disease in mouse models of T cell receptor gene therapy." Nat Med **16**(5): 565-570, 561p following 570.
- Berdien, B., U. Mock, et al. (2014). "TALEN-mediated editing of endogenous T-cell receptors facilitates efficient reprogramming of T lymphocytes by lentiviral gene transfer." Gene Ther **21**(6): 539-548.
- Berger, C., M. C. Jensen, et al. (2008). "Adoptive transfer of effector CD8+ T cells derived from central memory cells establishes persistent T cell memory in primates." J Clin Invest **118**(1): 294-305.
- Bhatnagar, P., Z. Li, et al. (2013). "Imaging of genetically engineered T cells by PET using gold nanoparticles complexed to Copper-64." Integr Biol (Camb) **5**(1): 231-238.
- Boissonnas, A., L. Fetler, et al. (2007). "In vivo imaging of cytotoxic T cell infiltration and elimination of a solid tumor." J Exp Med **204**(2): 345-356.
- Bonini, C., G. Ferrari, et al. (1997). "HSV-TK gene transfer into donor lymphocytes for control of allogeneic graft-versus-leukemia." Science **276**(5319): 1719-1724.

- Borghaei, H., L. Paz-Ares, et al. (2015). "Nivolumab versus Docetaxel in Advanced Nonsquamous Non-Small-Cell Lung Cancer." N Engl J Med **373**(17): 1627-1639.
- Borjesson, P. K., Y. W. Jauw, et al. (2006). "Performance of immuno-positron emission tomography with zirconium-89-labeled chimeric monoclonal antibody U36 in the detection of lymph node metastases in head and neck cancer patients." Clin Cancer Res **12**(7 Pt 1): 2133-2140.
- Borjesson, P. K., Y. W. Jauw, et al. (2009). "Radiation dosimetry of 89Zr-labeled chimeric monoclonal antibody U36 as used for immuno-PET in head and neck cancer patients." J Nucl Med **50**(11): 1828-1836.
- Botti, C., D. R. Negri, et al. (1997). "Comparison of three different methods for radiolabelling human activated T lymphocytes." Eur J Nucl Med **24**(5): 497-504.
- Brahmer, J., K. L. Reckamp, et al. (2015). "Nivolumab versus Docetaxel in Advanced Squamous-Cell Non-Small-Cell Lung Cancer." N Engl J Med **373**(2): 123-135.
- Brentjens, R. J., M. L. Davila, et al. (2013). "CD19-targeted T cells rapidly induce molecular remissions in adults with chemotherapy-refractory acute lymphoblastic leukemia." Sci Transl Med **5**(177): 177ra138.
- Bromberg, J. S., K. D. Chavin, et al. (1991). "Anti-CD2 monoclonal antibodies alter cell-mediated immunity in vivo." Transplantation **51**(1): 219-225.
- Bruno, R., C. B. Washington, et al. (2005). "Population pharmacokinetics of trastuzumab in patients with HER2+ metastatic breast cancer." Cancer Chemother Pharmacol **56**(4): 361-369.
- Buckanovich, R. J., A. Facciabene, et al. (2008). "Endothelin B receptor mediates the endothelial barrier to T cell homing to tumors and disables immune therapy." Nat Med **14**(1): 28-36.
- Buijs, W. C., W. J. Oyen, et al. (1998). "Dynamic distribution and dosimetric evaluation of human non-specific immunoglobulin G labelled with 111In or 99Tcm." Nucl Med Commun **19**(8): 743-751.
- Carpenter, P. A., S. Pavlovic, et al. (2000). "Non-Fc receptor-binding humanized anti-CD3 antibodies induce apoptosis of activated human T cells." J Immunol **165**(11): 6205-6213.
- Chan, P. C., C. Y. Wu, et al. (2011). "Evaluation of F-18-labeled 5-iodocytidine (18F-FIAC) as a new potential positron emission tomography probe for herpes simplex virus type 1 thymidine kinase imaging." Nucl Med Biol **38**(7): 987-995.
- Charo, J., C. Perez, et al. (2011). "Visualizing the dynamic of adoptively transferred T cells during the rejection of large established tumors." Eur J Immunol **41**(11): 3187-3197.
- Chatenoud, L. (2003). "CD3-specific antibody-induced active tolerance: from bench to bedside." Nat Rev Immunol **3**(2): 123-132.
- Cheal, S. M., B. Punzalan, et al. (2014). "Pairwise comparison of 89Zr- and 124I-labeled cG250 based on positron emission tomography imaging and nonlinear immunokinetic modeling: in vivo carbonic anhydrase IX receptor binding and internalization in mouse xenografts of clear-cell renal cell carcinoma." Eur J Nucl Med Mol Imaging **41**(5): 985-994.
- Cheever, M. A., J. P. Allison, et al. (2009). "The prioritization of cancer antigens: a national cancer institute pilot project for the acceleration of translational research." Clin Cancer Res **15**(17): 5323-5337.
- Chewning, J. H., K. J. Dugger, et al. (2009). "Bioluminescence-based visualization of CD4 T cell dynamics using a T lineage-specific luciferase transgenic model." BMC Immunol **10**: 44.

- Chodon, T., B. Comin-Anduix, et al. (2014). "Adoptive transfer of MART-1 T-cell receptor transgenic lymphocytes and dendritic cell vaccination in patients with metastatic melanoma." Clin Cancer Res **20**(9): 2457-2465.
- Clemente, C. G., M. C. Mihm, Jr., et al. (1996). "Prognostic value of tumor infiltrating lymphocytes in the vertical growth phase of primary cutaneous melanoma." Cancer **77**(7): 1303-1310.
- Cohen, C. J., Y. F. Li, et al. (2007). "Enhanced antitumor activity of T cells engineered to express T-cell receptors with a second disulfide bond." Cancer Res **67**(8): 3898-3903.
- Cohen, C. J., Y. Zhao, et al. (2006). "Enhanced antitumor activity of murine-human hybrid T-cell receptor (TCR) in human lymphocytes is associated with improved pairing and TCR/CD3 stability." Cancer Res **66**(17): 8878-8886.
- Collins, R. H., Jr., O. Shpilberg, et al. (1997). "Donor leukocyte infusions in 140 patients with relapsed malignancy after allogeneic bone marrow transplantation." J Clin Oncol **15**(2): 433-444.
- Crites, T. J., L. Chen, et al. (2012). "A TIRF microscopy technique for real-time, simultaneous imaging of the TCR and its associated signaling proteins." J Vis Exp(61).
- Curran, M. A., W. Montalvo, et al. (2010). "PD-1 and CTLA-4 combination blockade expands infiltrating T cells and reduces regulatory T and myeloid cells within B16 melanoma tumors." Proc Natl Acad Sci U S A **107**(9): 4275-4280.
- Curti, B. D., M. Kovacsovics-Bankowski, et al. (2013). "OX40 is a potent immune-stimulating target in late-stage cancer patients." Cancer Res **73**(24): 7189-7198.
- Daldrup-Link, H. E., R. Meier, et al. (2005). "In vivo tracking of genetically engineered, anti-HER2/neu directed natural killer cells to HER2/neu positive mammary tumors with magnetic resonance imaging." Eur Radiol **15**(1): 4-13.
- Davila, M. L., I. Riviere, et al. (2014). "Efficacy and toxicity management of 19-28z CAR T cell therapy in B cell acute lymphoblastic leukemia." Sci Transl Med **6**(224): 224ra225.
- Davis, J. L., M. R. Theoret, et al. (2010). "Development of human anti-murine T-cell receptor antibodies in both responding and nonresponding patients enrolled in TCR gene therapy trials." Clin Cancer Res **16**(23): 5852-5861.
- Di Pucchio, T., L. Pilla, et al. (2006). "Immunization of stage IV melanoma patients with Melan-A/MART-1 and gp100 peptides plus IFN-alpha results in the activation of specific CD8(+) T cells and monocyte/dendritic cell precursors." Cancer Res **66**(9): 4943-4951.
- Di Stasi, A., S. K. Tey, et al. (2011). "Inducible apoptosis as a safety switch for adoptive cell therapy." N Engl J Med **365**(18): 1673-1683.
- Dobrenkov, K., M. Olszewska, et al. (2008). "Monitoring the efficacy of adoptively transferred prostate cancer-targeted human T lymphocytes with PET and bioluminescence imaging." J Nucl Med **49**(7): 1162-1170.
- Dong, H., S. E. Strome, et al. (2002). "Tumor-associated B7-H1 promotes T-cell apoptosis: a potential mechanism of immune evasion." Nat Med **8**(8): 793-800.
- Dotti, G., M. Tian, et al. (2009). "Repetitive noninvasive monitoring of HSV1-tk-expressing T cells intravenously infused into nonhuman primates using positron emission tomography and computed tomography with 18F-FAU." Mol Imaging **8**(4): 230-237.
- Dobrovina, M. M., E. S. Dobrovina, et al. (2007). "In vivo imaging and quantitation of adoptively transferred human antigen-specific T cells transduced to express a human norepinephrine transporter gene." Cancer Res **67**(24): 11959-11969.

- Drobyski, W. R. and D. Majewski (1996). "Treatment of donor mice with an alpha beta T-cell receptor monoclonal antibody induces prolonged T-cell nonresponsiveness and effectively prevents lethal graft-versus-host disease in murine recipients of major histocompatibility complex (MHC)-matched and MHC-mismatched donor marrow grafts." Blood **87**(12): 5355-5369.
- Dubey, P., H. Su, et al. (2003). "Quantitative imaging of the T cell antitumor response by positron-emission tomography." Proc Natl Acad Sci U S A **100**(3): 1232-1237.
- Dudley, M. E., C. A. Gross, et al. (2010). "CD8+ enriched "young" tumor infiltrating lymphocytes can mediate regression of metastatic melanoma." Clin Cancer Res **16**(24): 6122-6131.
- Dudley, M. E., J. C. Yang, et al. (2008). "Adoptive cell therapy for patients with metastatic melanoma: evaluation of intensive myeloablative chemoradiation preparative regimens." J Clin Oncol **26**(32): 5233-5239.
- Egen, J. G. and J. P. Allison (2002). "Cytotoxic T lymphocyte antigen-4 accumulation in the immunological synapse is regulated by TCR signal strength." Immunity **16**(1): 23-35.
- Engels, B., H. Cam, et al. (2003). "Retroviral vectors for high-level transgene expression in T lymphocytes." Hum Gene Ther **14**(12): 1155-1168.
- Eriksson, O., A. Sadeghi, et al. (2011). "Distribution of adoptively transferred porcine T-lymphoblasts tracked by (18)F-2-fluoro-2-deoxy-D-glucose and position emission tomography." Nucl Med Biol **38**(6): 827-833.
- Evazalipour, M., M. D'Huyvetter, et al. (2014). "Generation and characterization of nanobodies targeting PSMA for molecular imaging of prostate cancer." Contrast Media Mol Imaging **9**(3): 211-220.
- Feig, C., J. O. Jones, et al. (2013). "Targeting CXCL12 from FAP-expressing carcinoma-associated fibroblasts synergizes with anti-PD-L1 immunotherapy in pancreatic cancer." Proc Natl Acad Sci U S A **110**(50): 20212-20217.
- Flavell, D. J., S. L. Warnes, et al. (2000). "Anti-CD7 antibody and immunotoxin treatment of human CD7(+)T-cell leukaemia is significantly less effective in NOD/LtSz-scid mice than in CB.17 scid mice." Br J Cancer **83**(12): 1755-1761.
- Freeman, G. J., A. J. Long, et al. (2000). "Engagement of the PD-1 immunoinhibitory receptor by a novel B7 family member leads to negative regulation of lymphocyte activation." J Exp Med **192**(7): 1027-1034.
- Fridman, W. H., F. Pages, et al. (2012). "The immune contexture in human tumours: impact on clinical outcome." Nat Rev Cancer **12**(4): 298-306.
- Galkina, E., J. Thatte, et al. (2005). "Preferential migration of effector CD8+ T cells into the interstitium of the normal lung." J Clin Invest **115**(12): 3473-3483.
- Galon, J., A. Costes, et al. (2006). "Type, density, and location of immune cells within human colorectal tumors predict clinical outcome." Science **313**(5795): 1960-1964.
- Gambhir, S. S., E. Bauer, et al. (2000). "A mutant herpes simplex virus type 1 thymidine kinase reporter gene shows improved sensitivity for imaging reporter gene expression with positron emission tomography." Proc Natl Acad Sci U S A **97**(6): 2785-2790.
- Gattinoni, L., E. Lugli, et al. (2011). "A human memory T cell subset with stem cell-like properties." Nat Med **17**(10): 1290-1297.
- Gaykema, S. B., A. H. Brouwers, et al. (2013). "89Zr-bevacizumab PET imaging in primary breast cancer." J Nucl Med **54**(7): 1014-1018.

- Goldenberg, D. M. (2002). "Targeted therapy of cancer with radiolabeled antibodies." J Nucl Med **43**(5): 693-713.
- Gordon, L. I., T. Witzig, et al. (2004). "Yttrium 90-labeled ibritumomab tiuxetan radioimmunotherapy produces high response rates and durable remissions in patients with previously treated B-cell lymphoma." Clin Lymphoma **5**(2): 98-101.
- Gorin, J. B., Y. Guilloux, et al. (2014). "Using alpha radiation to boost cancer immunity?" Oncoimmunology **3**(9): e954925.
- Green, L. A., K. Nguyen, et al. (2004). "A tracer kinetic model for 18F-FHBG for quantitating herpes simplex virus type 1 thymidine kinase reporter gene expression in living animals using PET." J Nucl Med **45**(9): 1560-1570.
- Griessinger, C. M., R. Kehlbach, et al. (2014). "In vivo tracking of Th1 cells by PET reveals quantitative and temporal distribution and specific homing in lymphatic tissue." J Nucl Med **55**(2): 301-307.
- Griessinger, C. M., A. Maurer, et al. (2015). "<sup>64</sup>Cu antibody-targeting of the T-cell receptor and subsequent internalization enables in vivo tracking of lymphocytes by PET." Proc Natl Acad Sci U S A **112**(4): 1161-1166.
- Griffioen, M., E. H. van Egmond, et al. (2009). "Retroviral transfer of human CD20 as a suicide gene for adoptive T-cell therapy." Haematologica **94**(9): 1316-1320.
- Grupp, S. A., M. Kalos, et al. (2013). "Chimeric antigen receptor-modified T cells for acute lymphoid leukemia." N Engl J Med **368**(16): 1509-1518.
- Guckel, B., C. Berek, et al. (1991). "Anti-CD2 antibodies induce T cell unresponsiveness in vivo." J Exp Med **174**(5): 957-967.
- Heemskerk, M. H., M. Hoogeboom, et al. (2003). "Redirection of antileukemic reactivity of peripheral T lymphocytes using gene transfer of minor histocompatibility antigen HA-2-specific T-cell receptor complexes expressing a conserved alpha joining region." Blood **102**(10): 3530-3540.
- Henrickson, M., J. Reid, et al. (1995). "Comparison of in vivo efficacy and mechanism of action of antimurine monoclonal antibodies directed against TCR alpha beta (H57-597) and CD3 (145-2C11)." Transplantation **60**(8): 828-835.
- Hitchens, T. K., L. Liu, et al. (2015). "Combining perfluorocarbon and superparamagnetic iron-oxide cell labeling for improved and expanded applications of cellular MRI." Magn Reson Med **73**(1): 367-375.
- Hodi, F. S., M. Butler, et al. (2008). "Immunologic and clinical effects of antibody blockade of cytotoxic T lymphocyte-associated antigen 4 in previously vaccinated cancer patients." Proc Natl Acad Sci U S A **105**(8): 3005-3010.
- Hodi, F. S., S. J. O'Day, et al. (2010). "Improved survival with ipilimumab in patients with metastatic melanoma." N Engl J Med **363**(8): 711-723.
- Hoeben, B. A., J. H. Kaanders, et al. (2010). "PET of hypoxia with 89Zr-labeled cG250-F(ab')<sub>2</sub> in head and neck tumors." J Nucl Med **51**(7): 1076-1083.
- Holliger, P. and P. J. Hudson (2005). "Engineered antibody fragments and the rise of single domains." Nat Biotechnol **23**(9): 1126-1136.
- Huang, M., R. K. Batra, et al. (2001). "Ectopic expression of the thyroperoxidase gene augments radioiodide uptake and retention mediated by the sodium iodide symporter in non-small cell lung cancer." Cancer Gene Ther **8**(8): 612-618.

- Huang, X., H. Guo, et al. (2008). "Sleeping Beauty transposon-mediated engineering of human primary T cells for therapy of CD19+ lymphoid malignancies." Mol Ther **16**(3): 580-589.
- Hughes, D. K. (2003). "Nuclear medicine and infection detection: the relative effectiveness of imaging with <sup>111</sup>In-oxine-, <sup>99m</sup>Tc-HMPAO-, and <sup>99m</sup>Tc-stannous fluoride colloid-labeled leukocytes and with <sup>67</sup>Ga-citrate." J Nucl Med Technol **31**(4): 196-201; quiz 203-194.
- Imai, C., K. Mihara, et al. (2004). "Chimeric receptors with 4-1BB signaling capacity provoke potent cytotoxicity against acute lymphoblastic leukemia." Leukemia **18**(4): 676-684.
- Introna, M., A. M. Barbui, et al. (2000). "Genetic modification of human T cells with CD20: a strategy to purify and lyse transduced cells with anti-CD20 antibodies." Hum Gene Ther **11**(4): 611-620.
- Jadvar, H., L. P. Yap, et al. (2012). "[<sup>18</sup>F]-2'-Fluoro-5-methyl-1-beta-D-arabinofuranosyluracil (18F-FMAU) in prostate cancer: initial preclinical observations." Mol Imaging **11**(5): 426-432.
- Jiang, T. and C. Zhou (2015). "The past, present and future of immunotherapy against tumor." Transl Lung Cancer Res **4**(3): 253-264.
- Johansson, A. G., T. Lovdal, et al. (1996). "Liver cell uptake and degradation of soluble immunoglobulin G immune complexes in vivo and in vitro in rats." Hepatology **24**(1): 169-175.
- Johnson, L. A., R. A. Morgan, et al. (2009). "Gene therapy with human and mouse T-cell receptors mediates cancer regression and targets normal tissues expressing cognate antigen." Blood **114**(3): 535-546.
- Joyce, J. A. and D. T. Fearon (2015). "T cell exclusion, immune privilege, and the tumor microenvironment." Science **348**(6230): 74-80.
- Kalos, M., B. L. Levine, et al. (2011). "T cells with chimeric antigen receptors have potent antitumor effects and can establish memory in patients with advanced leukemia." Sci Transl Med **3**(95): 95ra73.
- Kaminski, M. S., M. Tuck, et al. (2005). "<sup>131</sup>I-tositumomab therapy as initial treatment for follicular lymphoma." N Engl J Med **352**(5): 441-449.
- Kantoff, P. W., C. S. Higano, et al. (2010). "Sipuleucel-T immunotherapy for castration-resistant prostate cancer." N Engl J Med **363**(5): 411-422.
- Kantoff, P. W., T. J. Schuetz, et al. (2010). "Overall survival analysis of a phase II randomized controlled trial of a Poxviral-based PSA-targeted immunotherapy in metastatic castration-resistant prostate cancer." J Clin Oncol **28**(7): 1099-1105.
- Kanwar, B., D. W. Gao, et al. (2008). "In vivo imaging of mucosal CD4+ T cells using single photon emission computed tomography in a murine model of colitis." J Immunol Methods **329**(1-2): 21-30.
- Kessels, H. W., M. C. Wolkers, et al. (2001). "Immunotherapy through TCR gene transfer." Nat Immunol **2**(10): 957-961.
- Kieback, E., J. Charo, et al. (2008). "A safeguard eliminates T cell receptor gene-modified autoreactive T cells after adoptive transfer." Proc Natl Acad Sci U S A **105**(2): 623-628.
- Kim, Y. J., P. Dubey, et al. (2004). "Multimodality imaging of lymphocytic migration using lentiviral-based transduction of a tri-fusion reporter gene." Mol Imaging Biol **6**(5): 331-340.



- Kircher, M. F., J. R. Allport, et al. (2003). "In vivo high resolution three-dimensional imaging of antigen-specific cytotoxic T-lymphocyte trafficking to tumors." Cancer Res **63**(20): 6838-6846.
- Kirkwood, J. M., M. H. Strawderman, et al. (1996). "Interferon alfa-2b adjuvant therapy of high-risk resected cutaneous melanoma: the Eastern Cooperative Oncology Group Trial EST 1684." J Clin Oncol **14**(1): 7-17.
- Klar, R., S. Schober, et al. (2014). "Therapeutic targeting of naturally presented myeloperoxidase-derived HLA peptide ligands on myeloid leukemia cells by TCR-transgenic T cells." Leukemia **28**(12): 2355-2366.
- Klebanoff, C. A., S. E. Finkelstein, et al. (2004). "IL-15 enhances the in vivo antitumor activity of tumor-reactive CD8+ T cells." Proc Natl Acad Sci U S A **101**(7): 1969-1974.
- Klebanoff, C. A., L. Gattinoni, et al. (2005). "Central memory self/tumor-reactive CD8+ T cells confer superior antitumor immunity compared with effector memory T cells." Proc Natl Acad Sci U S A **102**(27): 9571-9576.
- Klug, F., H. Prakash, et al. (2013). "Low-dose irradiation programs macrophage differentiation to an iNOS(+)/M1 phenotype that orchestrates effective T cell immunotherapy." Cancer Cell **24**(5): 589-602.
- Koehne, G., M. Doubrovin, et al. (2003). "Serial in vivo imaging of the targeted migration of human HSV-TK-transduced antigen-specific lymphocytes." Nat Biotechnol **21**(4): 405-413.
- Kolb, H. J. (2008). "Graft-versus-leukemia effects of transplantation and donor lymphocytes." Blood **112**(12): 4371-4383.
- Kolb, H. J., J. Mittermuller, et al. (1990). "Donor leukocyte transfusions for treatment of recurrent chronic myelogenous leukemia in marrow transplant patients." Blood **76**(12): 2462-2465.
- Kolb, H. J., B. Simoes, et al. (2004). "Cellular immunotherapy after allogeneic stem cell transplantation in hematologic malignancies." Curr Opin Oncol **16**(2): 167-173.
- Kotredes, K. P. and A. M. Gamero (2013). "Interferons as inducers of apoptosis in malignant cells." J Interferon Cytokine Res **33**(4): 162-170.
- Koya, R. C., S. Mok, et al. (2010). "Kinetic phases of distribution and tumor targeting by T cell receptor engineered lymphocytes inducing robust antitumor responses." Proc Natl Acad Sci U S A **107**(32): 14286-14291.
- Kreiter, S., M. Vormehr, et al. (2015). "Mutant MHC class II epitopes drive therapeutic immune responses to cancer." Nature **520**(7549): 692-696.
- Kuball, J., M. L. Dossett, et al. (2007). "Facilitating matched pairing and expression of TCR chains introduced into human T cells." Blood **109**(6): 2331-2338.
- Kuball, J., B. Hauptrock, et al. (2009). "Increasing functional avidity of TCR-redirectioned T cells by removing defined N-glycosylation sites in the TCR constant domain." J Exp Med **206**(2): 463-475.
- Kubo, R. T., W. Born, et al. (1989). "Characterization of a monoclonal antibody which detects all murine alpha beta T cell receptors." J Immunol **142**(8): 2736-2742.
- Kummer, U., U. Zengerle, et al. (2001). "Increased in vivo mitogenicity of anti-TCR/CD3 monoclonal antibody through reduced interaction with Fc gamma receptors." Immunol Lett **75**(2): 153-158.

- Kwon, E. D., C. G. Drake, et al. (2014). "Ipilimumab versus placebo after radiotherapy in patients with metastatic castration-resistant prostate cancer that had progressed after docetaxel chemotherapy (CA184-043): a multicentre, randomised, double-blind, phase 3 trial." Lancet Oncol **15**(7): 700-712.
- Kwon, E. D., C. G. Drake, et al. (2014). "Ipilimumab versus placebo after radiotherapy in patients with metastatic castration-resistant prostate cancer that had progressed after docetaxel chemotherapy (CA184-043): a multicentre, randomised, double-blind, phase 3 trial." Lancet Oncol **15**(7): 700-712.
- Lamers, C. H., S. Sleijfer, et al. (2013). "Treatment of metastatic renal cell carcinoma with CAIX CAR-engineered T cells: clinical evaluation and management of on-target toxicity." Mol Ther **21**(4): 904-912.
- Larkin, J., V. Chiarion-Sileni, et al. (2015). "Combined Nivolumab and Ipilimumab or Monotherapy in Untreated Melanoma." N Engl J Med **373**(1): 23-34.
- Leach, D. R., M. F. Krummel, et al. (1996). "Enhancement of antitumor immunity by CTLA-4 blockade." Science **271**(5256): 1734-1736.
- Lee, D. W., J. N. Kochenderfer, et al. (2015). "T cells expressing CD19 chimeric antigen receptors for acute lymphoblastic leukaemia in children and young adults: a phase 1 dose-escalation trial." Lancet **385**(9967): 517-528.
- Lesokhin, A. M., T. M. Hohl, et al. (2012). "Monocytic CCR2(+) myeloid-derived suppressor cells promote immune escape by limiting activated CD8 T-cell infiltration into the tumor microenvironment." Cancer Res **72**(4): 876-886.
- Leukemia, T. I. C. S. G. o. C. M. (1994). "Interferon alfa-2a as compared with conventional chemotherapy for the treatment of chronic myeloid leukemia. The Italian Cooperative Study Group on Chronic Myeloid Leukemia." N Engl J Med **330**(12): 820-825.
- Lewin, M., N. Carlesso, et al. (2000). "Tat peptide-derivatized magnetic nanoparticles allow in vivo tracking and recovery of progenitor cells." Nat Biotechnol **18**(4): 410-414.
- Lewis, J., R. Laforest, et al. (2001). "Copper-64-diacetyl-bis(N4-methylthiosemicarbazone): An agent for radiotherapy." Proc Natl Acad Sci U S A **98**(3): 1206-1211.
- Li, B., H. Wang, et al. (2005). "Construction and characterization of a humanized anti-human CD3 monoclonal antibody 12F6 with effective immunoregulation functions." Immunology **116**(4): 487-498.
- Linette, G. P., E. A. Stadtmauer, et al. (2013). "Cardiovascular toxicity and titin cross-reactivity of affinity-enhanced T cells in myeloma and melanoma." Blood **122**(6): 863-871.
- Liu, L., Q. Ye, et al. (2012). "Tracking T-cells in vivo with a new nano-sized MRI contrast agent." Nanomedicine **8**(8): 1345-1354.
- Liu, Z. and Z. Li (2014). "Molecular imaging in tracking tumor-specific cytotoxic T lymphocytes (CTLs)." Theranostics **4**(10): 990-1001.
- Lobo, E. D., R. J. Hansen, et al. (2004). "Antibody pharmacokinetics and pharmacodynamics." J Pharm Sci **93**(11): 2645-2668.
- Lynch, T. J., I. Bondarenko, et al. (2012). "Ipilimumab in combination with paclitaxel and carboplatin as first-line treatment in stage IIIB/IV non-small-cell lung cancer: results from a randomized, double-blind, multicenter phase II study." J Clin Oncol **30**(17): 2046-2054.
- Maher, J., R. J. Brentjens, et al. (2002). "Human T-lymphocyte cytotoxicity and proliferation directed by a single chimeric TCRzeta /CD28 receptor." Nat Biotechnol **20**(1): 70-75.

- Mannheim, J. G., M. S. Judenhofer, et al. (2012). "Quantification accuracy and partial volume effect in dependence of the attenuation correction of a state-of-the-art small animal PET scanner." *Phys Med Biol* **57**(12): 3981-3993.
- Manuri, P. V., M. H. Wilson, et al. (2010). "piggyBac transposon/transposase system to generate CD19-specific T cells for the treatment of B-lineage malignancies." *Hum Gene Ther* **21**(4): 427-437.
- Maude, S. L., N. Frey, et al. (2014). "Chimeric antigen receptor T cells for sustained remissions in leukemia." *N Engl J Med* **371**(16): 1507-1517.
- McCracken, M. N., D. N. Vatakis, et al. (2015). "Noninvasive detection of tumor-infiltrating T cells by PET reporter imaging." *J Clin Invest* **125**(5): 1815-1826.
- McDevitt, M. R., R. D. Finn, et al. (1999). "Preparation of alpha-emitting <sup>213</sup>Bi-labeled antibody constructs for clinical use." *J Nucl Med* **40**(10): 1722-1727.
- Meir, R., K. Shamalov, et al. (2015). "Nanomedicine for Cancer Immunotherapy: Tracking Cancer-Specific T-Cells in Vivo with Gold Nanoparticles and CT Imaging." *ACS Nano* **9**(6): 6363-6372.
- Melero, I., A. Rouzaut, et al. (2014). "T-cell and NK-cell infiltration into solid tumors: a key limiting factor for efficacious cancer immunotherapy." *Cancer Discov* **4**(5): 522-526.
- Melero, I., W. W. Shuford, et al. (1997). "Monoclonal antibodies against the 4-1BB T-cell activation molecule eradicate established tumors." *Nat Med* **3**(6): 682-685.
- Mendler, C. T., T. Gehring, et al. (2015). "<sup>89</sup>Zr-Labeled Versus <sup>124</sup>I-Labeled alphaHER2 Fab with Optimized Plasma Half-Life for High-Contrast Tumor Imaging In Vivo." *J Nucl Med* **56**(7): 1112-1118.
- Mlecnik, B., M. Tosolini, et al. (2011). "Histopathologic-based prognostic factors of colorectal cancers are associated with the state of the local immune reaction." *J Clin Oncol* **29**(6): 610-618.
- Moolten, F. L. (1986). "Tumor chemosensitivity conferred by inserted herpes thymidine kinase genes: paradigm for a prospective cancer control strategy." *Cancer Res* **46**(10): 5276-5281.
- Morgan, R. A. (2012). "Live and let die: a new suicide gene therapy moves to the clinic." *Mol Ther* **20**(1): 11-13.
- Morgan, R. A., N. Chinnasamy, et al. (2013). "Cancer regression and neurological toxicity following anti-MAGE-A3 TCR gene therapy." *J Immunother* **36**(2): 133-151.
- Morgan, R. A., M. E. Dudley, et al. (2006). "Cancer regression in patients after transfer of genetically engineered lymphocytes." *Science* **314**(5796): 126-129.
- Morgan, R. A., J. C. Yang, et al. (2010). "Case report of a serious adverse event following the administration of T cells transduced with a chimeric antigen receptor recognizing ERBB2." *Mol Ther* **18**(4): 843-851.
- Murali-Krishna, K., J. D. Altman, et al. (1998). "Counting antigen-specific CD8 T cells: a reevaluation of bystander activation during viral infection." *Immunity* **8**(2): 177-187.
- Nakazawa, Y., L. E. Huye, et al. (2011). "PiggyBac-mediated cancer immunotherapy using EBV-specific cytotoxic T-cells expressing HER2-specific chimeric antigen receptor." *Mol Ther* **19**(12): 2133-2143.
- Neville, D. M., Jr., J. Scharff, et al. (1992). "In vivo T-cell ablation by a holo-immunotoxin directed at human CD3." *Proc Natl Acad Sci U S A* **89**(7): 2585-2589.

- Niederle, N., O. Kloke, et al. (1993). "Long-term treatment of chronic myelogenous leukemia with different interferons: results from three studies." Leuk Lymphoma **9**(1-2): 111-119.
- Nishimura, Y., M. Eto, et al. (1994). "Inhibition of skin xenograft rejection by depleting T-cell receptor alpha beta-bearing cells without T-cell receptor gamma delta-bearing cells or natural killer cells by monoclonal antibody." Immunology **83**(2): 196-204.
- O'Brien, S. G., F. Guilhot, et al. (2003). "Imatinib compared with interferon and low-dose cytarabine for newly diagnosed chronic-phase chronic myeloid leukemia." N Engl J Med **348**(11): 994-1004.
- Oude Munnink, T. H., E. G. de Vries, et al. (2012). "Lapatinib and 17AAG reduce 89Zr-trastuzumab-F(ab')<sub>2</sub> uptake in SKBR3 tumor xenografts." Mol Pharm **9**(11): 2995-3002.
- Palmer, D. C., C. C. Chan, et al. (2008). "Effective tumor treatment targeting a melanoma/melanocyte-associated antigen triggers severe ocular autoimmunity." Proc Natl Acad Sci U S A **105**(23): 8061-8066.
- Pandit-Taskar, N., J. O'Donoghue, et al. (2015). "First in Human 89Zr-Df-IAB2M anti-prostate specific membrane antigen (PSMA) minibody in patients with metastatic prostate cancer." Journal of Nuclear Medicine **56**(supplement 3): 400.
- Parkhurst, M. R., J. C. Yang, et al. (2011). "T cells targeting carcinoembryonic antigen can mediate regression of metastatic colorectal cancer but induce severe transient colitis." Mol Ther **19**(3): 620-626.
- Penheiter, A. R., S. J. Russell, et al. (2012). "The sodium iodide symporter (NIS) as an imaging reporter for gene, viral, and cell-based therapies." Curr Gene Ther **12**(1): 33-47.
- Perk, L. R., O. J. Visser, et al. (2006). "Preparation and evaluation of (89)Zr-Zevalin for monitoring of (90)Y-Zevalin biodistribution with positron emission tomography." Eur J Nucl Med Mol Imaging **33**(11): 1337-1345.
- Perk, L. R., M. J. Vosjan, et al. (2010). "p-Isothiocyanatobenzyl-desferrioxamine: a new bifunctional chelate for facile radiolabeling of monoclonal antibodies with zirconium-89 for immuno-PET imaging." Eur J Nucl Med Mol Imaging **37**(2): 250-259.
- Philip, B., E. Kokalaki, et al. (2014). "A highly compact epitope-based marker/suicide gene for easier and safer T-cell therapy." Blood **124**(8): 1277-1287.
- Porter, D. L., B. L. Levine, et al. (2011). "Chimeric antigen receptor-modified T cells in chronic lymphoid leukemia." N Engl J Med **365**(8): 725-733.
- Prins, R. M., C. J. Shu, et al. (2008). "Anti-tumor activity and trafficking of self, tumor-specific T cells against tumors located in the brain." Cancer Immunol Immunother **57**(9): 1279-1289.
- Provasi, E., P. Genovese, et al. (2012). "Editing T cell specificity towards leukemia by zinc finger nucleases and lentiviral gene transfer." Nat Med **18**(5): 807-815.
- Przepiorka, D., G. L. Phillips, et al. (1998). "A phase II study of BTI-322, a monoclonal anti-CD2 antibody, for treatment of steroid-resistant acute graft-versus-host disease." Blood **92**(11): 4066-4071.
- Quezada, S. A., T. R. Simpson, et al. (2010). "Tumor-reactive CD4(+) T cells develop cytotoxic activity and eradicate large established melanoma after transfer into lymphopenic hosts." J Exp Med **207**(3): 637-650.
- Rabinovich, B. A., Y. Ye, et al. (2008). "Visualizing fewer than 10 mouse T cells with an enhanced firefly luciferase in immunocompetent mouse models of cancer." Proc Natl Acad Sci U S A **105**(38): 14342-14346.

- Robbins, P. F., S. H. Kassim, et al. (2015). "A pilot trial using lymphocytes genetically engineered with an NY-ESO-1-reactive T-cell receptor: long-term follow-up and correlates with response." *Clin Cancer Res* **21**(5): 1019-1027.
- Robbins, P. F., R. A. Morgan, et al. (2011). "Tumor regression in patients with metastatic synovial cell sarcoma and melanoma using genetically engineered lymphocytes reactive with NY-ESO-1." *J Clin Oncol* **29**(7): 917-924.
- Rosenberg, S. A., M. T. Lotze, et al. (1987). "A progress report on the treatment of 157 patients with advanced cancer using lymphokine-activated killer cells and interleukin-2 or high-dose interleukin-2 alone." *N Engl J Med* **316**(15): 889-897.
- Rosenberg, S. A., M. T. Lotze, et al. (1989). "Experience with the use of high-dose interleukin-2 in the treatment of 652 cancer patients." *Ann Surg* **210**(4): 474-484; discussion 484-475.
- Rosenberg, S. A., B. S. Packard, et al. (1988). "Use of tumor-infiltrating lymphocytes and interleukin-2 in the immunotherapy of patients with metastatic melanoma. A preliminary report." *N Engl J Med* **319**(25): 1676-1680.
- Rosenberg, S. A., J. C. Yang, et al. (2011). "Durable complete responses in heavily pretreated patients with metastatic melanoma using T-cell transfer immunotherapy." *Clin Cancer Res* **17**(13): 4550-4557.
- Rosenberg, S. A., J. C. Yang, et al. (1994). "Treatment of 283 consecutive patients with metastatic melanoma or renal cell cancer using high-dose bolus interleukin 2." *JAMA* **271**(12): 907-913.
- Roszik, J., B. Rabinovich, et al. (2011). "Imaging of T cells expressing chimeric antigen receptors." *Immunotherapy* **3**(12): 1411-1414.
- Sakuishi, K., L. Apetoh, et al. (2010). "Targeting Tim-3 and PD-1 pathways to reverse T cell exhaustion and restore anti-tumor immunity." *J Exp Med* **207**(10): 2187-2194.
- Samaniego, F., Z. Berkova, et al. (2014). "90Y-ibritumomab tiuxetan radiotherapy as first-line therapy for early stage low-grade B-cell lymphomas, including bulky disease." *Br J Haematol* **167**(2): 207-213.
- Sato, N., H. Wu, et al. (2015). "(89)Zr-Oxine Complex PET Cell Imaging in Monitoring Cell-based Therapies." *Radiology* **275**(2): 490-500.
- Schneider, H., J. Downey, et al. (2006). "Reversal of the TCR stop signal by CTLA-4." *Science* **313**(5795): 1972-1975.
- Schumacher, T., L. Bunse, et al. (2014). "A vaccine targeting mutant IDH1 induces antitumor immunity." *Nature* **512**(7514): 324-327.
- Serafini, M., M. Manganini, et al. (2004). "Characterization of CD20-transduced T lymphocytes as an alternative suicide gene therapy approach for the treatment of graft-versus-host disease." *Hum Gene Ther* **15**(1): 63-76.
- Sfanos, K. S., T. C. Bruno, et al. (2009). "Human prostate-infiltrating CD8+ T lymphocytes are oligoclonal and PD-1+." *Prostate* **69**(15): 1694-1703.
- Sham, J. G., F. M. Kievit, et al. (2014). "Glypican-3-targeting F(ab')<sub>2</sub> for 89Zr PET of hepatocellular carcinoma." *J Nucl Med* **55**(12): 2032-2037.
- Shiheido, H., C. Chen, et al. (2014). "Modulation of the human T cell response by a novel non-mitogenic anti-CD3 antibody." *PLoS One* **9**(4): e94324.
- Shu, C. J., S. Guo, et al. (2005). "Visualization of a primary anti-tumor immune response by positron emission tomography." *Proc Natl Acad Sci U S A* **102**(48): 17412-17417.

- Shu, C. J., C. G. Radu, et al. (2009). "Quantitative PET reporter gene imaging of CD8+ T cells specific for a melanoma-expressed self-antigen." Int Immunol **21**(2): 155-165.
- Sim, G. C., N. Martin-Orozco, et al. (2014). "IL-2 therapy promotes suppressive ICOS+ Treg expansion in melanoma patients." J Clin Invest **124**(1): 99-110.
- Small E, D. T., Gerritsen WR, et al. (2009). "A phase III study of GVAX immunotherapy for prostate cancer in combination with docetaxel versus docetaxel plus prednisone in symptomatic, castration-resistant prostate cancer (CRPC)."
- Smith-Jones, P. M., B. Stolz, et al. (1994). "Gallium-67/gallium-68-[DFO]-octreotide--a potential radiopharmaceutical for PET imaging of somatostatin receptor-positive tumors: synthesis and radiolabeling in vitro and preliminary in vivo studies." J Nucl Med **35**(2): 317-325.
- Sommermeier, D., M. Hudecek, et al. (2015). "Chimeric antigen receptor-modified T cells derived from defined CD8 and CD4 subsets confer superior antitumor reactivity in vivo." Leukemia.
- Sommermeier, D. and W. Uckert (2010). "Minimal amino acid exchange in human TCR constant regions fosters improved function of TCR gene-modified T cells." J Immunol **184**(11): 6223-6231.
- Srinivas, M., M. S. Turner, et al. (2009). "In vivo cytometry of antigen-specific t cells using 19F MRI." Magn Reson Med **62**(3): 747-753.
- Stelter, L., H. Amthauer, et al. (2008). "An orthotopic model of pancreatic somatostatin receptor (SSTR)-positive tumors allows bimodal imaging studies using 3T MRI and animal PET-based molecular imaging of SSTR expression." Neuroendocrinology **87**(4): 233-242.
- Steward, B. W., Wild,C.P. (2014). World Cancer Report 2014.
- Swirski, F. K., C. R. Berger, et al. (2007). "A near-infrared cell tracker reagent for multiscopic in vivo imaging and quantification of leukocyte immune responses." PLoS One **2**(10): e1075.
- Taube, J. M., R. A. Anders, et al. (2012). "Colocalization of inflammatory response with B7-h1 expression in human melanocytic lesions supports an adaptive resistance mechanism of immune escape." Sci Transl Med **4**(127): 127ra137.
- Tavare, R., H. Escuin-Ordinas, et al. (2015). "An effective immuno-PET imaging method to monitor CD8-dependent responses to immunotherapy." Cancer Res.
- Tavare, R., H. Escuin-Ordinas, et al. (2016). "An Effective Immuno-PET Imaging Method to Monitor CD8-Dependent Responses to Immunotherapy." Cancer Res **76**(1): 73-82.
- Tavare, R., M. N. McCracken, et al. (2014). "Engineered antibody fragments for immuno-PET imaging of endogenous CD8+ T cells in vivo." Proc Natl Acad Sci U S A **111**(3): 1108-1113.
- Tavare, R., M. N. McCracken, et al. (2015). "Immuno-PET of Murine T Cell Reconstitution Postadoptive Stem Cell Transplantation Using Anti-CD4 and Anti-CD8 Cys-Diabodies." J Nucl Med **56**(8): 1258-1264.
- Tehrani, O. S., O. Muzik, et al. (2007). "Tumor imaging using 1-(2'-deoxy-2'-18F-fluoro-beta-D-arabinofuranosyl)thymine and PET." J Nucl Med **48**(9): 1436-1441.
- Thompson, R. H., S. M. Kuntz, et al. (2006). "Tumor B7-H1 is associated with poor prognosis in renal cell carcinoma patients with long-term follow-up." Cancer Res **66**(7): 3381-3385.
- Topalian, S. L., F. S. Hodi, et al. (2012). "Safety, activity, and immune correlates of anti-PD-1 antibody in cancer." N Engl J Med **366**(26): 2443-2454.

- Tran, E., M. Ahmadzadeh, et al. (2015). "Immunogenicity of somatic mutations in human gastrointestinal cancers." Science **350**(6266): 1387-1390.
- Tran, E., S. Turcotte, et al. (2014). "Cancer immunotherapy based on mutation-specific CD4+ T cells in a patient with epithelial cancer." Science **344**(6184): 641-645.
- Triebel, F., S. Jitsukawa, et al. (1990). "LAG-3, a novel lymphocyte activation gene closely related to CD4." J Exp Med **171**(5): 1393-1405.
- van de Watering, F. C., M. Rijpkema, et al. (2014). "Zirconium-89 labeled antibodies: a new tool for molecular imaging in cancer patients." Biomed Res Int **2014**: 203601.
- van den Eertwegh, A. J., J. Versluis, et al. (2012). "Combined immunotherapy with granulocyte-macrophage colony-stimulating factor-transduced allogeneic prostate cancer cells and ipilimumab in patients with metastatic castration-resistant prostate cancer: a phase 1 dose-escalation trial." Lancet Oncol **13**(5): 509-517.
- van Eerd, J. E., E. Vegt, et al. (2006). "Gelatin-based plasma expander effectively reduces renal uptake of <sup>111</sup>In-octreotide in mice and rats." J Nucl Med **47**(3): 528-533.
- van Elsas, A., A. A. Hurwitz, et al. (1999). "Combination immunotherapy of B16 melanoma using anti-cytotoxic T lymphocyte-associated antigen 4 (CTLA-4) and granulocyte/macrophage colony-stimulating factor (GM-CSF)-producing vaccines induces rejection of subcutaneous and metastatic tumors accompanied by autoimmune depigmentation." J Exp Med **190**(3): 355-366.
- van Meerten, T., R. S. van Rijn, et al. (2006). "Complement-induced cell death by rituximab depends on CD20 expression level and acts complementary to antibody-dependent cellular cytotoxicity." Clin Cancer Res **12**(13): 4027-4035.
- van Oosterhout, Y. V., L. van Emst, et al. (2000). "A combination of anti-CD3 and anti-CD7 ricin A-immunotoxins for the in vivo treatment of acute graft versus host disease." Blood **95**(12): 3693-3701.
- Vansteenkiste, J., M. Zielinski, et al. (2013). "Adjuvant MAGE-A3 immunotherapy in resected non-small-cell lung cancer: phase II randomized study results." J Clin Oncol **31**(19): 2396-2403.
- Verel, I., G. W. Visser, et al. (2003). "<sup>89</sup>Zr immuno-PET: comprehensive procedures for the production of <sup>89</sup>Zr-labeled monoclonal antibodies." J Nucl Med **44**(8): 1271-1281.
- Viola-Villegas, N. T., K. K. Sevak, et al. (2014). "Noninvasive Imaging of PSMA in prostate tumors with (<sup>89</sup>Zr)-Labeled huJ591 engineered antibody fragments: the faster alternatives." Mol Pharm **11**(11): 3965-3973.
- Walter, S., T. Weinschenk, et al. (2012). "Multi-peptide immune response to cancer vaccine IMA901 after single-dose cyclophosphamide associates with longer patient survival." Nat Med **18**(8): 1254-1261.
- Wang, X., C. Berger, et al. (2011). "Engraftment of human central memory-derived effector CD8+ T cells in immunodeficient mice." Blood **117**(6): 1888-1898.
- Wang, X., W. C. Chang, et al. (2011). "A transgene-encoded cell surface polypeptide for selection, in vivo tracking, and ablation of engineered cells." Blood **118**(5): 1255-1263.
- Weetall, M., M. E. Digan, et al. (2002). "T-cell depletion and graft survival induced by anti-human CD3 immunotoxins in human CD3epsilon transgenic mice." Transplantation **73**(10): 1658-1666.
- Weide, B., S. Pascolo, et al. (2009). "Direct injection of protamine-protected mRNA: results of a phase 1/2 vaccination trial in metastatic melanoma patients." J Immunother **32**(5): 498-507.

- Wu, C., Y. Zhu, et al. (2006). "Immunohistochemical localization of programmed death-1 ligand-1 (PD-L1) in gastric carcinoma and its clinical significance." Acta Histochem **108**(1): 19-24.
- Wu, F., W. Zhang, et al. (2013). "Human effector T cells derived from central memory cells rather than CD8(+)T cells modified by tumor-specific TCR gene transfer possess superior traits for adoptive immunotherapy." Cancer Lett **339**(2): 195-207.
- Yadav, M., S. Jhunjhunwala, et al. (2014). "Predicting immunogenic tumour mutations by combining mass spectrometry and exome sequencing." Nature **515**(7528): 572-576.
- Yaghoubi, S. S., M. A. Couto, et al. (2006). "Preclinical safety evaluation of 18F-FHBG: a PET reporter probe for imaging herpes simplex virus type 1 thymidine kinase (HSV1-tk) or mutant HSV1-sr39tk's expression." J Nucl Med **47**(4): 706-715.
- Yaghoubi, S. S., M. C. Jensen, et al. (2009). "Noninvasive detection of therapeutic cytolytic T cells with 18F-FHBG PET in a patient with glioma." Nat Clin Pract Oncol **6**(1): 53-58.
- Yang, J. C., M. Hughes, et al. (2007). "Ipilimumab (anti-CTLA4 antibody) causes regression of metastatic renal cell cancer associated with enteritis and hypophysitis." J Immunother **30**(8): 825-830.
- Zhang, L., J. R. Conejo-Garcia, et al. (2003). "Intratumoral T cells, recurrence, and survival in epithelial ovarian cancer." N Engl J Med **348**(3): 203-213.
- Zhou, X., G. Dotti, et al. (2015). "Inducible caspase-9 suicide gene controls adverse effects from alloplete T cells after haploidentical stem cell transplantation." Blood **125**(26): 4103-4113.
- Zhu, Y., B. L. Knolhoff, et al. (2014). "CSF1/CSF1R blockade reprograms tumor-infiltrating macrophages and improves response to T-cell checkpoint immunotherapy in pancreatic cancer models." Cancer Res **74**(18): 5057-5069.



## 8 ABBREVIATIONS

%ID	Percent injected dose
%ID/g	Percent injected dose per gram
<sup>111</sup> In	Indium-111
<sup>18</sup> F-FDG	Fluor-18-Fluorodesoxyglucose
<sup>64</sup> Cu-PTSM	64-Cu-pyruvaldehydebis(N4-methylthiosemicarbazone
7-AAD	7-aminoactinomycine-D
<sup>89</sup> Zr	Zirconium-89
<sup>99m</sup> Tc-HMPAO	Technetium-99m-hexamethylpropylene amine oxime
ALL	Acute lymphocytic leukemia
AML	Acute myeloid leukemia
APC	Antigen presenting cells
aTCRmu	Anti murine TCR antibody
BLI	Bioluminescence imaging
CAR	Chimeric antigen receptors
CDC	Complement dependent cytotoxicity
CEA	Carcinoembryonic antigen
CML	Chronic myelogenous leukemia
CPM	Counts per minute
CT	X-ray computed tomography
CTLA-4	Cytotoxic T-lymphocyte antigen-4
DC	Dendritic cell
DEPC	Diethyldicarbonat
DFO-Bz-NCS	P-isothiocanatobenzyl derivate of desferrioxamine
DLI	Donor lymphocyte infusions
DNA	Deoxyribonucleic acid
EGFR	Epithelial growth factor receptor
ELISA	Enzyme linked immunosorbent Assay
FcR	Fc-Receptor
FDA	Food and Drug administration USA
GCV	Ganciclovir
gDNA	Genomic DNA

GFP	Green fluorescent protein
GM-CSF	Granulocyte macrophage colony stimulating factor
GM-CSF	Granulocyte macrophage colony stimulating factor
gp100	Glycoprotein 100
GvHD	Graft-versus-host disease
GvL	Graft-versus-leukemia effect
hNET	human norepinephrine transporter
hNIS	human sodium iodide transporter
HRP	horseradish peroxidase
HSV1-tk	herpes simplex virus1-thymidine kinase
i.t.	Intratumoral
i.v.	Intravenous
IFN	Interferon
IgG	Immunoglobuline G
IL	Interleukin
kDa	Kilo-Dalton
MAGE-A3	Melanoma associated antigen A3
MART-1	Melanoma antigen recognized by T cells 1
MFI	Mean fluorescence intensity
MHC	Major histocompatibility complex
MIP	Maximal intensity projection
MPO	Myeloperoxidase
MRI	Magnetic resonance tomography
NSCLC	Non-small cell lung carcinoma
p.i.	Post injection
PAP	Prostatic acid phosphatase
PBL	Peripheral blood lymphocytes
PBMC	Peripheral blood mononuclear cells
PCR	Polymerase chain reaction
PD-1	Programmed cell death 1 protein
PD-L1	Programmed cell death 1 protein ligand
PET	Positron emission tomography

PFC	Perfluorocarbon
PSMA	Human prostate specific membrane antigen
qPCR	Quantitative Polymerase chain reaction
RCC	Renal cell carcinoma
ROI	Region of interest
s.c.	Subcutaneous
s.d.	Standard deviation
SPECT	Single photon emission computed tomography
SPIO	Superparamagnetic iron oxide
TAA	Tumor-associated antigens
TALEN	Transcription-activator-like effector nucleases
TBI	Total body irradiation
T <sub>CM</sub>	Central memory T-cells
TCR	T-cell receptor
T <sub>EM</sub>	Effector memory T-cells
TIL	Tumor infiltrating lymphocytes
TME	Tumor microenvironment
T-Reg	Regulatory T-cells
T <sub>SCM</sub>	T memory stem cells
WHO	World health organization
WT	Wild-type

## 9 ACKNOWLEDGEMENTS

First of all I would like to thank Prof. Krackhardt for giving me the opportunity to perform my dissertation in her lab, her outstanding supervision and support in all different aspects of this PhD-project. She was always highly interested and supportive for this project. Furthermore I would like to thank Prof. Peschel as well as Prof. Schwaiger for their support and providing laboratory and imaging-equipment. Dr. Calogero d'Alessandria and Nahid Yusufi for their collaboration, great help and preparation of tracers. Furthermore I would like to thank Prof. Ziegler for their collaboration and the accompaniment of this project as a member of my PhD-Committee together with Prof. Antes. Many thanks to the preclinical imaging team, especially Sybille Reder for their efforts that made it possible to perform PET-imaging on this level. I would like to thank Dr. Michaela Aichler and Dr. Katja Steiger as well as Dr. Melanie Straub for their support with pathological expertise and performance of the immunohistochemical stainings.

A very special thanks to all group members of the AG Krackhardt: Dr. Xiaoling Liang showed me with great patience all methods necessary for in vivo experiments. Dr. Richard Klar, who characterized the TCR used in this study. He had always an open ear and many very good suggestions regarding this project. Eva Bräunlein and Stefan Audehm for enriching my life with many very helpful scientific but also personal discussions and their support. Henrique Bianchi and Ricarda Wagner for the support and help with the in vivo studies. Many thanks to Stephanie Rämisch and especially to Irina Fuchs for such great technical support and their optimism.

Furthermore, I would like to thank my family for their support and indispensable motivation. Last but not least I would like to thank Rainer endowing me so much love and support in every circumstances and having an incredible patience over such a long time. Without his help I would not be able to perform this work in such a way.

## 10 CURRICULUM VITAE

### Personal information

Name	<b>Mall, Sabine</b>
E-Mail	sabine.mall@tum.de
Date of birth	23.09.1985
Nationality	Italian

### University education

10.2010 - today	Doctoral thesis at the Technical University Munich Klinikum rechts der Isar, 3 <sup>rd</sup> medical department (hematology/oncology) Group of Prof.Dr.med.Angela Krackhardt
06.2009 - 06.2010	Diploma thesis at the Medical University Vienna Institute of cancer research Group of Prof.Dr.Wolfgang Mikulits
10.2004 – 06.2010	Diploma in molecular biology at the University Vienna

### Education

10.1999 - 06.2004	Pädagogisches Gymnasium J.Ferrari, Meran
10.1991 - 06.1999	Primary school, Prad am Stilfserjoch

### Publications

**Mall S**, Yusufi N, Wagner R, Klar R, Bianchi H, Steiger, K, Straub M, Audehm S, Laitinen I, Aichler M, Peschel C, Ziegler S, Mustafa M, Schwaiger M, D`Alessandria C, Krackhardt AM. **Mapping of T-cell receptor-engineered human T cells at the tumor site by Immuno-PET.** *Cancer Research. in revision*

Klar R, Schober S, Rami M, **Mall S**, Merl J, Hauck SM, Ueffing M, Admon A, Slotta-Huspenina J, Schwaiger M, Stevanović S, Oostendorp RA, Busch DH, Peschel C, Krackhardt AM. **Therapeutic targeting of naturally presented myeloperoxidase-derived HLA peptide ligands on myeloid leukemia cells by TCR-transgenic T cells.** *Leukemia*. 2014 Dec;28(12):2355-66.

Weigand LU, Liang X, Schmied S, **Mall S**, Klar R, Stötzer OJ, Salat C, Götze K, Mautner J, Peschel C, Krackhardt AM. **Isolation of human MHC class II-restricted T cell receptors from the autologous T-cell repertoire with potent anti-leukaemic reactivity.** *Immunology*. 2012 Nov;137(3):226-38.

Höfig I, Atkinson MJ, **Mall S**, Krackhardt AM, Thirion C, Anastasov N. **Poloxamer synperonic F108 improves cellular transduction with lentiviral vectors.** *J Gene Med*. 2012 Aug;14(8):549-60.

van Zijl F, **Mall S**, Machat G, Pirker C, Zeillinger R, Weinhaeusel A, Bilban M, Berger W, Mikulits W. **A human model of epithelial to mesenchymal transition to monitor drug efficacy in hepatocellular carcinoma progression.** *Mol Cancer Ther*. 2011 May;10(5):850-60.

## Cogress participation

2015, Cancer Immunotherapy Meeting CIMT, Mainz (poster): **Development of clinically implementable imaging strategies for tracking T-cell receptor transgenic effector cells.** **Mall S**, Yusufi N, Klar R, Bianchi H, Laitinen I, Steiger K, Aichler M, Feuchtinger A, Walch A, Schwaiger M, Peschel C, D'Alessandria C, Krackhardt AM.

2014, Immunotherapy of Cancer Conference, München (poster): **Development of clinically implementable imaging strategies for tracking T-cell receptor transgenic effector cells.** **Mall S**, Yusufi N, Klar R, Bianchi H, Laitinen I, Steiger K, Aichler M, Walch A, Schwaiger M, Peschel C, D'Alessandria C, Krackhardt AM.

2013, International Symposium of Cellular Therapy, Erlangen, (poster): **Development of clinically implementable imaging strategies for tracking T-cell receptor transgenic effector cells.** **Mall S**, D'Alessandria C, Reder S, Frank A, Aichler A, Walch A, Schwaiger M, Peschel C, Essler M, Krackhardt AM.

2012, Cancer Immunotherapy Meeting CIMT, Mainz, (poster, oral presentation): **Development of clinically implementable imaging strategies for tracking T-cell receptor transgenic effector cells.** **Mall S**, D'Alessandria C, Reder S, Frank A, Laitinen I, Aichler A, Walch A, Schwaiger M, Peschel C, Krackhardt AM.